SENSOR-BASED MACHINE OLFACTION WITH

NEUROMORPHIC MODELS OF THE OLFACTORY SYSTEM

A Dissertation

by

BARANIDHARAN RAMAN

Submitted to the Office of Graduate Studies of
Texas A&M University
in partial fulfillment of the requirements for the degree of

DOCTOR OF PHILOSOPHY

December 2005

Major Subject: Computer Science

SENSOR-BASED MACHINE OLFACTION WITH

NEUROMORPHIC MODELS OF THE OLFACTORY SYSTEM

A Dissertation

by

BARANIDHARAN RAMAN

Submitted to the Office of Graduate Studies of
Texas A&M University
in partial fulfillment of the requirements for the degree of

DOCTOR OF PHILOSOPHY

Approved by:

Chair of Committee,	Ricardo Gutierrez-Osuna
Committee Members,	Yoonsuck Choe
	Bruce H. McCormick
	Behbood Zoghi
Head of Department,	Valerie Taylor

December 2005

Major Subject: Computer Science

ABSTRACT

Sensor-based Machine Olfaction with Neuromorphic Models of the Olfactory

System. (December 2005)

Baranidharan Raman, B.Eng., University of Madras, India;

M.S., Texas A&M University

Chair of Advisory Committee: Dr. Ricardo Gutierrez-Osuna

Electronic noses combine an array of cross-selective gas sensors with a pattern recognition engine to identify odors. Pattern recognition of multivariate gas sensor response is usually performed using existing statistical and chemometric techniques. An alternative solution involves developing novel algorithms inspired by information processing in the biological olfactory system.

The objective of this dissertation is to develop a neuromorphic architecture for pattern recognition for a chemosensor array inspired by key signal processing mechanisms in the olfactory system. Our approach can be summarized as follows. First, a high-dimensional odor signal is generated from a chemical sensor array. Three approaches have been proposed to generate this combinatorial and high dimensional odor signal: temperature-modulation of a metal-oxide chemoresistor, a large population of optical microbead sensors, and infrared spectroscopy. The resulting high-dimensional odor signals are subject to dimensionality reduction using a self-organizing model of chemotopic convergence. This convergence transforms the initial combinatorial high-dimensional code into an organized spatial pattern (i.e., an odor image), which decouples

odor identity from intensity. Two lateral inhibitory circuits subsequently process the highly overlapping odor images obtained after convergence. The first shunting lateral inhibition circuits perform gain control enabling identification of the odorant across a wide range of concentration. This shunting lateral inhibition is followed by an additive lateral inhibition circuit with center-surround connections. These circuits improve contrast between odor images leading to more sparse and orthogonal patterns than the one available at the input. The sharpened odor image is stored in a neurodynamic model of a cortex. Finally, anti-Hebbian/ Hebbian inhibitory feedback from the cortical circuits to the contrast enhancement circuits performs mixture segmentation and weaker odor/background suppression, respectively. We validate the models using experimental datasets and show our results are consistent with recent neurobiological findings.

To My Mom, Dad and Sai

ACKNOWLEDGEMENTS

I would like to thank my advisor, Dr. Ricardo Gutierrez-Osuna, for introducing me to this fascinating area of research, and providing me support and guidance for accomplishing this work. I have learned from him the art of writing and presenting research. I am also thankful to Ricardo for his commendable effort in providing me feedback for every version of my dissertation and all my papers.

I also would like to thank my committee members, Dr. Yoonsuck Choe, Dr. Bruce H. McCormick and Dr. Behbood Zoghi, for their interest in this research and their invaluable suggestions and encouragement.

I would like to thank the PRISM lab members, Dr. Alexandre Perera-Lluna, Dr. Takao Yamanaka, Agustin Gutierrez-Galvez, Steve Ortiz, Marco Zavala, and Jobany Rodrigeuz, who have made this a rather pleasurable experience. The numerous Friday meetings at Coffee Station led to several ideas that are now part of this dissertation.

I would like to thank Jody Naderi for her support and care.

I would also like to thank my friends, Swathi, Manish, Rajesh, Vidyaraman, Bharath, Priyanka, Satya, and Manas, for their encouragement and faith in me.

This acknowledgement will be incomplete without my gratitude towards my Uncle Rengarajan for his financial support and encouragement, which allowed me to pursue my graduate education. I am also indebted to my family members and relatives for their love and care.

Above all, I would like to thank my mom, Sundara, my dad, Raman, and my beloved brother, Saianand, for their absolute confidence in me, and their care and

support without which none of this would have been possible. They were, are, and will always be the source of inspiration in all my endeavors.

TABLE OF CONTENTS

LIST OF FIGURES

FIGURE   Page

LIST OF TABLES

TABLE   Page

CHAPTER I

INTRODUCTION

The sense of smell is the most primitive of the known senses. In humans, smell is often viewed as an aesthetic sense, as a sense capable of eliciting enduring thoughts and memories. For many animal species however, olfaction is the primary sense. Olfactory cues are extensively used for food foraging, trail following, mating, bonding, navigation, and detection of threats (Axel 1995). Irrespective of its purpose i.e., as a primary sense or as an aesthetic sense, there exists an astonishing similarity in the organization of the peripheral olfactory system across phyla (Hildebrand and Shepherd 1997). This suggests that the biological olfactory system may have been optimized over evolutionary time to perform the essential but complex task of recognizing odorants from their molecular features, and generating the perception of smells.

Inspired by biology, artificial systems for chemical sensing and odor measurement, popularly referred to as the 'electronic nose technology' or 'e-nose' for short, have emerged in the past two decades. An electronic nose combines an array of cross-selective chemical sensors and a pattern recognition engine to recognize odors (Persaud and Dodd 1982). The ability of these instruments to detect and discriminate volatile compounds and odorants has demonstrated their potential as a low-cost high-throughput alternative to analytical instrume[1]nts and sensory analysis.

This dissertation follows the style of Biological Cybernetics.

A number of parallels between biological and artificial olfaction are well known to the e-nose community. Two of these parallels are at the core of sensor-based machine olfaction[1] (SMBO), as stated in the seminal work of Persaud and Dodd (1982). First, biology relies on a population of olfactory receptor neurons (ORNs) that are broadly tuned to odorants. In turn, SBMO employs chemical sensor arrays with highly overlapping selectivities. Second, neural circuitry downstream the olfactory epithelium improves the signal-to-noise ratio and the specificity of the initial receptor code, enabling wider odor detection ranges than those of individual receptors. Pattern recognition of chemical sensor signals performs similar functions through preprocessing, dimensionality reduction, and classification/regression algorithms [Gutierrez-Osuna 2002].

Most of the current approaches for processing multivariate data from e-noses are the direct application of statistical and chemometric pattern recognition techniques [Gutierrez-Osuna 2002]. In this dissertation, we focus on an alternative approach: computational models inspired by information processing in the biological olfactory system. Our goal is to develop a complete pattern-recognition architecture for chemosensor arrays inspired by (our current understanding of) key signal processing mechanisms in the olfactory pathway. This neuromorphic approach to signal-processing represents a unique departure from current practices in the e-nose community, one that we expect will move us beyond multivariate chemical sensing and in the direction of

---

[1] We will refer to artificial olfaction as sensor-based machine olfaction (SBMO) or e-noses interchangeably in this document.

true machine olfaction: relating sensor/instrumental signals to the perceptual characteristics of the odorant being sensed.

I.1. The biological olfactory system

The anatomy of the human olfactory system is illustrated in Fig. 1. The entire olfactory pathway can be divided into three general stages: (1) olfactory epithelium, where primary reception takes place, (2) olfactory bulb, where an organized olfactory image is formed and, (3) olfactory cortex, where odor associations are stored (Buck 1996). These anatomically and functionally distinct relays perform a variety of signal processing tasks, resulting in the sensation that we know as an odor. Fig. 2 identifies six olfactory signal-processing primitives in the olfactory pathway (Laurent 1999, Pearce 1997):

(1)   population coding by olfactory receptor neurons (ORNs),

(2)   dimensionality reduction through chemotopic convergence of ORNs,

(3)   gain control through lateral inhibition from periglomerular (PG) cells,

(4)   contrast enhancement through lateral inhibition from granule (GR) cells,

(5)   storage and association of odor memories in the olfactory cortex, and,

(6)   mixture segmentation and background suppression through cortical feedback.
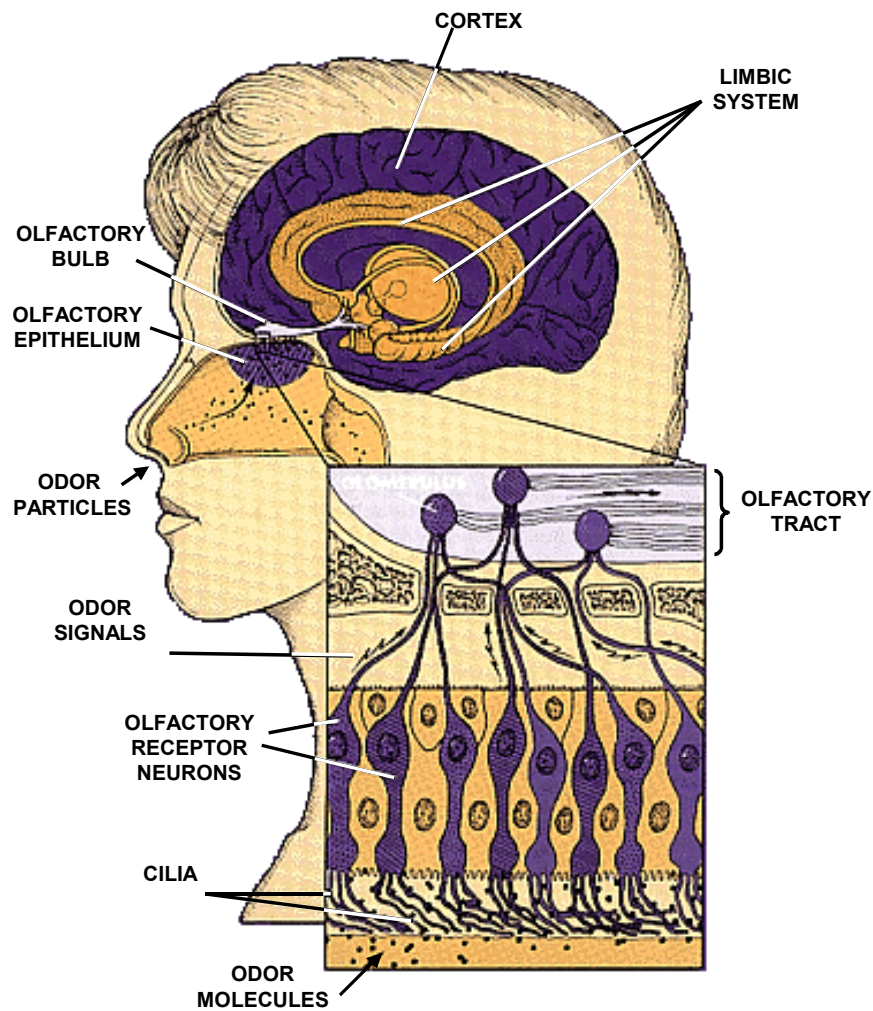
Fig. 1: Olfactory information processing[2]. Odorant molecules entering the nostrils bind to receptor neuron in the olfactory epithelium. Odor signals from the receptor neurons are then relayed to olfactory bulb where the bulk of signal processing takes place. Bulbar outputs are then passed onto olfactory cortex, where they are interpreted as different odors.

_____

[2] Adapted from: http://www.sfn.org/content/Publications/BrainBriefings/smell.html
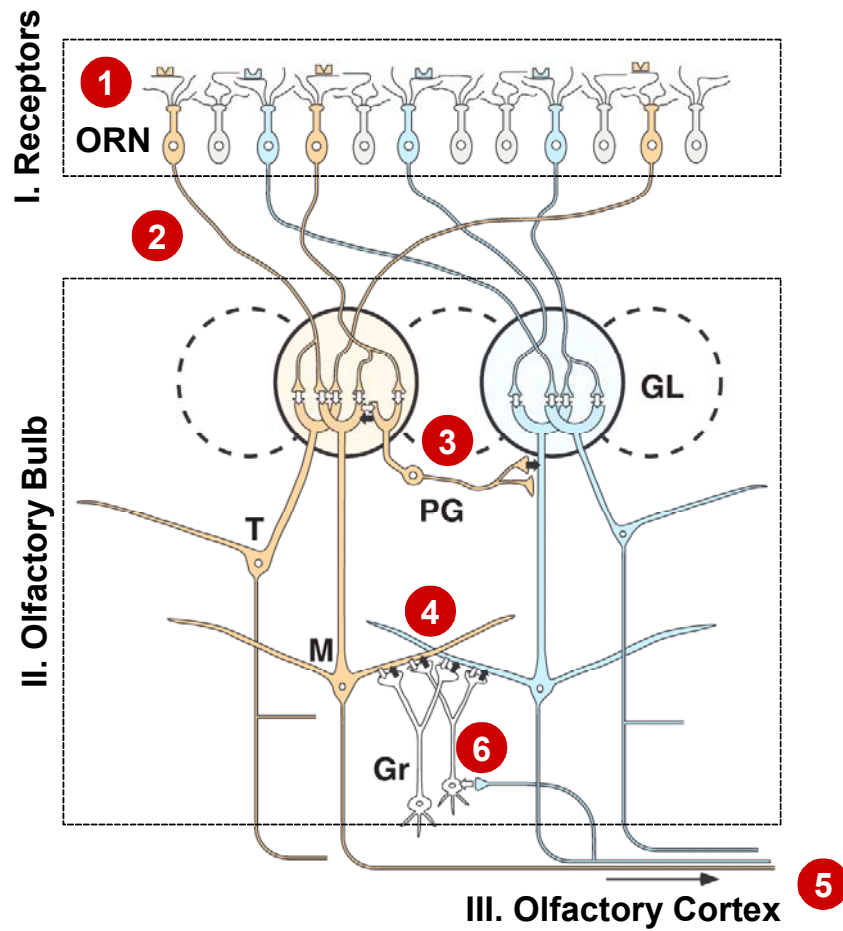
Fig. 2: Different anatomical stages and signal-processing primitives in the olfactory pathway (adapted from Mori et al. 1999): (1) population coding, (2) chemotopic convergence, (3) gain control, (4) contrast enhancement, (5) storage and association of odor memories and (6) bulbar modulation through cortical feedback.

The *first primitive* is concerned with transduction of the chemical stimulus into an electrical signal. Odorants are volatile compounds with low molecular weight (30-300 Dalton), typically organic, hydrophobic and polar (Schiffman and Pearce 2003).

Three notable theories have been proposed that relate molecular properties of an odorant with its overall quality: *vibrational, steric*, and *odotope* theories (Dyson 1938; Moncrieff 1949; Shepherd 1987). The *vibrational* theory first proposed by Dyson (1938) and later revisited by Wright (1982) and Turin (1996) (Lefingwell 2002), suggests that vibrations due to stretching and bending of odor molecules are the determinants of odor identity and quality. On the other hand, the *steric* theory initially put forth by Moncreiff (1949) and later extended by Amoore (1970) (Lefingwell 2002) proposes that odor quality is determined by the shape and size of the odorant molecules. More recently, the *odotope or weak shape theory* was proposed by Shepherd (1987). According to this theory, odor quality is determined by various molecular features of an odorant (commonly referred to as odotopes), such as carbon chain length or different functional groups.

Though the precise relationship between the molecular properties and the odorant quality is still not known; much has been recently discovered about the olfactory transduction mechanism. Odorant molecules that enter the nostrils bind to olfactory receptor neurons, which belong to a family of G-protein coupled receptors (Axel 1991). As illustrated in Fig. 3, these receptors cross the cell membrane seven times (seven-transmembrane) forming pockets where the odorants bind. The odorant-bound receptor triggers a cascade of molecular events that transform the chemical signal into a neural signal. A detailed illustration of this mechanism is shown in Fig. 4. First, tens of G-proteins are released by the activated receptor, which in turn activate the transducer Adenylyl cyclase (AC). Once activated the adenylyl cyclase converts the abundant Adenosine TriPhosphate (ATP) intracellular molecules into cyclic-3',5'-

AdenosylMonoPhosphate (cAMP) secondary messengers. The cAMP binds to the cyclic nucleotide channel (CNG) and opens it to allow Na^{2+} and Ca^{2+} cations inside. This depolarizes the cell and, if the gates are open long enough, causes it to fire an action potential (Firestein 2001).
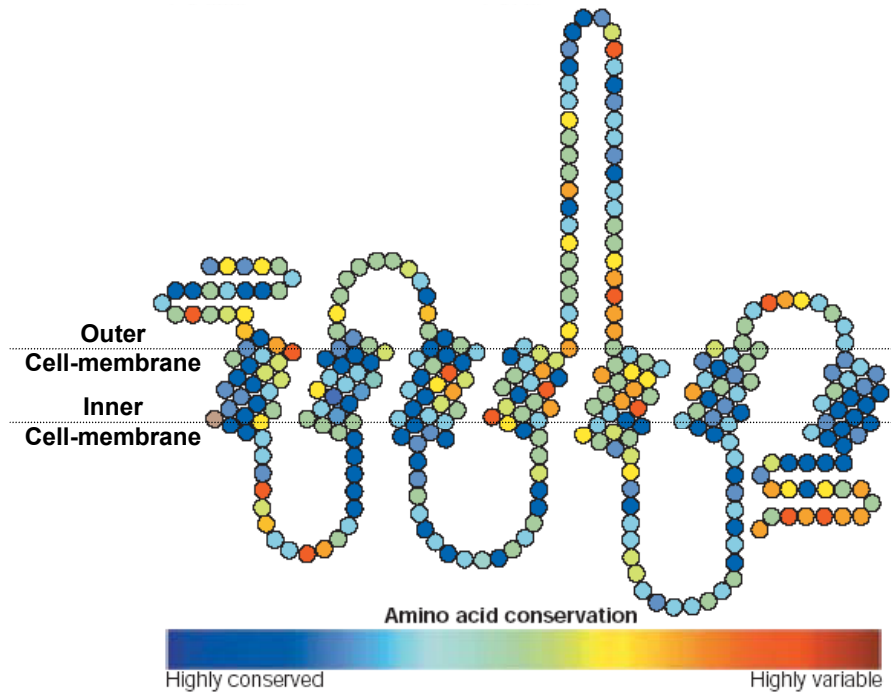
Fig. 3: G-protein coupled odorant receptors make seven loops through the cell membrane, forming pockets for holding odor molecules. Each receptor type is specified by a particular sequence of a string of amino acids. Rearranging the amino acid sequence results in a different receptor type. Approximately 1,000 different receptors have been known to exist in the case of mammals. (reprinted from Mombaerts 2004; Laurent 2005).

A complete model of the transduction (Malaka 1995) is beyond the scope of this work; let it suffice that the spiking frequency of an ORN is a monotonically increasing function of the odorant concentration for a given receptor-odorant binding affinity. Each ORN responds to a range of odorants and each odorant is encoded by a large population of such cross-selective ORNs. To illustrate the combinatorial nature of the odor code available at the olfactory epithelium, Fig. 5 shows the response of sixty different ORNs to twenty odorants (Sicard and Holey 1982). Each receptor exhibits broad tuning and responds to a number of odorants.
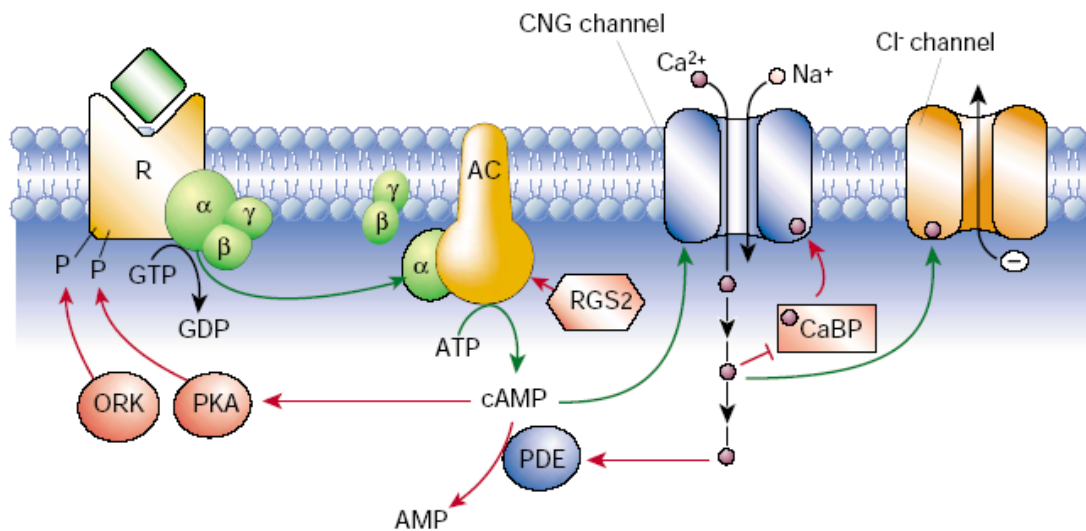
Fig. 4: Olfactory signal transduction mechanism. Binding of an odorant molecule to a receptor triggers a cascade of molecular mechanisms, finally leading to depolarization of the neuron and generation of an action potential (reprinted from Firestein 2001).
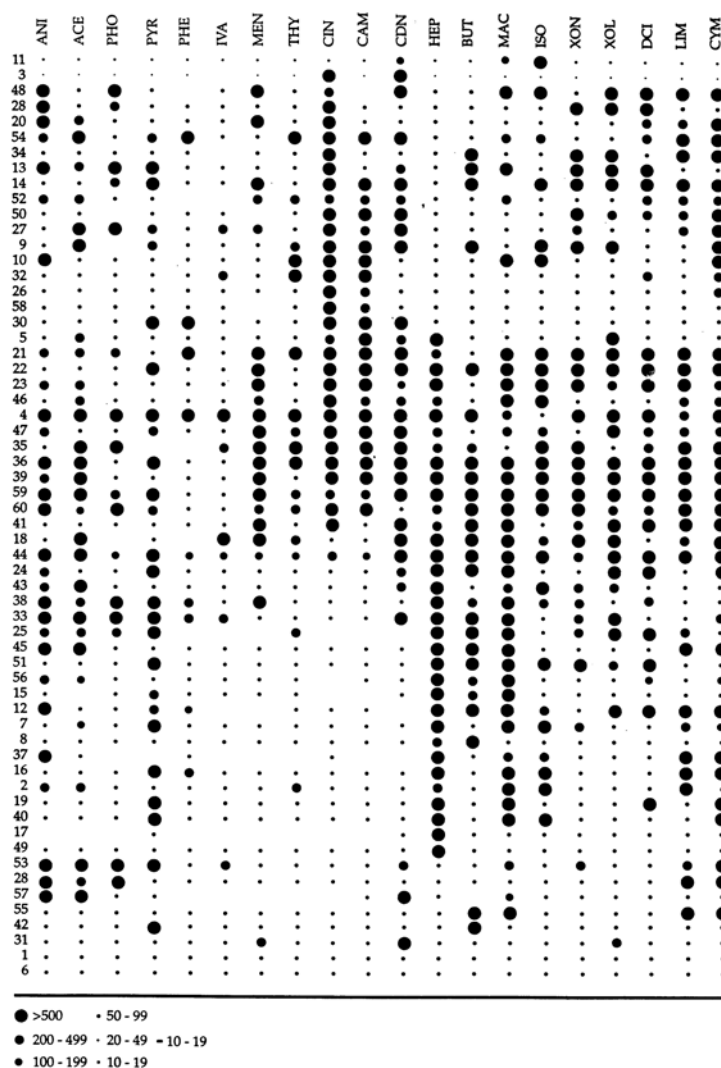
Fig. 5: Combinatorial coding by ORNs. Columns indicate odors; rows indicate receptor cells identified by a serial number given in the leftmost column. ACE – acetophenone, ANI – anisole, BUT – n-butanol, CAM – DL-camphor, CDN – cyclodecanone, CIN – 1,8-cineole, CYM – p-cymene, DCI – D-critonellol, HEP– n-heptanol, ISO – isoamylacetate, IVA – isophenol, PHO – thiophenol, PYR – pyridine, THY – thymol, XOL – cyclohexanol, XON – cyclohexanone. The spot size is roughly proportional to spike frequency (spike/min). (Reprinted from Sicard and Holey 1982).

The next three signal-processing primitives take place at the olfactory bulb (OB). The *second primitive* involves massive convergence of ORN axons onto one or a few glomeruli (GL) [Mori et al. 1999; Laurent 1999], which are spherical structures of neuropil on which ORNs synapse mitral cells. Fig. 6 shows the convergence of ORNs expressing the same P2 receptor onto a single GL in the mouse OB [Bulfone et al. 1998]. This form of convergence serves two computational functions. First, massive summation of ORN inputs averages out uncorrelated noise, allowing the system to detect odorants below the detection threshold of individual ORNs. This is discussed later in section I.3. Second, chemotopic organization leads to a more compact odorant representation than that available at the epithelium, providing the means to decouple odor quality from odor intensity. This is the basis for the traditional view of GL as labeled lines (one GL: one odor) or, more recently, as odotope detectors (one GL: one molecular feature) [Mori et al. 1999]. The GL maps of four different odors: pentanoic acid, methyl pentanoate, pentanol, and pentanal, and a single analyte (methyl pentanoate) at different concentrations are shown in Fig. 7. These maps were obtained in rat olfactory bulb using optical imaging techniques involving 2-deoxyglucose uptakes. It can be seen that the identity of the odor is encoded by a unique spatial pattern across GLs, whereas the odor concentration is related to the intensity and spread of this pattern (Johnson and Leon 2000).
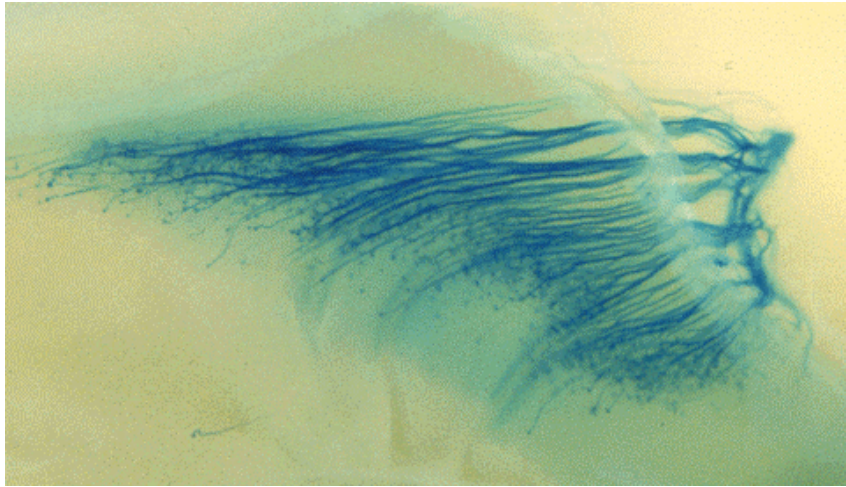
Fig. 6: Convergence of ORNs expressing P2 receptor onto a single GL in the mouse OB (Bulfone et al. 1998).

a) Glomerular maps across odors

pentanoic acid   methyl pentanoate   pentanol   pentanal
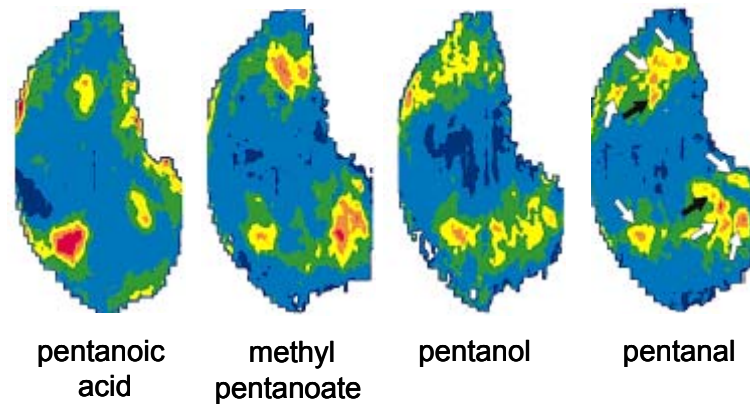
b) Glomerular maps across concentration (methyl pentanoate)
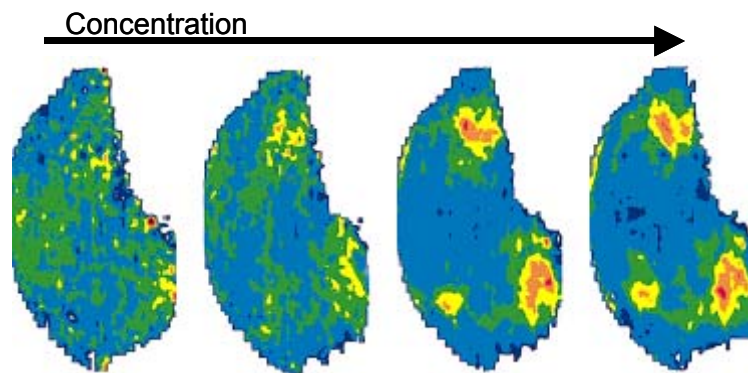
Concentration

Fig. 7: Glomerular-layer activity patterns in rat olfactory bulb: identity is encoded by a unique spatial pattern across GLs (top row); concentration is related to the intensity and spread of this pattern (bottom row) (Johnson and Leon 2000).

The initial glomerular image is further transformed in the olfactory bulb by means of two distinct lateral inhibitory circuits. The first of these circuits (*third primitive* in Fig. 2) takes place between proximal GLs through periglomerular (PG) cells. As noted by Freeman (1999), the interaction through PG cells may serve as a

"volume control" mechanism, enabling the identification of odorants over several log units of concentration. Recently, local neurons in the moth antennal lobe (analogous to PG cells in the olfactory bulb of mammals) have been found to operate as multifunctional units, causing local inhibition at lower odor concentrations and global inhibition at higher concentrations (Christensen et al. 2001). This result is particularly interesting and will be discussed later in Chapter IV.

The *fourth primitive* is represented by dendro-dendritic interactions between excitatory mitral/tufted (M/T) and inhibitory granule (GR) cells. These self and lateral inhibitory circuits form the negative feedback loops that are responsible for the observed oscillatory behavior in OB (Segev 1999). More importantly, local inhibition introduces time as an additional coding dimension by generating temporal patterning of the initial spatial code at the GL layer (Shepherd et al. 2003). The precise role of the granular lateral inhibition circuits is, however, under debate. Two hypotheses have been suggested for the role of these circuits. The first and more traditional view is that lateral inhibition sharpens the molecular tuning range of individual mitral cells with respect to that of their corresponding ORNs (Mori et al. 1999). This is illustrated in Fig. 8, where the GL unit (indicated by B) responds to a wide range of odorants (aldehydes with hydrocarbon chain length from five to nine), whereas the M cell receiving this input (indicated by D) exhibits a shaper tuning range (D responds to aldehydes with hydrocarbon chain length from six to eight) due to lateral inhibition from neighboring M cells through GR cells. Taken to the extreme, this function reduces to the Winner-Take-All strategy of competitive learning. The second hypothesis for the role of lateral

inhibition is that it leads to a "global redistribution" of activity such that the bulb-wide representation of an odorant, rather than the individual tuning ranges, becomes specific and concise over time (Laurent 1999). Fig. 9 shows the odor trajectories formed by the spatio-temporal activity of projection neurons in the honeybee antennal lobe (analogous to M cells in mammalian OB); AL activity evolves over time, moving away and settling into odor specific regions. This neuro-dynamics view of lateral inhibition is thus heavily related to temporal coding. This temporal coding mechanism will be discussed further in Chapter V.
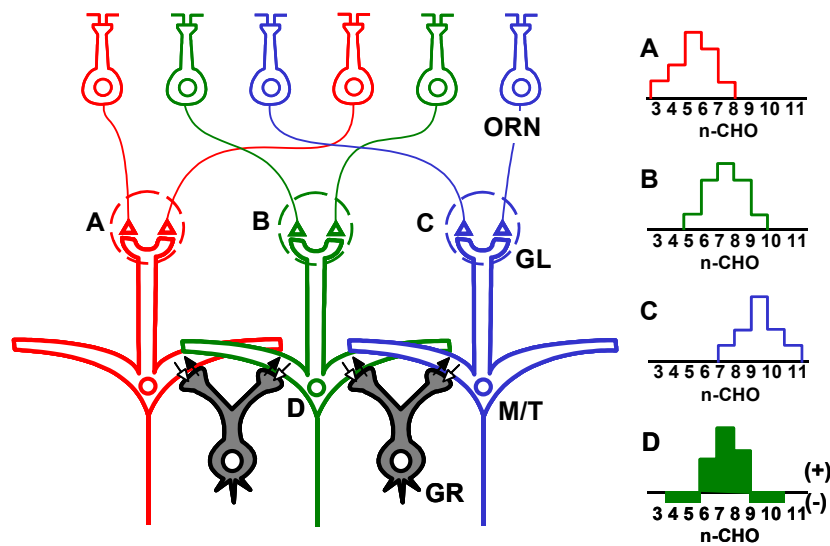
Fig. 8: Sharpening of molecular tuning range through lateral inhibition. A, B, and C are GL units that respond to aldehydes with hydrocarbon chain length from three to eight, five to ten and seven to eleven, respectively. Mitral cell D, which receives input from B, exhibits a shaper tuning range than B and responds to aldehydes with hydrocarbon chain length from six to eight due to lateral inhibition from neighboring mitral cells (adapted from Yokoi et al. 1995).
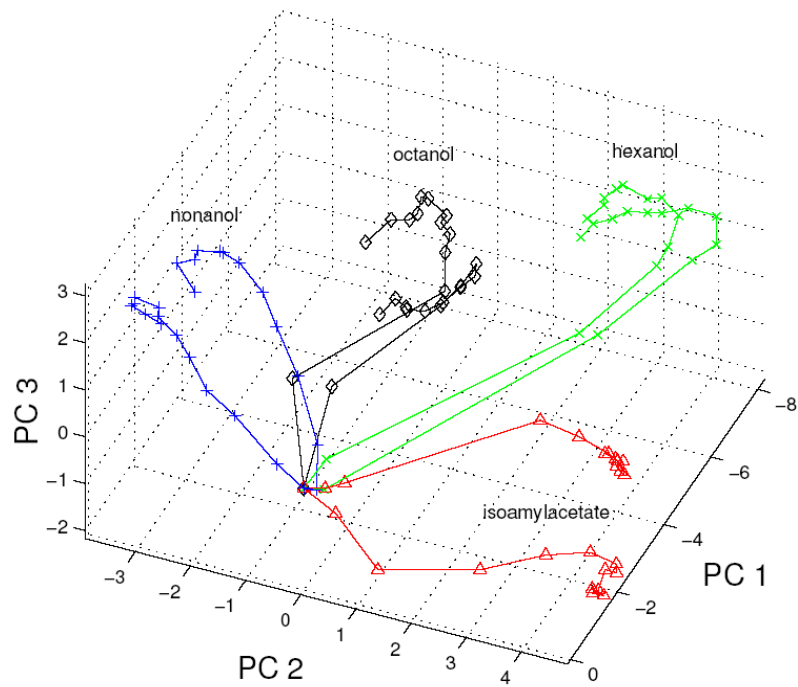
Fig. 9: Odor trajectories formed by spatio-temporal activity in the honeybee AL. The spatio-temporal response of the twenty-one PNs was projected along their first three principal components for visualization purposes. The trajectories begin close to each other, and evolve over time to converge into odor specific attractors. (reprinted from Galan et al. 2003).

The *fifth primitive* involves the formation of "odor objects" and their subsequent storage in the piriform cortex (PC). Pyramidal neurons (P), the principal cells in the PC, receive sparse, non-topographic, excitatory connections from M/T axons in the OB through the lateral olfactory tract (LOT). These projections are both convergent and divergent (many-to-many). This suggests that P cells detect combinations of co-occurring molecular features of the odorant, and therefore function as "coincidence

detectors" (Wilson and Stevenson 2003). The PC is also characterized by sparse, distributed connections between P cells. These lateral connections have been shown to play an important role in storing odors with minimum interference and pattern completion of degraded stimuli (Wilson and Bower 1988). Together, these two anatomical features of the PC (many-to-many connection from OB and lateral association connections between P cells) form the basis for the synthetic processing of odors (Wilson and Stevenson 2003).

The *sixth primitive* involves centrifugal connections from the cortex onto GR interneurons in the olfactory bulb. Several computational functions have been associated with these feedback connections, including odor segmentation and habituation (Li and Hertz 2000), hierarchical clustering (Ambrose-Ingerson et al. 1990), and chaotic bulbar dynamics (Yao and Freeman 1990).

We have presented a review of our current understanding of information processing strategies in the biological olfactory system. Next, we present an overview of current sensing technologies and pattern recognition approaches in e-noses.

I.2. The electronic nose

An electronic nose is an instrument that combines an array of cross-selective chemical sensors and a pattern recognition engine to recognize odors (Persaud and Dodd 1982). The processing of multivariate sensor responses is usually performed by means of statistical pattern recognition (Gutierrez-Osuna 2002), as illustrated in Fig. 10 (Nagle et al. 1998).
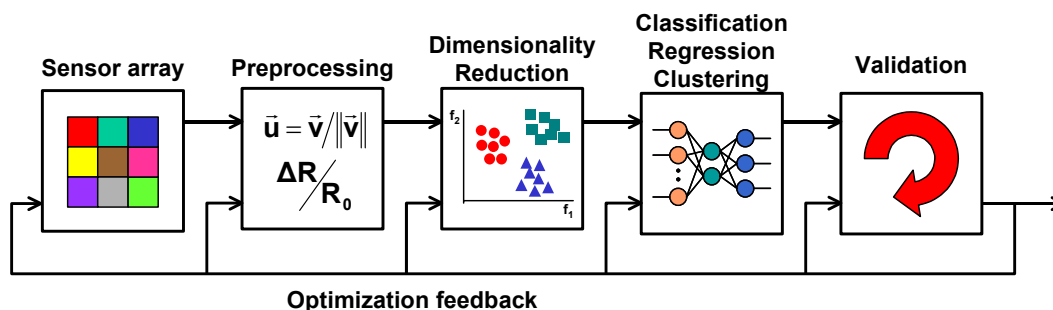
Fig. 10: Building blocks of sensor-based machine olfaction architecture: (i) sensor array, (ii) signal preprocessing, (iii) dimensionality reduction, (iv) classification, and (v) validation (reprinted from Gutierrez-Osuna 2002).

I.2.1. Review of sensor technologies

A number of sensor technologies have been employed for the purpose of detecting and identifying chemicals, including metal-oxide (MOS) and conducting polymer (CP) chemoresistors, quartz microbalance (QMB) resonators, surface acoustic waves (SAW) devices, and optical-fiber based devices. Fig. 11 provides an illustration of the underlying principles used by these different types of sensors.

MOS sensors detect odorants through changes in conductance of the sensing material due to oxidation/reduction reactions caused by the odorant (Nagle et al. 1998). In the case of CP sensors, the odorants interact with the polymer (usually polypyrole, polythiophene or polyaniline) by directly accepting ions from the polymer chain, interacting with the dopant ions (e.g., chloride ions) or diffusing into the polymer lattice causing it to swell (Nagle et al. 1998; Yinon 2003). These interactions change the conductivity of the material, which is read out as the sensor signal (Nagle et al. 1998).
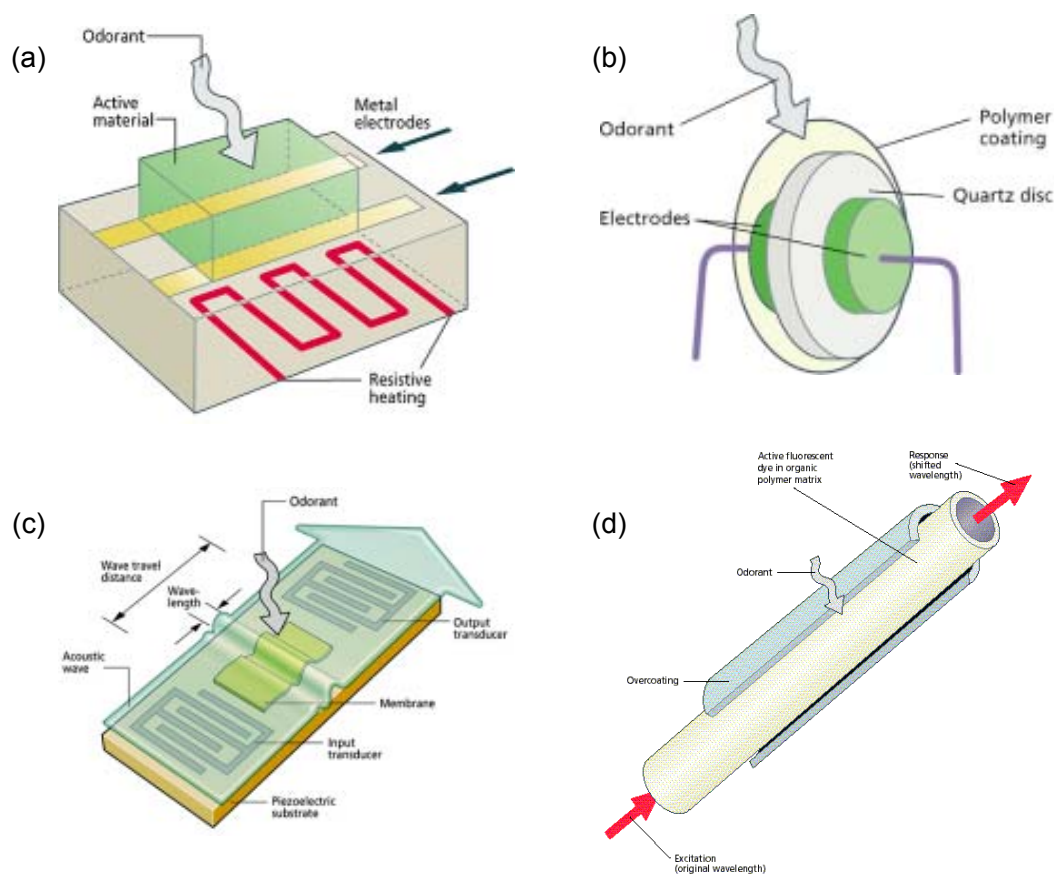
Fig. 11: Chemical sensing technologies: (a) Metal-oxide sensors (MOS)/ Conducting Polymer (CP) chemoresistors; (b) Quartz crystal microbalance (QCM) resonators; (c) Surface Acoustic Waves (SAW) devices; (d) Optical fiber sensors (Nagle et al. 1998).

QCM and SAW sensors employ a completely different sensing principle for detecting odorants compared to MOS and CP sensors. In the case of QCM, odorants adsorb to the surface of a piezoelectric quartz crystal, altering its mass and therefore shifting its resonant frequency (Nagle et al. 1998). On the other hand, in SAW sensors, an A.C voltage is applied to the input electrode, generating an acoustic wave that propagates through the surface of the piezoelectric material. Odorants adsorb to the

active material in the propagation path, which alters the surface characteristics and affects the velocity of the acoustic wave. The change in the velocity, measured by monitoring the phase shifts of the signal at the output electrode, becomes the sensor response (Nagle et al. 1998).

In the case of optical fiber sensors, fluorescent dyes are immobilized in the polymer matrices placed on one end of the fibers. Exposure to odorants alters the micro-environmental polarity of the dyes in the polymer matrices. The dyes respond with a corresponding shift in their fluorescent spectrum, which becomes the sensor response (Dickinson et al. 1996). The reader is referred to (Nagle et al. 1998) for an introductory review of odor sensing technologies. The transduction principles for MOS sensor and optical fiber sensors, which are used in this dissertation, will be discussed in detail in Chapter II.

I.2.2. Review of pattern recognition for chemical sensor arrays

The multivariate sensor array response is then regarded as a fingerprint of the stimulus. These raw signals are first preprocessed to accomplish several functions, such as drift compensation, feature extraction and reduction of sample-to-sample variance (Nagle et al. 1998). Preprocessing is followed by a dimensionality reduction stage. Linear techniques such as principal component analysis (PCA) and linear discriminant analysis (LDA), non-linear techniques such as Kohonen self-organizing maps (SOM) and several feature selection approaches have been widely used for this purpose (Nagle et al. 1998; Pearce 1997). These lower-dimensional odor signals are then passed to a pattern

classification algorithm to predict the identity of the stimulus from among a finite set of previously learned classes.

A number of pattern classifiers have been used with gas sensor arrays. Fig. 12 shows a summary of statistical methods that have been used for pattern analysis with gas sensor arrays. Readers are referred to (Schiffman and Pearce 2003; Gutierrez-Osuna 2002) for a thorough review of these methods. These statistical techniques have been used extensively for handling generic pattern recognition tasks such as dimensionality reduction, 1-of-m classification, and clustering (Pearce 1997; Gutierrez-Osuna 1998 and references therein). Problems unique to chemical sensors such as estimating chemical concentrations in a mixture (Ortega et al. 2000; Sundic et al. 2003), canceling background odors (Gutierrez-Osuna and Powar 2003), handling odor mixtures (Capone et al. 2001; Yamanaka 2004), drift compensation (Gutierrez-Osuna 2000; Holmberg and Arthursson 2002), event detection (Perera et al. 2003) and prediction of sensory scores (Gutierrez-Osuna 2002) have also been tackled using these methods. The last problem, that of predicting organoleptic properties of odorants from their response on a sensor array, is arguably the ultimate challenge of machine olfaction, but also the least successful to date.
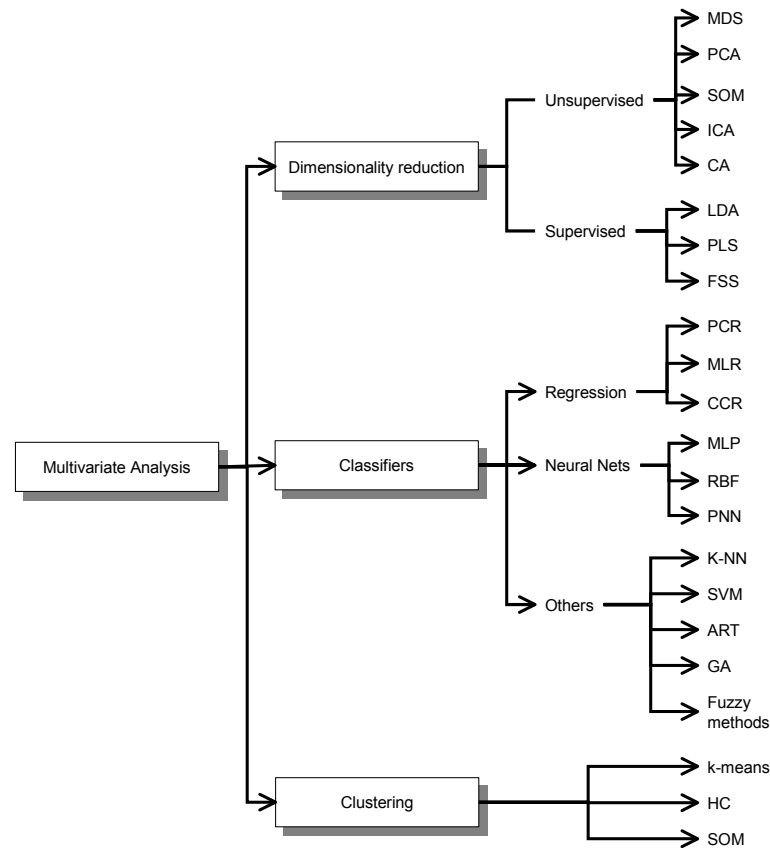
Fig. 12: Statistical methods for multivariate pattern analysis techniques applied with gas sensor arrays (Schiffman and Pearce 2003; Gutierrez-Osuna 2000, 2002; DeCoste et al. 2001). MDS- Multi-dimensional scaling, PCA- Principal Component Analysis, SOM- Self-Organized Maps, ICA- Independent Component Analysis, CA- Cluster Analysis, LDA- Linear Discriminant Analysis, PLS- Partial Least Squares, FSS- Feature Selection Search, PCR- Principal Component Regression, MLR- Multi Linear Regression, CCR- Canonical Correlation Regression, MLP- Multi-Layer Perceptron, RBF- Radial Basis Functions, PNN- Probabilistic Neural Network, k-NN- k-Nearest Neighbors, SVM- Support Vector Machines, ART- Adaptive Resonance Theory, GA- Genetic Algorithms, and HC- Hierarchical Clustering.

I.3. Neuromorphic processing for chemical sensor arrays

Leveraging a growing body of knowledge from computational neuroscience (Davies and Eichenbaum 1991), neuromorphic models of the olfactory system have become a recent subject of attention for the purpose of processing data from chemical sensor arrays.

Ratton et al. (1997) have employed the olfactory model of Ambros-Ingerson et al. (1990), which simulates the closed-loop interactions between the olfactory bulb and higher cortical areas. The model performs a hierarchical processing of an input stimulus into increasingly finer descriptions by repetitive projection of bulbar activity to (and feedback from) the olfactory cortex.   Ratton et al. (1997) have applied the model to classify data from a micro-hotplate metal oxide sensor excited with a saw-tooth temperature profile. Sensor data was converted into a binary representation by means of thermometer and Gray coding, which was then used to simulate the spatial activity at the olfactory bulb.   Their results show that classical approaches (Gram-Schmidt orthogonalization, fast Fourier transform and Haar wavelets) yield better classification performance. This result should come as no surprise given that the thermometer and Gray codes are unable to faithfully simulate the spatial activity at the olfactory bulb, where the most critical representation of an odor stimulus is formed.

White et al. (1998, 1999) have employed a spiking neuron model of the peripheral olfactory system to process signals from fiber-optic sensor array. In their model, the response of each sensor is converted into a pattern of spikes across a population of ORNs, which then projects to a unique mitral cell. Different odors produce unique spatio-temporal activation patterns across mitral cells, which are then

discriminated with a delay line neural network (DLNN). Their OB-DLNN model is able to produce a decoupled odor code: odor quality being encoded by the spatial activity across units, and odor intensity by the response latency of the units.

Pearce et al. (2001) have investigated the issue of concentration hyperacuity by means of massive convergence of ORNs onto GL. Modeling spike trains of individual ORNs as Poisson processes, the authors show that an enhancement in sensitivity of $\sqrt{n}$ can be achieved at the GL, where n is the number of convergent ORNs. Experimental results on an array of optical micro-beads are presented to validate the theoretical predictions.

Otto et al. (2000) have employed the KIII model of Freeman et al. (1998) to process data from FT-IR spectra (Quarder et al. 2001; Claussnitzer et al. 2001) and chemical sensors (Otto et al. 2000). The KIII is a neurodynamics model that faithfully captures the spatio-temporal activity in the olfactory bulb, as observed in electro-encephalogram (EEG) recordings. In (Quarder et al. 2001), the FT-IR spectrum of each analyte was decimated, Hadamard-transformed and normalized before being used as an input vector into the KIII model. The authors show that the principal components of the mitral cell state-space attractors can be used to discriminate different analytes. Their results, however, indicate that the KIII is unable to match the performance of a Regularized Discriminant Analysis classifier.

Gill and Pearce (2003) have used an array of optical micro-bead sensors to investigate the issues of development, organization and maintenance of connections in the early olfactory pathway. Two populations of micro-bead sensors: active (exposed to

various odorants) and inactive (exposed only to air) were used to simulate the distribution of ORNs in the olfactory epithelium. Oja's Hebbian learning rule was used to develop activity-dependent weights between the sensor (receptor) layer and the GL layer; a Mexican hat function was used to model the lateral interactions between GLs mediated by PG cells. Similar to experimental findings on mice (Zheng et al. 2000), their results show segregation of the active and inactive ORN populations into separate GLs suggesting the influence of odorant-evoked activity in the organization and maintenance of OB connections. Further their results suggest that the lateral interaction between GLs through PG cells play an important role in realizing the topological organization of the ORN projections. However, this predicted role of PG cells has not been confirmed through experimental studies.

Gutierrez-Osuna et al. (2003a, 2003b) has investigated the use of habituation for processing odor mixtures with chemical sensor arrays. A statistical pattern recognition model was presented in (Gutierrez-Osuna and Powar 2003), where habituation is triggered by a global cortical feedback signal, in a manner akin to Li and Hertz (2000). A neuromorphic approach based on the KIII model was proposed in (Gutierrez-Osuna and Gutierrez-Galvez 2003), where habituation is simulated by local synaptic depression of mitral channels. Inspired by the role of GL as functional units (Pearce 1997), sensor array patterns are preprocessed with a family of odor selective discriminant functions before being fed to the KIII model. Their results showed that the KIII model is able to recover the majority of the errors, introduced in the sensor-array and discriminant-function stages, by means of its Hebbian pattern-completion capabilities.

With the exception of prior work in our group, the use of neuromorphic models has focused on 1-of-m classification (Ratton et al. 1997; Otto et al. 2000; White et al. 1998) and sensitivity enhancement (Pearce et al. 2001). Problems of dimensionality reduction, gain control and intensity/quality coding have not been investigated using neuromorphic approaches. In this dissertation, we address this issue and propose neuromorphic solutions to these problems.

I.4. Proposed work: Biologically-inspired computational models for machine olfaction

Based on the computational view of the olfactory pathway presented in section I.1, this dissertation proposes a biologically-inspired architecture for the processing of gas sensor array signals. Shown in Fig. 13, the architecture consists of six building blocks, modeled after the six signal processing primitives identified in the olfactory pathway. First, a high dimensional odor signal is generated from the sensor arrays using a variety of methods that will be discussed in Chapter II. This high dimensional odor signal undergoes dimensionality reduction through chemotopic convergence, producing an odor image that decouples odor identity from intensity. The odor images formed through convergence are highly overlapping, and are subsequently processed by two lateral inhibitory circuits. The first circuit performs gain control, enabling identification of the odorant across a wide range of concentration. The second lateral inhibitory circuit enhances the initial contrast between odor images. The sharpened odor image is stored in a content addressable memory (CAM). Finally, interaction between the CAM and the

contrast enhancement circuits performs mixture segmentation and background suppression.

In the following chapters we will propose computational models of these six signal-processing primitives, which are all novel to machine olfaction. We will validate these models on experimental datasets generated using sensor arrays employing MOS and optical fiber sensors and Infrared absorption spectroscopy.
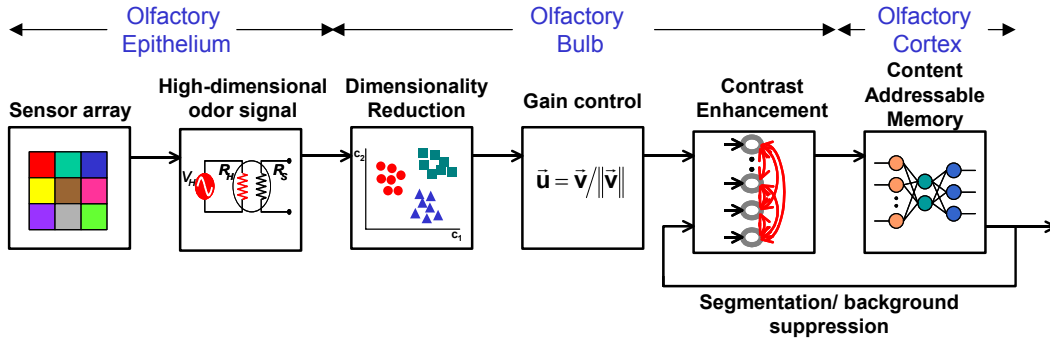
Fig. 13: Building blocks for biologically-inspired pattern recognition in sensor-based machine olfaction. The six stages correspond to the six signal processing primitives identified in the olfactory pathway (refer to Fig. 2).

I.5. Contributions of this work

The principal contributions of this dissertation research can be summarized as follows:

(1) We have developed computational models of key signal processing primitives in the olfactory system, and integrated them in a neuromorphic architecture suitable for machine olfaction with gas sensor arrays.

(2) We have characterized the proposed models and validated them on experimental datasets from temperature-modulated metal oxide chemoresistors and a large population of optical microbead sensors.

(3) We have conducted a preliminary investigation to examine the relationships between molecular features of odorants detected by their infrared absorption spectra, and their olfactory bulb images, and their overall smell descriptors.

I.6. Organization of this document

The rest of this dissertation is organized as follows: Chapter II describes three separate methods that can be used to generate a high-dimensional, combinatorial input signal from gas sensor arrays. Chapter III presents a computational model of receptor neuron convergence that generates compact odorant representations similar to those observed in the olfactory bulb. Chapter IV presents a model of shunting lateral inhibition that removes concentration effects from the multivariate response of a gas sensor array. Chapter V presents an additive model of lateral inhibition with center-surround connections that improves contrast between odor images formed after chemotopic convergence. Chapter VI presents a model of bulbar-cortical interactions capable of achieving background suppression and mixture segmentation. Chapter VII integrates the six primitives to create a unified neuromorphic signal processing architecture for machine olfaction. Chapter VIII presents a summary of results and identifies directions for future research.

Supplementary materials are provided as three separate appendices. Appendix A includes a table with the range of IR absorption spectra for different functional groups;

this reference material is useful for illustrating the IR principle in Chapter II. Appendix B presents a computational model for olfactory receptors that can be used to generate high-dimensional signals from the low-dimensional feature spaces typically obtained with e-nose instruments. Appendix C presents a spiking model of the OB; this model shows that the proposed primitives are not tied to any particular neural network model (e.g., spiking vs. rate model).

CHAPTER II

HIGH-DIMENSIONAL ODOR CODING WITH PSEUDO-SENSORS

The first stage in the olfactory pathway consists of a large array (~10-100 million) of sensory neurons, each of which selectively expresses one or a few genes from a large (~1,000) family of receptor proteins (Buck and Axel, 1991). Each receptor is capable of detecting multiple odorants, and each odorant can be detected by multiple receptors, leading to a massively combinatorial olfactory code at the receptor level. It has been shown (Alkasab et al. 2002; Zhang and Sejnowski 1999) that this broad tuning of receptors may be an advantageous strategy for sensory systems dealing with a very large detection space. This is certainly the case for the human olfactory system, which has been estimated to discriminate up to 10,000 different odorants (Schiffman and Pearce, 2003). Further, the massively redundant representation improves signal-to-noise ratio, providing increased sensitivity in the subsequent processing layers (Pearce et al. 2002).

Unlike the biological olfactory system, the artificial system uses very few sensors, commonly one replica of up to 32-64 different sensor types. This fundamental mismatch between the two systems in their input dimensionality must be overcome in order to be able to exploit the processing strategies employed by the biological olfactory system. In order to generate a combinatorial and high dimensional odor representation from chemical sensor arrays, similar to that available in the olfactory epithelium, we will adopt the following three mechanisms:

- Temperature modulation in metal-oxide sensors,

- Sensing with a large population of optical microbead arrays, and

- Infrared absorption spectroscopy.

The objective of this chapter is to present and analyze each one of these dimensionality expansion techniques.

II.1. MOS sensor array

The first method to simulate a large population of cross-selective sensors involves temperature modulation of metal oxide (MOS) chemoresistors. The various components of a MOS sensor are shown in Fig. 14. The sensing material is a metal oxide (tin, zinc, titanium, or iridium) coated with a noble metal catalyst (palladium or platinum) (Nagle et al. 1998). The active material is placed on a substrate made of silicon, glass or plastic, and heated by applying a voltage to a resistive heating built into the device. When the heated active material comes in contact with the odorant, it undergoes reduction/oxidation chemical reaction depending on the nature of the environment. In an oxidizing atmosphere, oxygen ions resulting from the decomposition of oxygen molecules in the ambient, or other electron acceptors adsorb to the surface of the material and trap free electrons from the conduction band of the semiconductor as shown in Fig. 15(a). This results in a decrease in the conductance of the sensing material. In a reducing atmosphere, on the other hand, the adsorbed oxygen atoms react with the reducing ambient molecules, releasing the trapped electrons to the sensing material as shown in Fig. 15(b). This results in an increase in the conductance of the sensing

material. The change in conductivity of the active material is measured by observing the

change in resistance across the electrode pair below the active material.
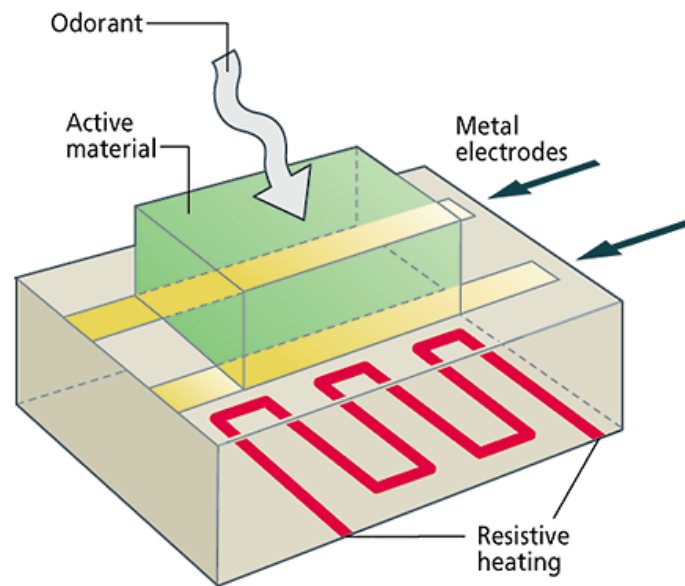
Fig. 14: General structure of a metal-oxide semiconductor chemoresistor (Nagle et al.

1998).

(a)

O_2 SnO$_2$ grains O_2

O_2

$O_2 + e^- \rightarrow O_2^-$
$\frac{1}{2}O_2 + e^- \rightarrow O^-$
$\frac{1}{2}O_2 + 2e^- \rightarrow O^{2-}$

eVs in air

electrons

(b)

CO O_2 CO O_2

CO

O_2

$O_2^- + CO \rightarrow CO_2 + e^-$
$O^- + CO \rightarrow CO_2 + e^-$
$O^{2-} + CO \rightarrow CO_2 + 2e^-$

eVs in the presence of reducing gas

Fig. 15: (a) Atmospheric oxygen adsorbed on the surface of the metal oxide trap free electrons from the conduction band of the semiconductor. This causes a potential barrier (eVs), which prevents electrons from moving freely, reducing the sensor conductance. (b) In the presence of reducing gas, the adsorbed oxygen atoms react with the reducing ambient molecules, releasing the trapped electrons. The potential barrier (eVs) decreases allowing electrons to move freely increasing the sensor conductance. (adapted from Figaro 1996).

II.1.1. Temperature modulation

In the case of MOS materials, the relative selectivity to different volatiles is known to be a function of the operating temperature at the surface of the material (Lee and Reddy 1999). This operating temperature is typically maintained at a constant set-point (specified by the manufacturer). This form of excitation is commonly referred to as *isothermal* operation. However, due to the temperature-selectivity dependence of MOS devices, more information can be extracted from the sensor by simply modulating the heater voltage during exposure to a volatile and capturing the dynamic response of the sensor at each heater voltage. The process is illustrated in Fig. 16. A sinusoidal voltage is applied to the sensor's heater, and the dynamic response of the sensing element is recorded simultaneously. If the heater voltage is modulated slowly enough relative to the thermal time constants of the device, the response of the sensor at each heater voltage can be considered a separate "pseudo-sensor", and used to simulate a large population of ORNs.
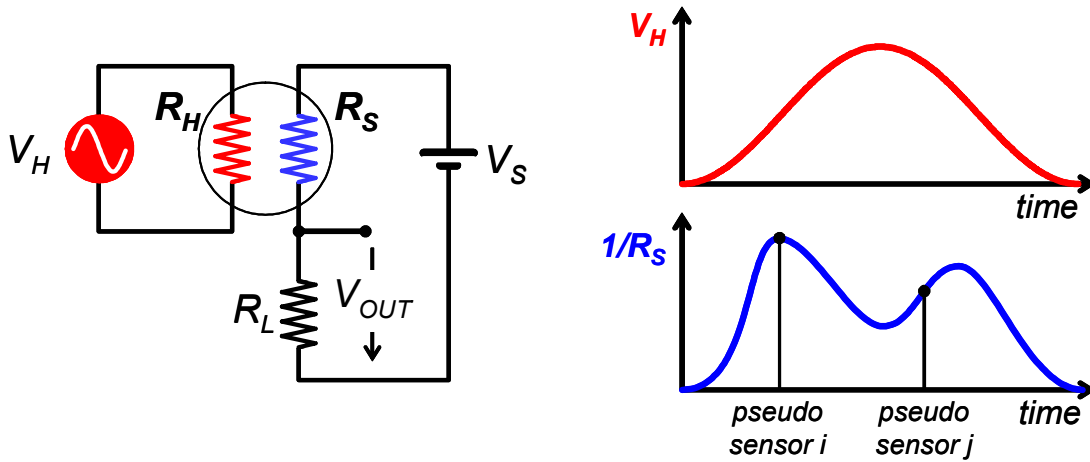
Fig. 16: Temperature modulation for metal-oxide sensors. A sinusoidal voltage V_H is applied to a resistive heather R_H, and the sensor resistance R_S is measured as a voltage drop across a load resistor R_L on a half-bridge. Due to the temperature-selectivity dependence, the response of a sensor at a particular temperature can be treated as a separate "pseudo-sensor," and used to simulate a large population of ORNs.

II.1.2. Selectivity data set (Powar 2002)

In order to generate a high-dimensional sensor response to overcome the dimensionality mismatch between the artificial olfactory system and its biological counterpart and validate the models presented in the following chapters, we perform temperature modulation of two Figaro MOS sensors (TGS 2600, TGS 2620) (Figaro 1996). A sinusoidal heater voltage (1-7 V range) with a 150 seconds time period, shown in Fig. 17, is used for this purpose. The sensor response is sampled at 10 Hz, leading to a population of 1500 pseudo-sensors from each sensor. The sensor array is exposed to the static headspace of mixtures from three analytes: acetone (*A*), isopropyl alcohol (*B*) and

ammonia (*C*), at three dilution levels in distilled water (the neutral). The lowest dilution of the analytes is 0.3 v/v% for acetone, 1.0 v/v% for isopropyl alcohol and 33 v/v% for ammonia. These baseline dilutions were chosen so that the average isothermal response (i.e., a constant heater voltage of 5V) across the two sensors was similar for the three analytes, thus ensuring that they could not be trivially discriminated (Gutierrez-Osuna and Raman 2004). Two serial dilutions by a factor of 1/3 were also acquired, resulting in 21 samples per day (4 mixtures × 3 concentrations). The process was repeated on three separate days, for a total of 63 samples. The temperature-modulated response of the two sensors to the three concentrations of the single analytes is shown in Fig. 18. Each analyte leads to a unique pattern, defined by the amplitude and location of a maximum in conductance. Two maxima are easily resolved in the case of isopropyl alcohol.
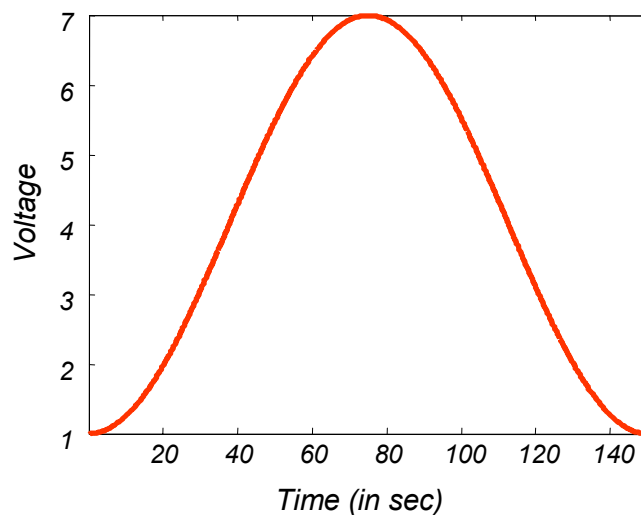
Fig. 17: Sinusoidal heater voltage profile used for modulating the operating temperature of the MOS sensors.
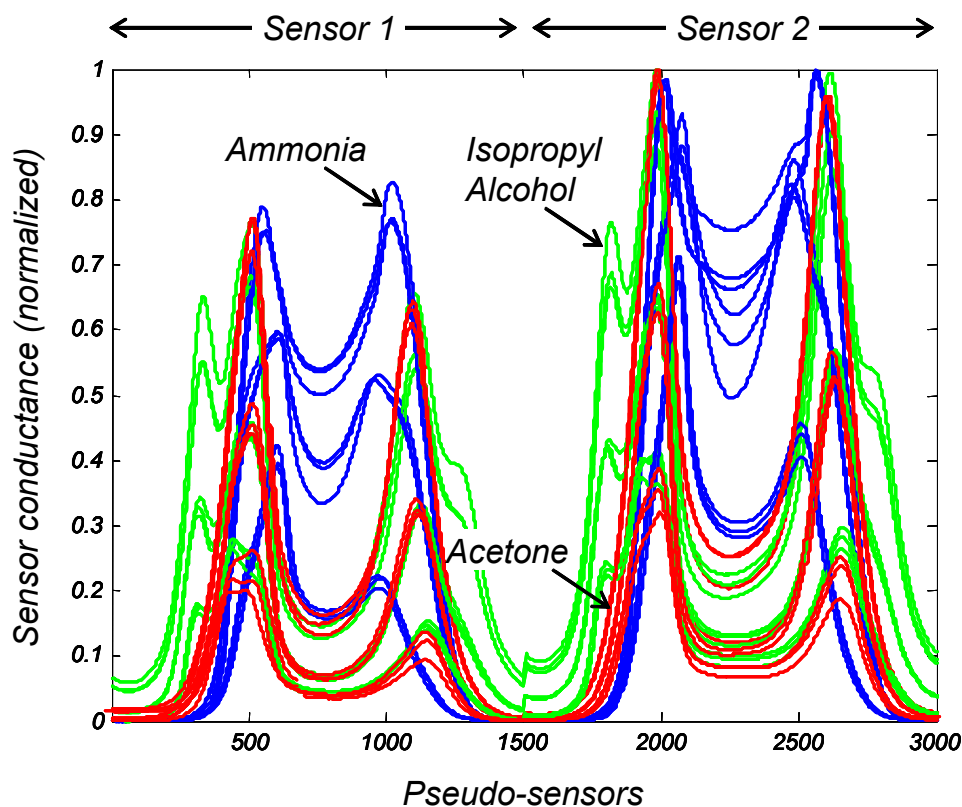
Fig. 18: Temperature-modulated response of two MOS sensors (concatenated) to acetone (odor A), isopropyl alcohol (odor B) and ammonia (odor C) at three concentrations. Three replicates per analyte and concentration are shown in the figure to illustrate the repeatability of the patterns.

The temperature-modulated response of one MOS sensors to binary and ternary mixtures at the highest concentration is shown in Fig. 19. It can be seen that the sensor responses show some degree of additivity with respect to the single analyte responses, particularly in the case of binary mixtures. We will show later that this type of additivity in the sensor response is necessary for segmenting mixtures into their constituents.
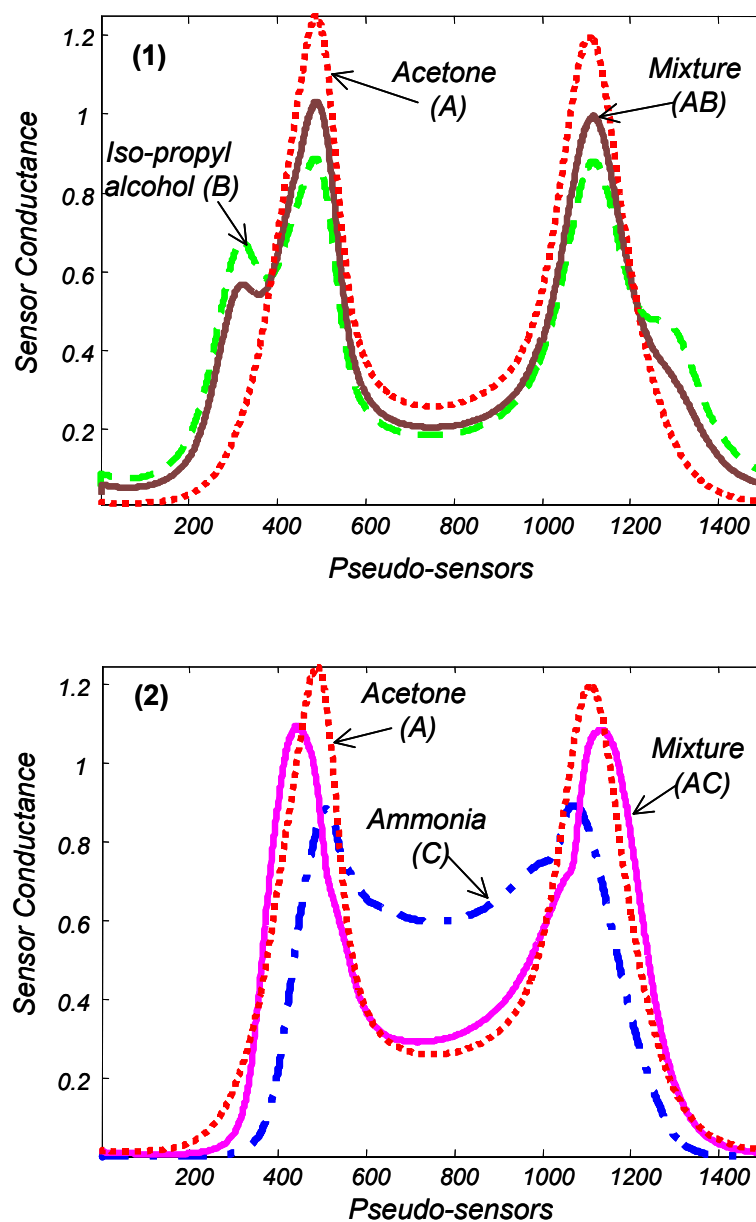
Fig. 19: Temperature-modulated response of a TGS 2620 MOS sensor to three pure analytes and their binary mixtures: (1) acetone (A), isopropyl alcohol (B) and their binary mixture (AB); (2) acetone (A), ammonia (C) and their binary mixture (AC); (3) isopropyl alcohol (B), ammonia (C) and their binary mixture (BC); (4)acetone (A), isopropyl alcohol (B), ammonia (C) and their ternary mixture (ABC).

38
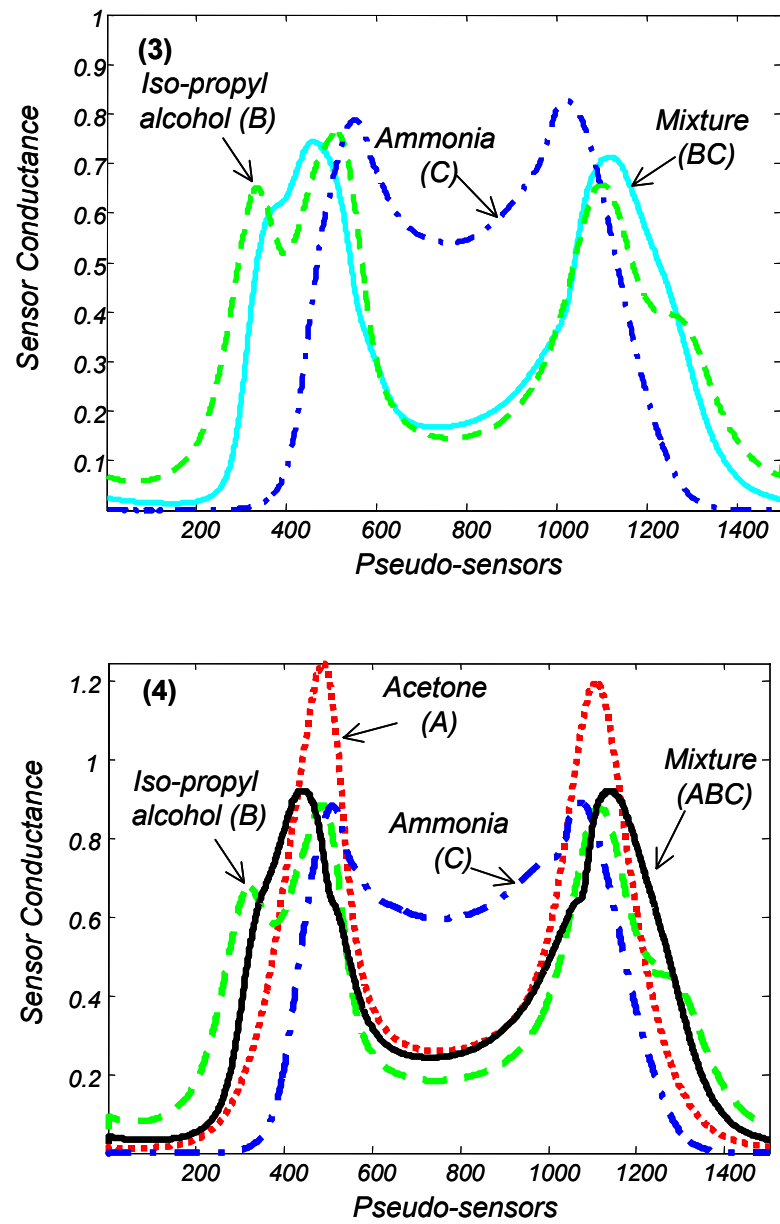
(Fig. 19: continued)

II.2. Optical microbead array

Walt and colleagues at Tufts University have proposed a novel method for chemical sensing based on optical microbead sensors. The microbead arrays typically include hundreds of broadly-tuned bead sensors, each belonging to a discrete class, randomly dispersed across the tip of an optical fiber (Dickinson et al. 1999). The high-dimensional, combinatorial response generate by the microbead arrays to odorants makes them an attractive alternative for use with neuromorphic models.

II.2.1. Microbead transduction principle

The basic transduction mechanism of microarray bead sensor arrays is as follows. Each microbead is coated with a polymer matrix onto which a salvotochromic dye (e.g. Nile red) is immobilized. The microbead is then placed on the distal end of an individual optical fibers, as shown in Fig. 20(inset A). The salvotochromic dyes change their color based on the polarity of the microenvironment, i.e. polymer surface polarity or odor exposure. Immobilizing these salvotochromic dyes in polymer matrices that vary in polarity, hydrophobicity, porosity, elasticity, and swelling tendency, creates unique sensing regions that interact differently with odor molecules, giving unique response to various odors (Dickinson et al. 1996).

Fig. 20 shows the basic odor sensing process using the microbead sensor arrays. Odor vapor diffuses into the polymer coated on the distal end of the fiber and modifies the microenvironment polarity. This causes the dyes to change their fluorescence intensity, which is captured with a CCD camera and plotted over time.
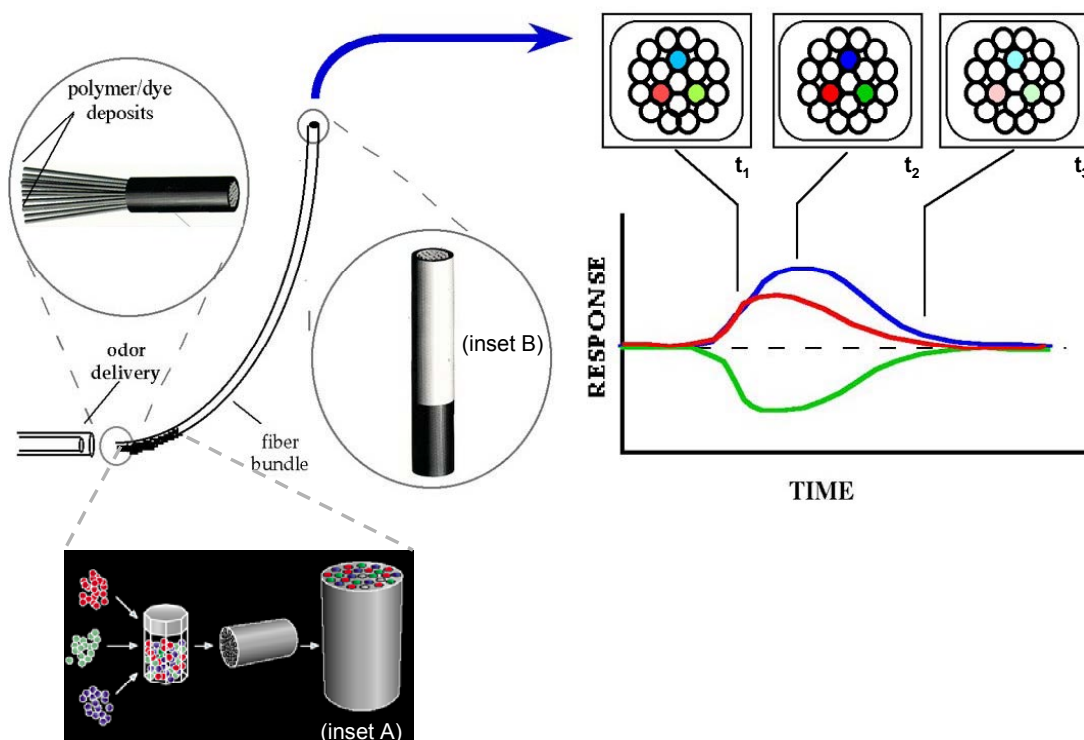
Fig. 20: Odor sensing using microbead arrays: Odor vapor is delivered to the distal end of the fiber. Exposure to odor vapor induces a change in fluorescence that is recorded and plotted versus time. (inset A) microspheres coated with a polymer matrix, onto which a salvotochromic dye (e.g. Nile red) is immobilized, randomly fill the distal end of the fiber. (inset B) distal end of the optical fiber from which the response is read (adapted from Dickinson et al. 1996).

II.2.2. Illumina data set

We will use a database from Illumina. Inc[3], comprising of transient responses of 586 microbead sensors to five analytes: Acetone (A), Ethyl Alcohol (EA), Ethyl hydroxide (EtOH), Methyl hydoxide (MeOH), and Toulene. Fig. 21 shows the transient response of 100 microbead sensors to acetone. The odorant was introduced at t=14 sec and removed at t=35 sec. The response of each sensor to the odorant is obtained by computing the difference between its steady state response (t=34 s) and baseline value (t=13 s).

---

[3] Data from Illumina microbead arrays, which are not commercially available, will be obtained through an existing collaboration between Illumina and our research group.
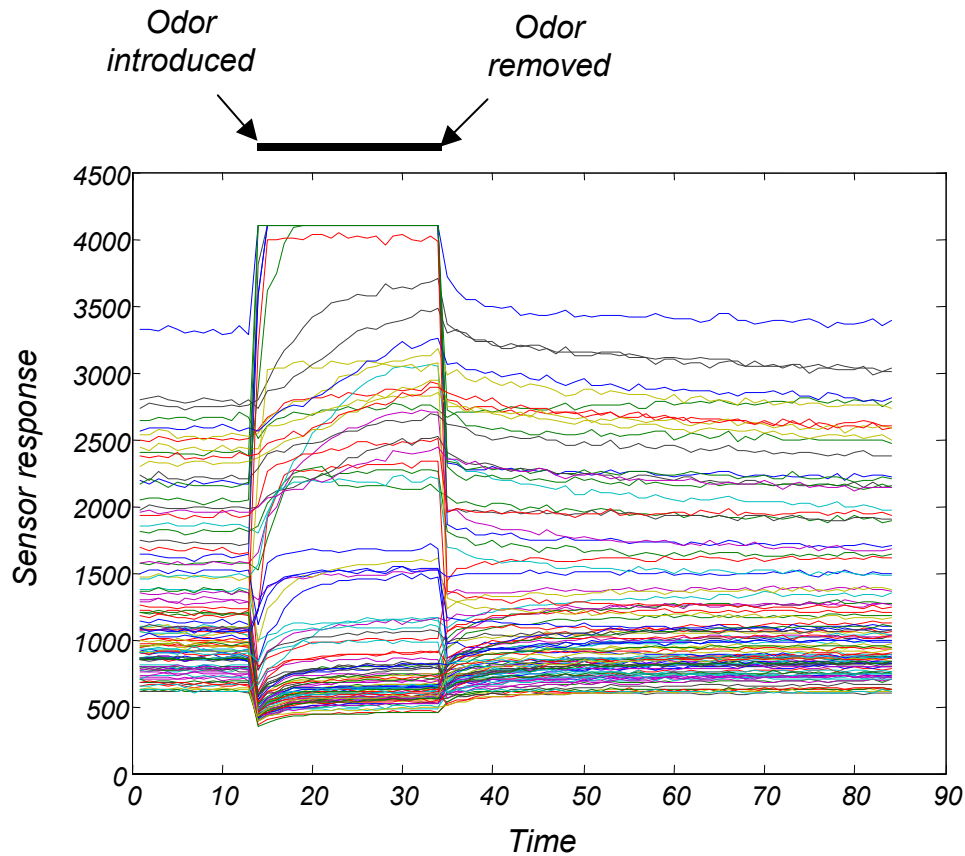
Fig. 21: Response of 100 microbead sensors to acetone (courtesy of Illumina, Inc.). The odor, acetone in this case, is introduced at t=14sec and removed at t=35 sec.

II.3. Infrared spectroscopy

The third approach that will be used in this dissertation to generate a high-dimensional response involves infrared absorption spectroscopy. Though very little is known about the molecular determinants of an odorant, it is widely believed that each GL unit (to which similar ORNs converge) acts like a "molecular feature detector" that identifies a particular molecular property, such as type and position of a functional group (Mori et

al. 1999). In the realm of instrumental data, infrared (IR) absorption spectroscopy is the closest match to this form of molecular detection.

II.3.1. IR principle

IR spectroscopy is based on the fact that different inter-atomic bonds in a molecule absorb IR radiation at unique wavelengths in the mid-IR range (4000-0 cm^{-1}). The absorption spectrum can be divided into two distinct regions: the so-called "functional-group" region (4000-1500 cm^{-1}) and the "fingerprint" region (<1500cm^{-1}). The former contains information about the functional groups that are present in the molecule (e.g., alcohols, aldehydes, ketones, esters etc.,), whereas the latter contains a global absorption pattern that is unique to each organic compound. A sample IR spectrum (iso-amyl acetate; an ester with a fruity smell) obtained from the National Institute of Standards and Technology (NIST) Chemistry Web Book database is shown in Fig. 22. Different peaks in the absorption spectrum correspond to the various functional groups present in iso-amyl acetate. As a reference, a table of different functional groups and their IR absorption regions is included in Appendix A.
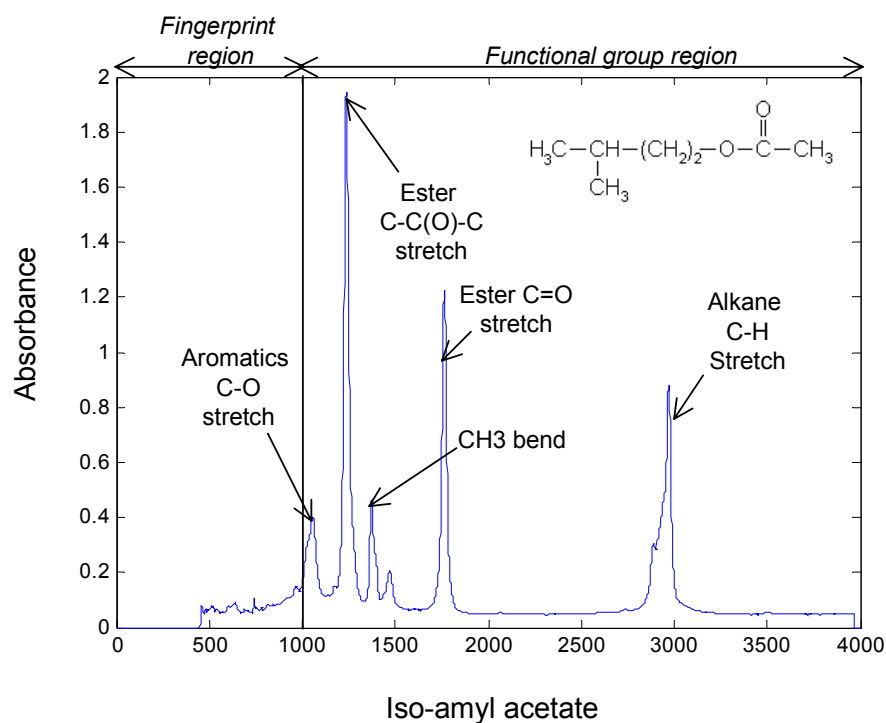
Fig. 22: IR absorption spectrum of iso-amyl acetate (an ester with a fruity smell). Each peak is labeled by the functional group responsible for the absorption.

II.3.2. NIST IR database

We will use a database comprising of infrared absorption spectra (wave number range 0 – 4000 cm^{-1}) of ninety-three chemicals obtained from NIST (Linstrom and Mallard 2003). Each feature in the absorption spectrum indicates the intensity of light absorbed by a molecule at a particular wavenumber, thus defining a high dimensional odor signal of 4,000 features.

II.4. Application of the experimental datasets

The high dimensional datasets generated with the MOS and optical microbead sensor arrays will be used to validate the computational models presented in the following chapters. Both *Selectivity* and *Illumina dataset* include sensor responses to different single analytes and will be used to validate models of chemotopic convergence for dimensionality reduction (Chapter III) and additive lateral inhibition for contrast enhancement (Chapter V). The *Selectivity* dataset is the only dataset that includes sensor response to single analytes at different concentration and their binary and ternary mixtures. Hence we will use this dataset to validate the shunting inhibition model for concentration normalization (Chapter IV), the model of bulb-cortex interaction for mixture segmentation and background suppression (Chapter VI) and the final integrated model (Chapter VII). The *NIST* IR spectrum database will be used specifically to demonstrate the ability of the chemotopic convergence model to generate artificial odor maps that are qualitatively similar to those found in rat olfactory bulb.

CHAPTER III

DIMENSIONALITY REDUCTION USING CHEMOTOPIC CONVERGENCE

The second stage of olfactory information processing deals with the generation of a compact odorant representation. The projection from the olfactory epithelium onto the olfactory bulb is organized such that ORNs expressing same receptor gene converge onto one or a few GL (Vassar et al. 1994). This convergence transforms the initial combinatorial high-dimensional code into an organized spatial pattern (i.e. an odor image), which decouples odor identity from intensity (Gutierrez-Osuna 2002). In addition, massive convergence improves the signal-to-noise-ratio (SNR) by integrating signals from multiple receptor neurons (Laurent 1999; Pearce et al. 2001). In this chapter, we adapt the self-organizing model of chemotopic convergence presented by us in (Gutierrez-Osuna 2002) to generate odor maps from the three input modalities discussed in Chapter II. We also study the benefits of this dimensionality reduction model, and analyze thee extent to which the resulting odor maps are consistent with those reported in neurobiology.

III.1. Chemotopic convergence model

Gutierrez-Osuna (Gutierrez-Osuna 2002) has presented a theoretical model of chemotopic convergence in olfactory bulb. The model is based on three principles: (i) ORNs with similar affinities project onto neighboring GL, (ii) GLs in OB are spatially arranged as a two-dimensional surface, and (iii) neighboring GL tend to respond to similar odors (Meister and Bonhoeffer 2001; Johnson and Leon 2000). Therefore, a natural choice to model the ORN-GL convergence is the self-organizing map (SOM) of Kohonen (1982).

We adapt the model presented in (Gutierrez-Osuna 2002) to process high-dimensional experimental data from each of the three input modalities discussed in Chapter II. In what follows, we will refer to pseudo-sensors (either defined by different modulating temperatures, microbeads or IR absorption bands), as ORNs. The SOM nodes to which the pseudo-sensors converge will be considered as GL in a simulated olfactory bulb.

To form a chemotopic mapping, we must first define a selectivity measure upon which ORNs can be clustered together. In this work, this is accomplished by treating the ORN response across a set of odorants as an affinity vector:

$$ORN_i = \left[ORN_i^{O_1}, \ ORN_i^{O_2}, ..., ORN_i^{O_C} \right] \tag{3.1}$$

where ORN_i^{O} is the response of ORN_i to odor O, and C is the number of odorants.

The convergence model operates as follows. The SOM is presented with a population of ORNs, each represented by a vector in C-dimensional affinity space, and

trained to model this distribution. Once the SOM is trained, each ORN is then assigned to the closest GL in affinity space, thereby forming a convergence map from which the response of each GL is computed as:

$$G_j^O = \sum_{i=1}^{N} W_{ij} ORN_i^O \tag{3.2}$$

where N is the number of ORNs in the array, and $W_{ij}=1$ if ORN_i converges to GL_j and zero otherwise. It is the novelty in training the SOM in the affinity space (discussed in detail in section III.1.1) that we will show leads to spatial odor maps that are qualitatively consistent with those found in neurobiology (Johnson and Leon 2000; Joerges et al. 1997; Friedrich and Korsching 1997).

To help visualize this model, Fig. 23 illustrates a problem with three odors (labeled as A, B and C). The affinities of pseudo-sensors are shown as a colorbar below the senor response. This is a simplification to illustrate the concept, as the actual affinity space for this problem will be three-dimensional. The chemotopic mapping is achieved by assigning the pseudo-sensors with similar affinities to the same SOM node. The activity of the entire SOM lattice is then considered as an artificial odor map.
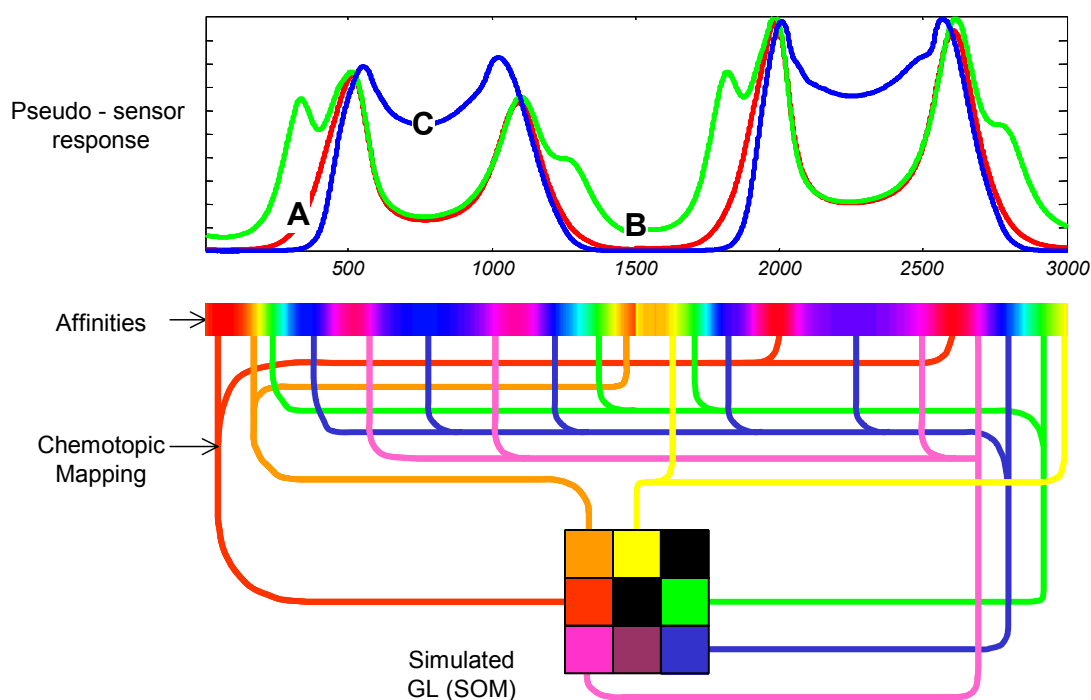
Fig. 23: Illustration of chemotopic convergence: the relative response to three analytes (labeled A, B and C) is used to define the affinity (shown as a colorbar) of the sensor at each operating temperature. Pseudo-sensors with similar affinities project to the same SOM node as a result of chemotopic convergence. Activity across the SOM lattice can be considered as an artificial odor map.

This convergence model works well when the different sensors are reasonably uncorrelated, since then the projection of ORNs across the SOM lattice approximates a uniform distribution, i.e., maximum entropy [Lancet et al. 1993; Laaksonen et al. 2003]. Unfortunately, the population of pseudo-sensors created by the methods proposed in Chapter II are collinear (*Selectivity* and *Illumina*) or over-sampled (*NIST IR*). As a result, a few GL tend to receive the majority of ORNs, which capture the "common-

mode" response of the sensor, overshadowing the most discriminatory information in the temperature-modulated response. To avoid this issue, the activity of each GL is normalized by the number of ORNs that converge to it:

$$G_j = \frac{\sum_{i=1}^{N} W_{ij} R_i}{\sum_{i=1}^{N} W_{ij}} \qquad (3.3)$$

Note that this solution is not driven by biological plausibility but largely by the limitations of our sensors.

III.1.1. Chemotopic convergence as feature clustering in affinity space

Conventional statistical pattern recognition approaches to dimensionality reduction operate in the feature space, where each input dimension corresponds to a particular feature (or sensor). Samples that belong to the same (odor) class cluster together in feature space, as shown in Fig. 24 (a). In contrast to feature space, each dimension in affinity space corresponds to a particular (odor) class. Features that provide similar information regarding the different classes cluster together in affinity space. As an example, in Fig. 24(b) all features of type S_1 provide high response to class B and low response to class A; as a result they can be clustered together. In contrast, all features of type S_2 provide high response to class A and low response to class B, therefore they can form a separate cluster. This basic principle underlies the chemotopic convergence model presented in section III.1: the SOM is used to cluster sensor features that have similar affinities (similar class information).
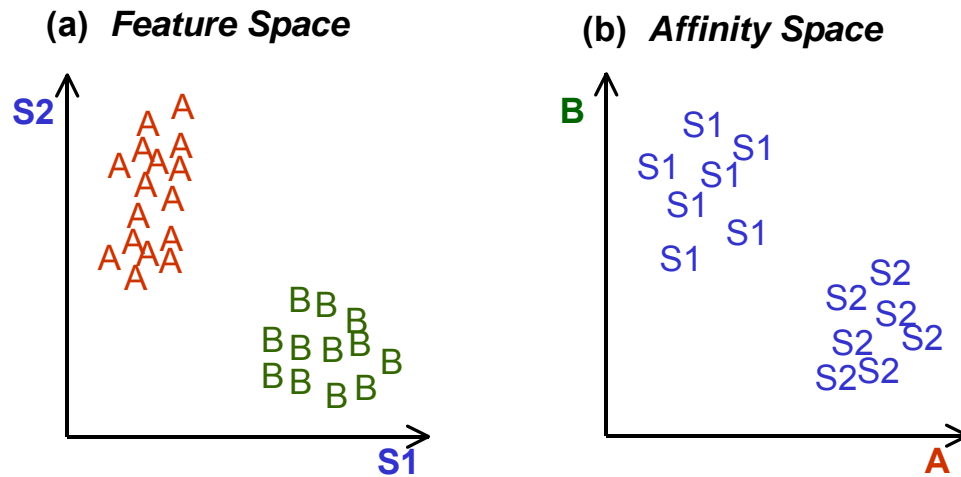
Fig. 24: Clustering in feature space and in affinity space. (a) Samples of the same class produce similar response across sensor array, and therefore cluster together in feature space. (b) Features that produce similar response to different odors (classes) cluster together in the affinity (class) space.

To visually illustrate this feature-clustering scheme, lets consider a toy problem consisting of discriminating three geometric silhouettes: Circles (C), Squares (S) and Triangles (T). Fig. 25(a) shows silhouettes used for training the model, where different labels are used to identify different types of features (e.g. CS indicates features that respond only to Circle and Square, T indicates features that respond only to Triangle, and so on). Following the convergence model, the features (pixels of the image) are chemotopically projected onto eight SOM nodes. Fig. 25(b) shows the features that are assigned to each SOM node, (represented by the lighter areas in the figure) after training in affinity space. It can be clearly seen that chemotopic convergence groups features

that convey similar class information, thus reducing the dimensionality of the input signals.
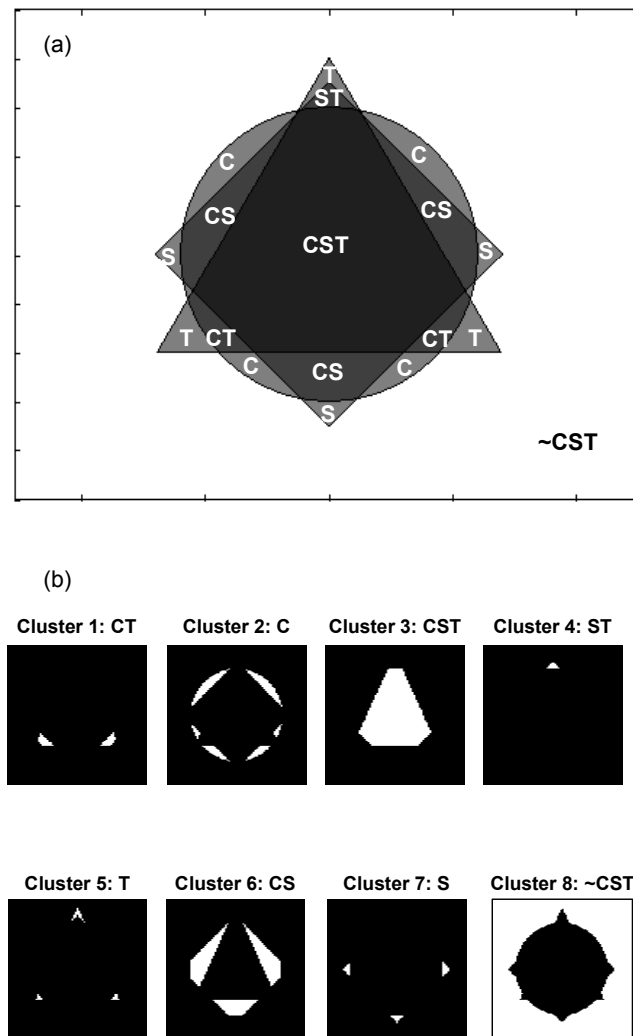
Fig. 25: (a) Toy problem with three classes: Circle, Square and Triangle. Different labels are used to identify different types of features (e.g. CS indicates features that are only active in Circle and Square, T indicates features that are active only in Triangle, and so on). (b) Eight feature clusters generated after chemotopic convergence with eight SOM nodes. Each SOM node receives projection from a single features cluster.

III.2. Experimental results

In this section, we apply the chemotopic convergence model on the experimental datasets obtained using temperature modulated MOS sensors (*Selectivity* dataset) and optical microbead sensors (*Illumina* dataset). The performance of the model is analyzed by comparing odor separability before (raw data) and after chemotopic convergence.

III.2.1. Validation on the Selectivity database

The high dimensional odor signal (3000 pseudo-sensors) generated by temperature modulating two MOS sensors is projected onto a GL layer with 400 nodes, arranged as a 20x20 SOM lattice, based on the convergence model described in section III.1. The SOM arranges itself after training to model the affinity space as shown in Fig. 26. Only one of the samples for the highest concentration of each odor was used to train the SOM; all the remaining samples and concentrations were used for validation purposes.

Fig. 27 shows the odor maps generated from the high dimensional sensor response to acetone (A), isopropyl alcohol (B) and ammonia (C) at three concentrations. It can be seen that odor quality is encoded by a unique spatial pattern across the SOM lattice, whereas odor concentration is related to the intensity and spread of this pattern. The locus of activity for a given odor corresponds to those SOM nodes that receive projections from the temperature features of maximum gain (peak in the temperature modulated response) to that odor. Fig. 28 shows the odor maps generated for the binary and ternary mixtures of the pure analytes. The processing of these odor maps for identifying the constituents of a mixture or suppressing the weaker (background) odor is

discussed in Chapter VI. It should be noted that these maps show a high degree of overlap; this issue is addressed by the two lateral inhibitory circuits that are presented in Chapters IV and V.
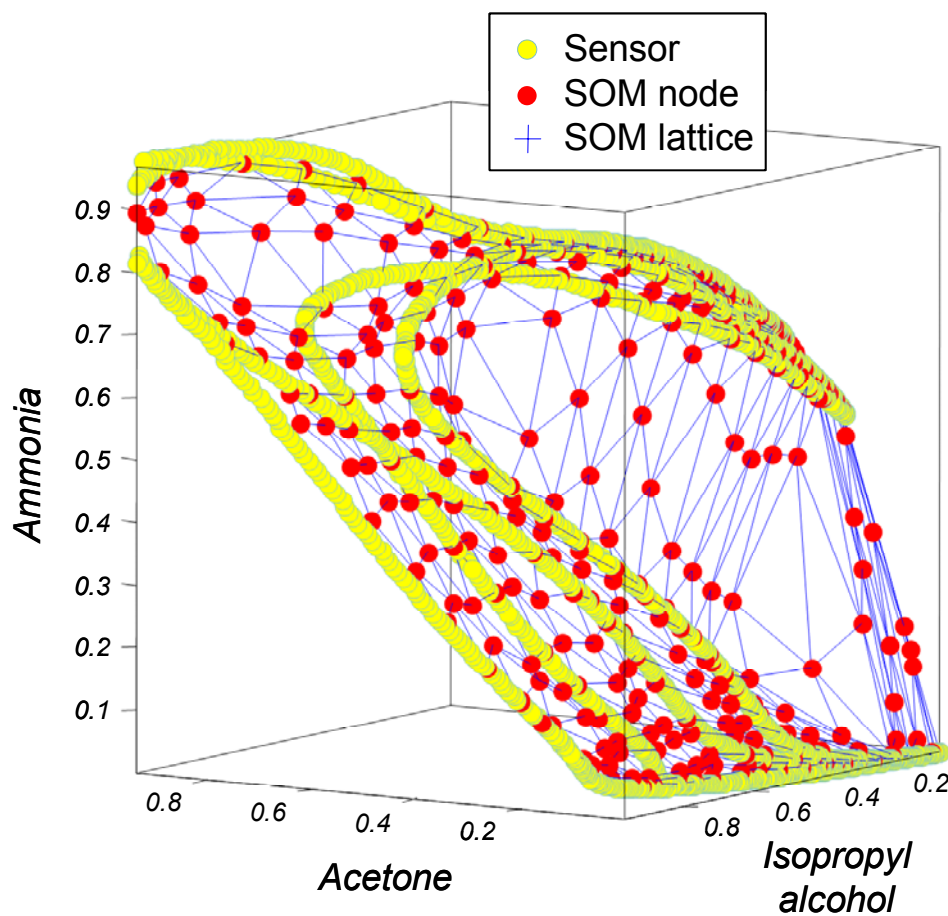
Fig. 26: Distribution of glomerular SOM nodes and pseudo-sensor repertoire in affinity space for the MOS sensor *Selectivity database* (3,000 ORNs, 20x20 lattice).
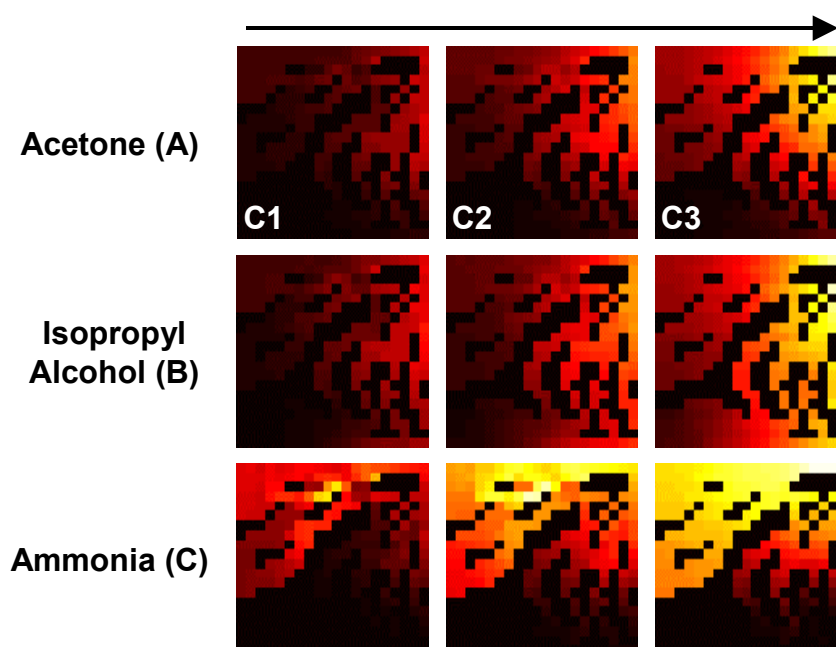
Fig. 27: Glomerular maps generated using a 20x20 lattice of GLs and 3,000 pseudo sensors from the temperature-modulated response profile of two MOS sensors to three analytes at three concentrations (*Selectivity database*).
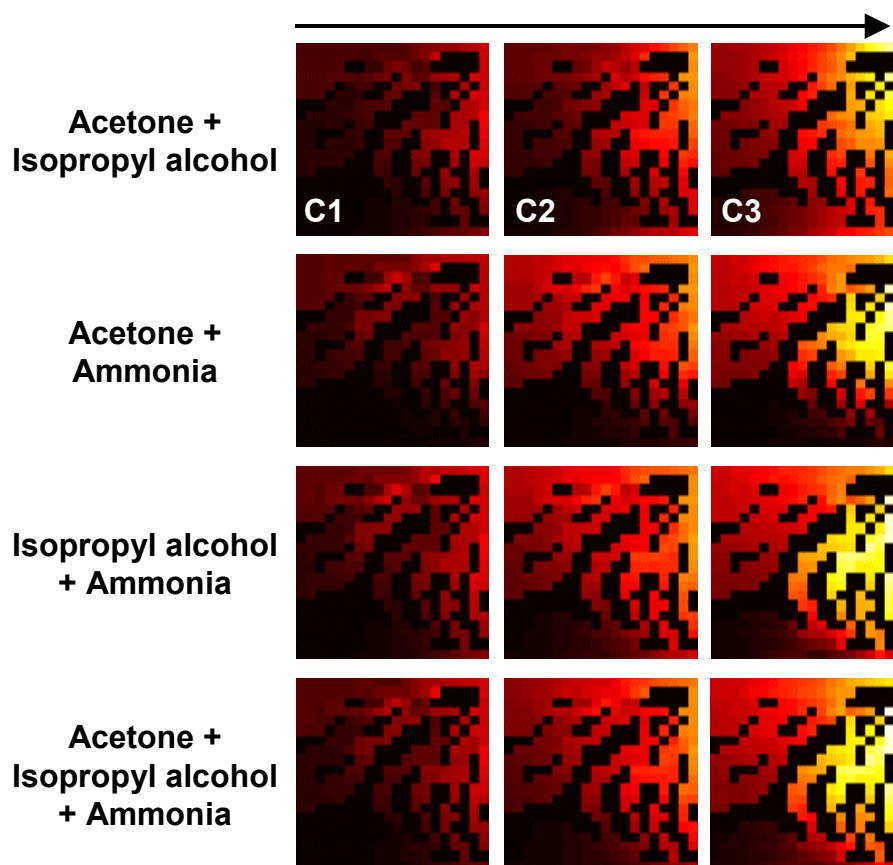
Fig. 28: Glomerular maps of the binary and ternary mixtures of the three analytes at three concentrations (*Selectivity database*).

III.2.2. Validation on the Illumina database

Similar to the study on *Selectivity* dataset, the sensor response of 586 optical sensors in the *Illumina* bead array are chemotopically projected onto a GL layer with 400 nodes, arranged as a 20x20 SOM lattice. Only one sample per odor was used to train the SOM; all the remaining samples were used for validation purposes. Fig. 29 shows the odor maps of five analytes: acetone (A), ethyl alcohol (EA), ethyl hydroxide (Et-OH), methyl hydroxide (Me-OH) and toulene (T). Five samples per odor are shown to illustrate

repeatability. It can be observed that the odor quality is encoded by a unique spatial pattern across the SOM lattice.
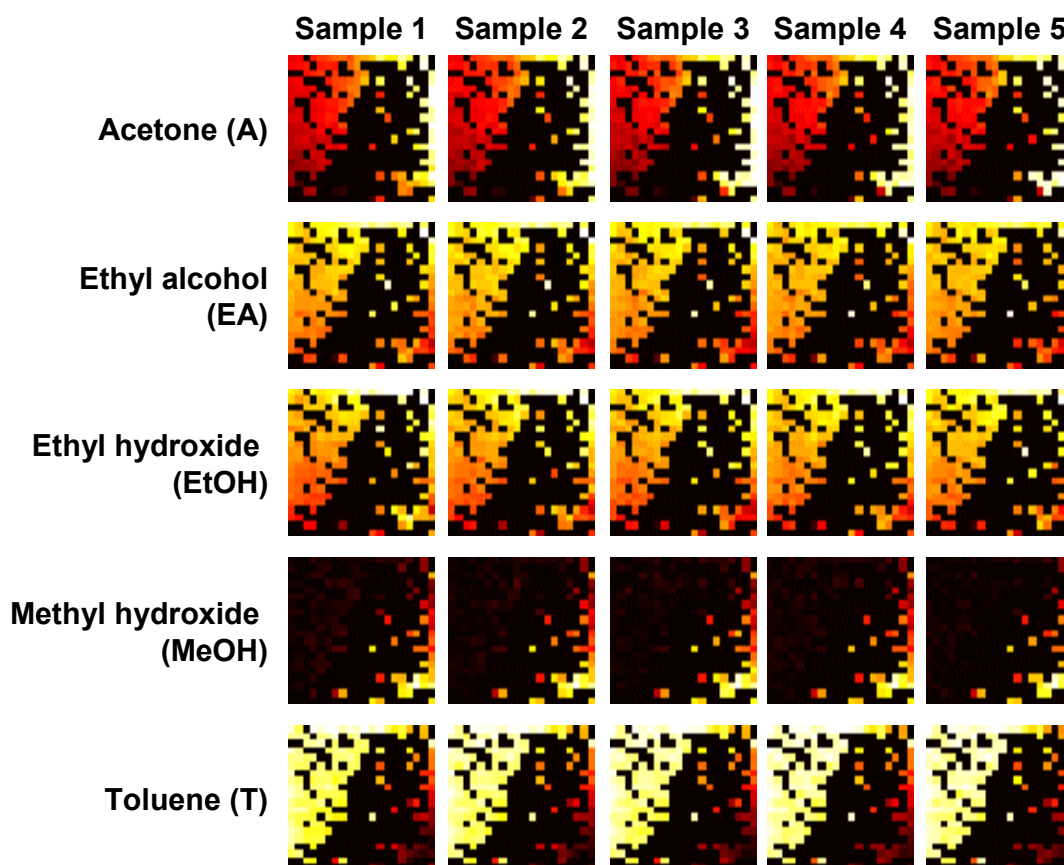
Fig. 29: Glomerular maps for the five analytes generated using a 20x20 lattice of GLs and 586 sensors in the Illumina microbead array.

III.3. Characterization of the model

To quantify the advantage of the proposed model for pattern recognition purposes, we employ a measure of class separability derived from Fisher's linear discriminant analysis (Fukanaga 1990):

$$J = \frac{tr(S_B)}{tr(S_W)} \tag{3.4}$$

where S_W and S_B are the within-class and between-class scatter matrices, respectively, defined as follows:

$$S_W = \sum_{q=1}^{Q} \sum_{x \in \omega_q} (x - \mu_q)(x - \mu_q)^T \tag{3.5}$$

$$S_B = \sum_{q=1}^{Q} (\mu_q - \mu)(\mu_q - \mu)^T \tag{3.6}$$

$$\mu_q = \frac{1}{n_q} \sum_{x \in \omega_q} x \;\; and \;\; \mu = \frac{1}{n} \sum_{\forall x} x \tag{3.7}$$

where x is a feature vector, Q is the number of odor classes, μ_q and n_q are the mean vector and number of examples for odor q, respectively, n is the total number of examples in the dataset, and μ is the mean vector of the entire distribution. Being the ratio of the spread between classes relative to the spread within each class, the measure J increases monotonically as classes become increasingly more separable.

Fig. 30 shows the odor separability as the number of SOM nodes in the lattice is increased. In the case of the *Selectivity* dataset, odor separability increases rapidly with the number of nodes, and saturates as the size of SOM lattices becomes large. Results on the *Illumina* dataset also reveal similar characteristics, except in this case the sum of responses of all 586 microbead sensors (1x1 SOM lattice) surprisingly provides maximum separability. This is because, the odor separability in the case of the *Illumina* dataset, is computed only using sensor responses to analytes at a single concentration. In both datasets, convergence mapping shows better performance compared to those of

principal component analysis and the baseline from raw data. This is a direct result of the supervised nature of the convergence mapping, which leads to more orthogonal patterns than those available at the input thereby enhancing the signal-to-noise-ratio.
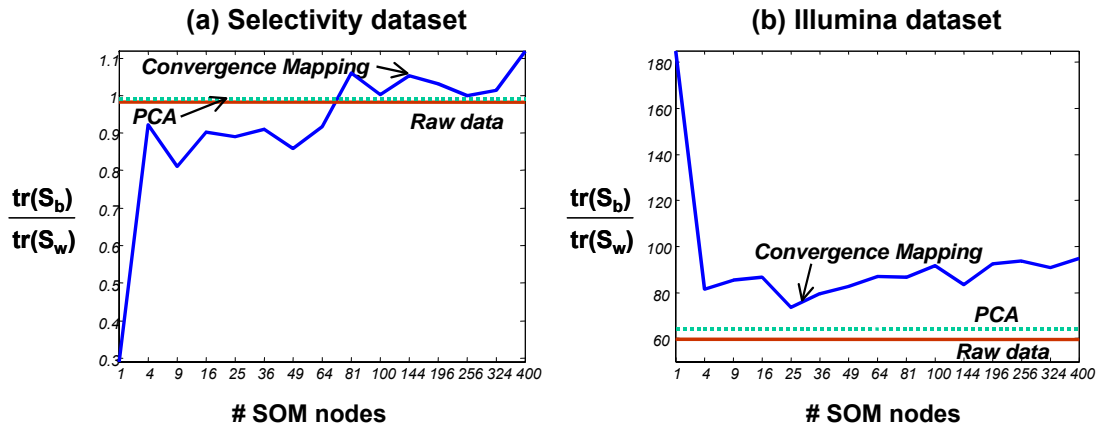
Fig. 30: Comparison of odor separability (1) from raw data, and (2) following chemotopic convergence with SOM lattices of increasing size (1×1 to 20×20). Only one of the samples for the highest concentration of each odor was used to train the SOM in each case. The generated chemotopic maps (with larger lattices) provide better odor separability than principal component analysis (capturing 99.9% variance) and the baseline from raw data.

III.4. Discussion: consistency with neurobiology

So far we have demonstrated the use of chemotopic convergence as a dimensionality reduction scheme to generate compact odor representation from a high dimensional

sensor response. In this section, we discuss the extent to which the odor maps generated by the convergence model are consistent with results from neurobiology.

Though very little is known about the molecular determinants of an odorant, it is widely believed that each GL unit to which similar ORNs converge acts like a "molecular feature detector" that identifies a particular property, such as type and position of a functional group (Mori et al. 1999). In the realm of instrumental data, infrared (IR) absorption spectroscopy is the closest match to this form of molecular detection. Hence we will use the IR absorption spectrum (*NIST IR* dataset) to generate artificial odor maps and show that the generated spatial patterns are qualitatively similar to those obtained in the rat olfactory bulb[4].

To generate artificial odor maps, a population of 4,000 pseudo-sensors is generated from the IR spectrum by treating the absorbance level at each wave number as a separate pseudo-sensor. The pseudo-sensors population is subsequently projected chemotopically onto a GL layer with 100 nodes, arranged as a 10x10 SOM lattice. The odor images are then low-pass filtered using a 5x5 Gaussian kernel. Fig. 31 shows the odor maps for ten different smell percepts[5] from the IR database. The following observations can be made based on the odor images obtained from their IR absorption spectrum:

---

[4] A database of odor maps from the rat olfactory bulb is available at http://leonlab.bio.uci.edu/.

[5] The organleptic descriptors were obtained from Flavornet.

(i)   Esters that smell like tropical fruits (banana and pineapple) produce similar odor maps, which are different from the maps of chemicals with apricots or citrus fruits descriptors,

(ii)   *Citrus* odor maps are similar to those that smell *Fatty*,

(iii) *Sweat* and *Cheese* also produce similar odor maps, and,

(iv)   Methyl salicylate and Menthol, which are both minty, produce distinct odor maps.

Spatial odor images for these compounds in the dorsal part of rat OB are shown in Fig. 32. These odor maps were obtained using optical imaging techniques involving 2-deoxyglucose uptakes in the dorsal part of the rat olfactory bulb (Johnson and Leon 2000). Similar to the images obtained from the IR spectra, esters with tropical fruit smells produce similar activation patterns across the OB, which is different from chemicals with apricot and citrus descriptors. Odor maps for *Citrus* and *Fat* descriptors, *Sweat* and *Cheese* descriptors overlap similar to the IR-generated odor maps. *Minty* smelling Methyl salicylate and Menthol produced distinct odor maps.

Hierarchical cluster analysis of the seventeen chemicals present in both the *NIST-IR* dataset and the rat OB image dataset reveal similar groupings, as shown in Fig. 33(a, b). In both cases, four distinct clusters can be identified that correspond to the following four smell descriptors: *Fruity*, *Cheese* or *Sweat*, *Fat* or *Citrus* and *Nuts*. Methyl salicylate, which smells *Minty*, is grouped with the nuts category in both cases. Hexanoic acid, which is a fatty acid that smells like *Sweat*, is grouped under *Fat* or

Citrus smell descriptor using the rat OB images and in the *Sweat* cluster using IR odor maps.

These results suggest that convergence mapping, combined with IR absorption spectra, may be an appropriate method to capture perceptual characteristics of the odorants from their molecular features.

III.5. Summary

In this chapter we have presented a computational model for the chemotopic convergence of ORNs onto GLs. A Kohonen SOM is used to topologically cluster pseudo-sensors obtained from the three experimental datasets. This results in a two-dimensional odor map that decouples odor quality from intensity. The identity of the odor is captured by the unique spatial pattern across SOM nodes, whereas concentration is related to the intensity and spread of this pattern. These results are consistent with those observed in the biological olfactory bulb through optical imaging. The next stage of processing involves contrast enhancement of the odor images formed through convergence by two lateral inhibitory circuits.

Iso-Amyl Acetate   Ethly Butyrate

Banana

Nonyl acetate

Apple

Propyl Butyrate   Ethly Propionate

Pineapple

gamma-Undekalakton

Apricot

Heptanal   Limonene

Citrus
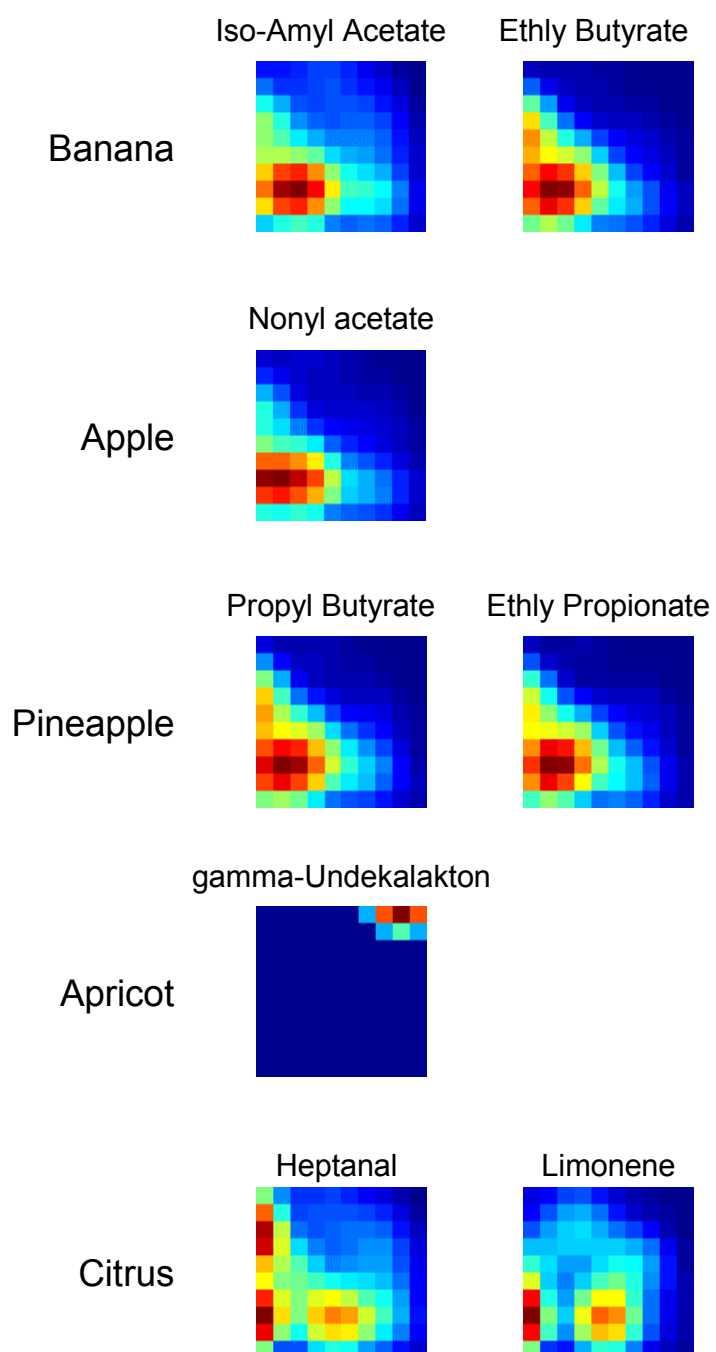
Fig. 31: Odor maps to the same ten different smell percepts as the OB images generated from the IR spectrum using the chemotopic convergence model.

Dimethyl pyrazine   Acetyl Pyridine   Benzaldehyde

Nuts

Hexanal   Heptanal   1-Octanol

Fat

Caproic acid   Valeric acid   IsoValeric acid

Sweat

Eucalyptol   Menthol   Methyl salicylate

Minty

Butyric acid
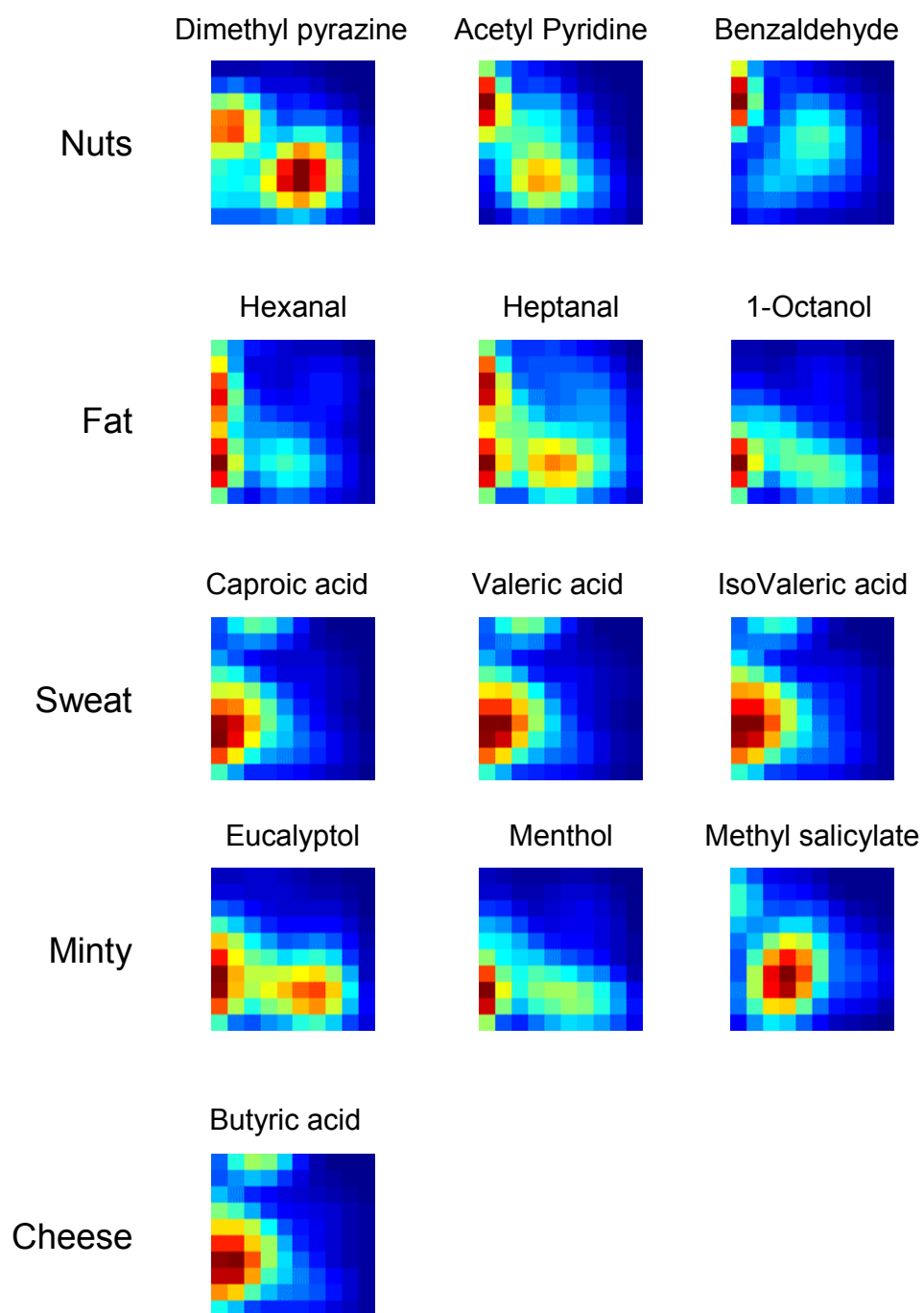
Cheese
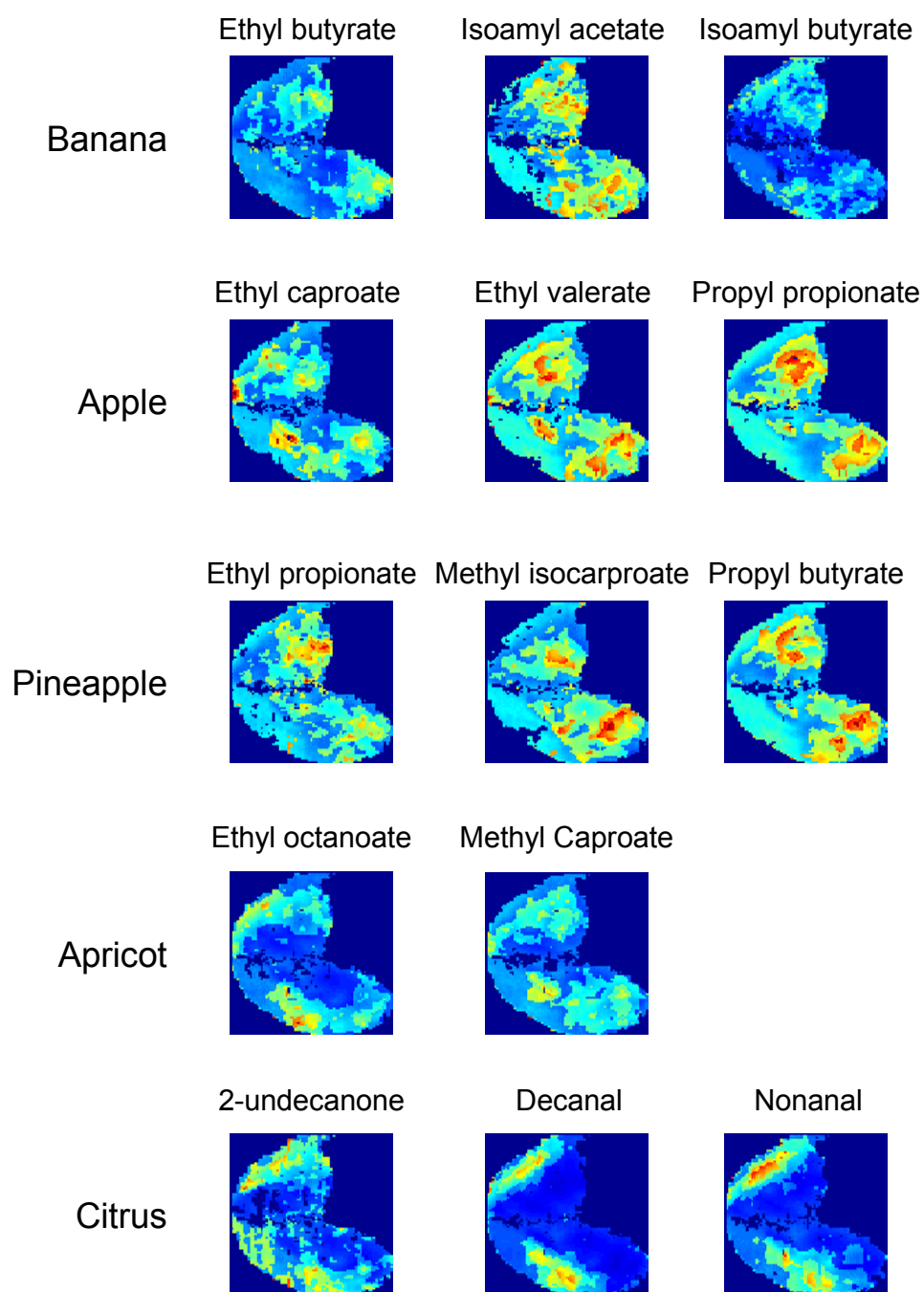
(Fig. 31: continued)

Fig. 32: Odor maps obtained in the rat olfactory bulb to ten different smell percepts: i) banana, ii) pineapple, iii) apple, iv) apricot, v) citrus, vi) nuts, vii) cheese, viii) sweat, ix) minty and x) fat.

2,3 dimethyl pyrazine   2-acetyl pyridine   Benzaldehyde

Nuts

Octanoic acid   Butyric acid

Cheese

Iso-valeric acid   Caproic acid   Valeric acid

Sweat

L-Menthol   Methyl Salicilate   Carvone(-)

Minty

1-hexanol   Octanol   1-heptanol

Fat
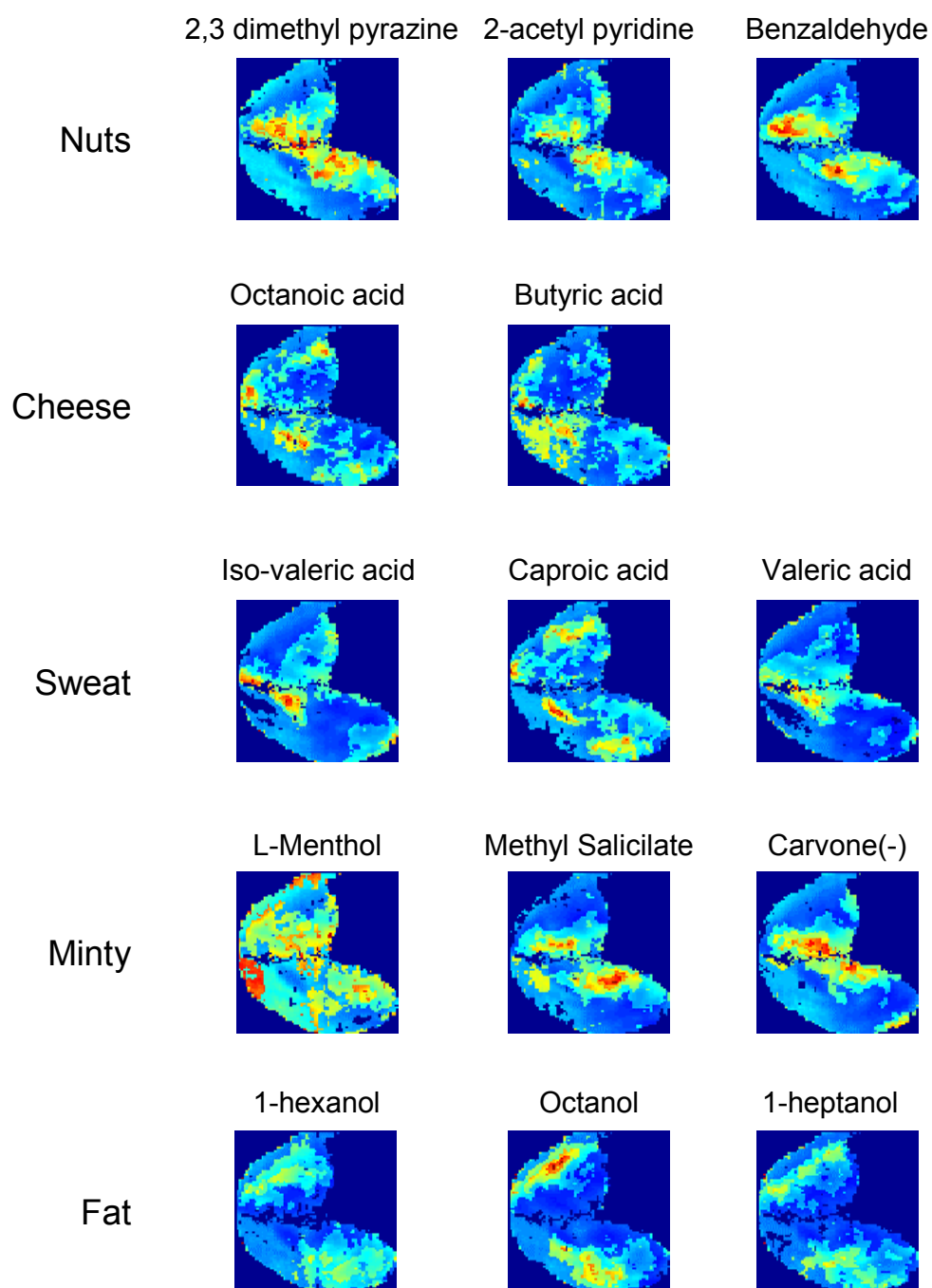
(Fig. 32: continued)

Fig. 33: Dendrograms (complete-linkage) revealing similar clusters a) from OB odor maps b) from artificial odor maps formed from their IR absorption spectra. The seventeen common chemicals found in both databases used in this study are as follows: 1 – Acetyl Pyridine (*Nuts*), 2 – Iso-amyl Acetate (*Fruity*), 3 – Benzaldehyde (*Nuts*), 4 – Butanoic Acid or Butyric acid (*Cheese*), 5 – 2,3-Dimethyl pyrazine (*Nuts*), 6 – Ethyl Butyrate (*Fruity*), 7 – Ethyl Propionate (*Fruity*), 8 – Heptanal (*Citrus*, *Fatty*), 9 – Heptanol (*Fatty*), 10 – Hexanal (*Fatty*), 11 – Hexanoic acid or Caproic acid   (*Sweat*), 12 – Hexanol (*Fatty*), 13 – Methyl Salicylate (*Minty*), 14 – Octanol (*Fatty*), 15 – Pentanoic Acid or Valeric acid (*Sweat*), 16 – Propyl Butyrate (*Fruity*), 17 – Iso-Valeric Acid (*Sweat*).   Asterix identifies chemicals with smell descriptors different from other members in the cluster.

(a) Clusters from OB odor maps

Cheese, Sweat *Nuts* *Fat* *Fruits* *Fat or Citrus*

15 17 4 1 3 5 13* 2 7 6 16 8 10 9 11* 12 14
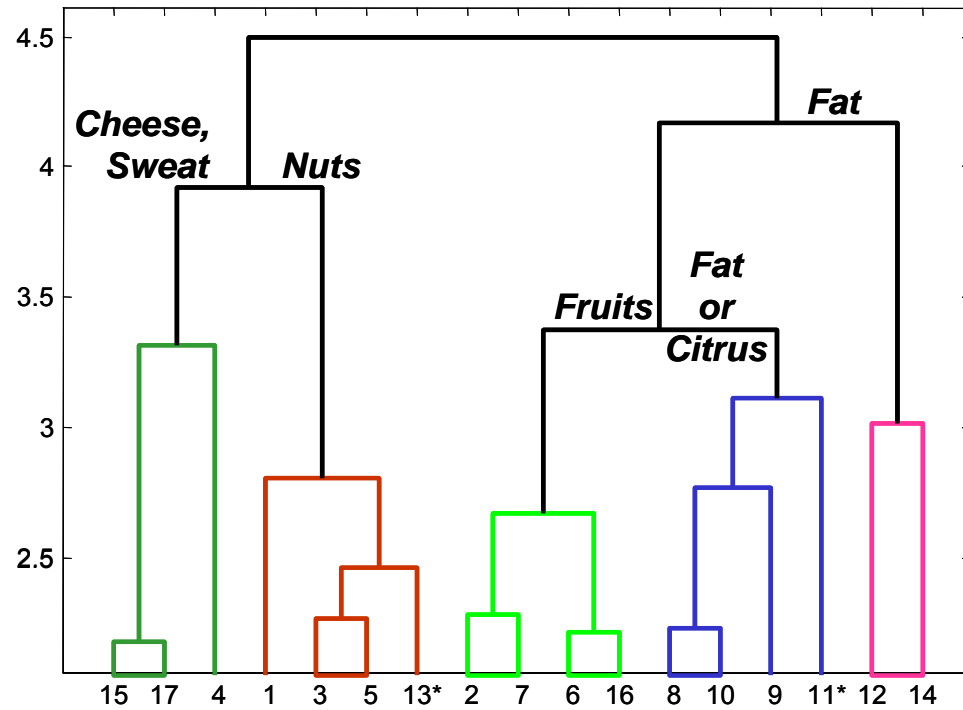
(b) Clusters from IR odor maps

Cheese, Sweat *Fruits* *Fat or Citrus* *Nuts*

11 15 4 17 2 6 16 7 8 10 9 12 14 1 3 5 13*
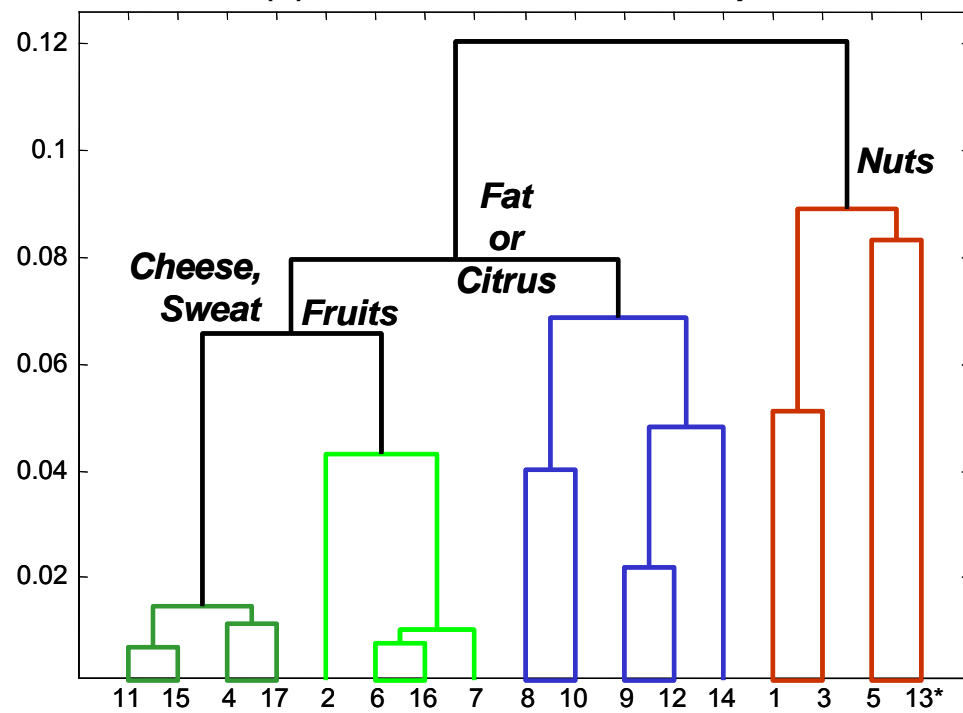
CHAPTER IV

CONCENTRATION NORMALIZATION THROUGH SHUNTING INHIBITION

The third stage of olfactory signal processing involves gain or "volume" control, a mechanism that enables invariant identification of odorants across a wide concentration range. The odor and concentration specific spatial patterns formed at the input of the olfactory bulb by the chemotopic convergence (Chapter III) are input to a layer of lateral inhibitory circuits driven by periglomerular interneurons. These lateral interactions are known to be shunting-type (divisive inhibition), and have been hypothesized to serve as a "volume control" mechanism (Freeman 1999). Recently these glomerular circuits have been found to have center-surround type connectivity and have been suggested to perform pattern normalization, noise reduction and contrast enhancement (Aungst et al. 2003). In this chapter, we present a computational model of these gain-control circuits, and analyze the role of the spread of lateral inhibition in achieving concentration removal with the network. We validate the concentration-normalization performance of the model on the *Selectivity dataset*, which consists of temperature-modulated responses of MOS sensors to three analytes at three different concentrations.

IV.1. Model of shunting lateral inhibition

The shunting lateral inhibition mediated by periglomerular interneurons is realized using a model of divisive normalization proposed by Grossberg (1976) as shown below:

$$\frac{dx_i^O}{dt} = -Dx_i^O + (B - x_i^O)G_i^O - x_i^O \sum_{k \neq i} c_{ki} G_k^O \qquad (4.1)$$

where G_i^O is the activity of SOM node i (i.e., after chemotopic convergence), x_i^O is the

corresponding neuron output to odor O, $-Dx_i^O$ is a decay term that models the dynamics

of a neuron, $(B - x_i^O)G_i^O$ is the shunting self-excitation, B is the maximum activity of

neuron ($0 \leq x_i^O \leq B$), and $-x_i^O \sum_{k \neq i} c_{ki} G_k^O$ is the shunting inhibition from other neurons

(Grossberg 1976). The complete model of the shunting lateral inhibition occurring at

the input of the olfactory bulb is schematically shown in Fig. 34. The connection matrix

C modeling the shunting inhibition is set as follows:

$$c_{ki} = \begin{cases} U(a,b) & d(k,i) < \dfrac{\sqrt{M}}{r} \\ 0 & otherwise \end{cases} \qquad (4.2)$$

where $U(a,b)$ is a uniform distribution between a and b, and d is the distance between

units measured as a Euclidean distance within the lattice

($d = \sqrt{(row_k - row_i)^2 + (col_k - col_i)^2}$; row and col being the row and column

coordinates of a neuron in the lattice), M is the number of SOM nodes, and r determines

the width of the lateral inhibitory connections. Fig. 35 provides an illustration of these

three model parameters.
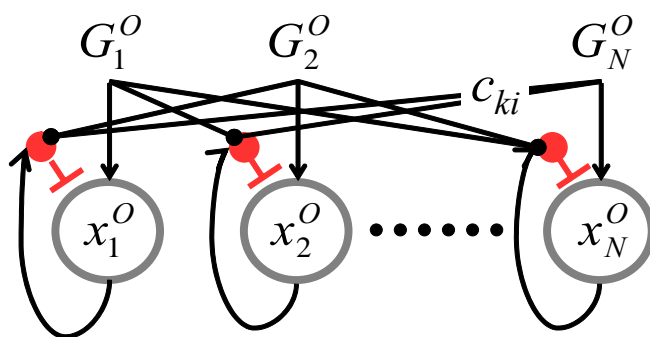
Fig. 34: Shunting lateral inhibition at the input of the olfactory bulb.

(a) Exponential decay

(b) Saturation effect

(c) Center on-off surround
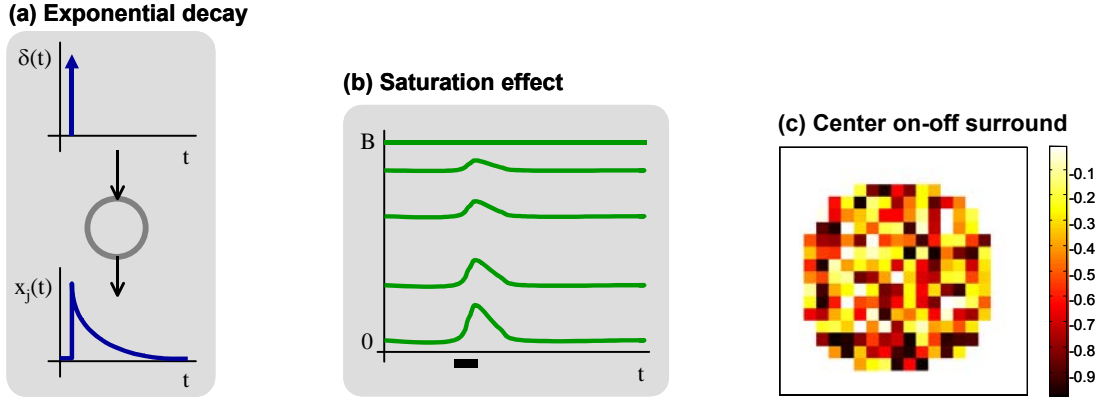
Fig. 35: Illustration of the shunting inhibition model parameters: (a) the term $-Dx_i^O$ in equation (4.1) models the impulse response as an exponential decay; (b) the term $\left(B - x_i^O\right)G_i^O$ captures saturation effects, according to which the response of a neuron to an input becomes smaller as the neuron's current activation approaches the maximum response level (B) (Gerstner and Kitler 2002); (c) the connection matrix C, modeling the lateral connectivity. Note that in this case activation of one GL ('on-center') causes widespread inhibition of surrounding GLs ('off-surround') similar to the results reported in (Aungst et al. 2003).

Equating equation (4.1) to zero, it trivially follows that the steady-state output of each neuron is:

$$x_i^O = \frac{BG_i^O}{D + G_i^O + \sum_{k \neq i} c_{ki} G_k^O} \tag{4.3}$$

which, for $c_{ki} = 1 \ \forall \ k,i$, and D=0, becomes proportional to the (L1) normalized response of its input relative to the total network activity:

$$x_i^O = \frac{BG_i^O}{\displaystyle\sum_{\forall k} G_k^O} \qquad (4.4)$$

The original study by Grossberg (1976) only considered global connections for the purpose of pattern normalization. However, in this work, we show that by adjusting the spread of the lateral inhibitory connections using equation (4.2), the degree of concentration normalization can be controlled parametrically.

IV.2. Experimental results

To validate the model, temperature-modulated patterns for three analytes acetone (A), isopropyl alcohol (B) and ammonia (C), at three different concentrations are first chemotopically projected using the convergence model described in Chapter III. A GL layer with 400 nodes, arranged as a 20x20 SOM lattice, is used to perform chemotopic mapping of sensor response. The outputs of the convergence model are then used as the inputs to the shunting inhibition model in equation (4.1).

The PCA scatterplot of steady-state activity across the network is shown in Fig. 36. Without shunting inhibition (a), the model preserves most of the concentration information, as can be seen in Fig. 36 (a), where the principal sources of variance is concentration information. In contrast, with global shunting inhibition (c) the network is able to remove most of the concentration information and provide maximum separability between odors. Finally, different degrees of cancellation can be achieved by controlling the spread of the shunting lateral inhibitory connections, as shown in Fig. 36(b). Also, it can be observed in the case of models with shunting inhibition, the first principal

components contains mostly odor information and the second principal component contains mostly concentration information. A detailed characterization of the model is presented next.

No shunting inhibition (after convergence)
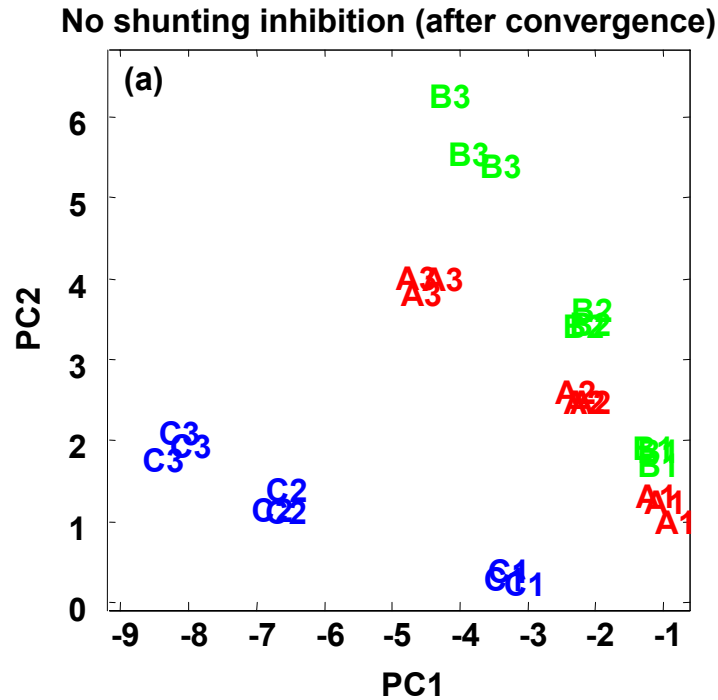
Fig. 36: PCA scatterplot of SOM activity following normalization with the shunting inhibition network (A1: lowest concentration of analyte A, C3: highest concentration of analyte C). Model parameters *B=1, D=0.1*. (a) PCA scatterplot of steady-state activity across the network after chemotopic convergence (no shunting inhibition) (b) PCA scatterplot of steady-state activity across the network with *local* shunting inhibition (c) PCA scatterplot of steady-state activity across the network with *global* shunting inhibition.
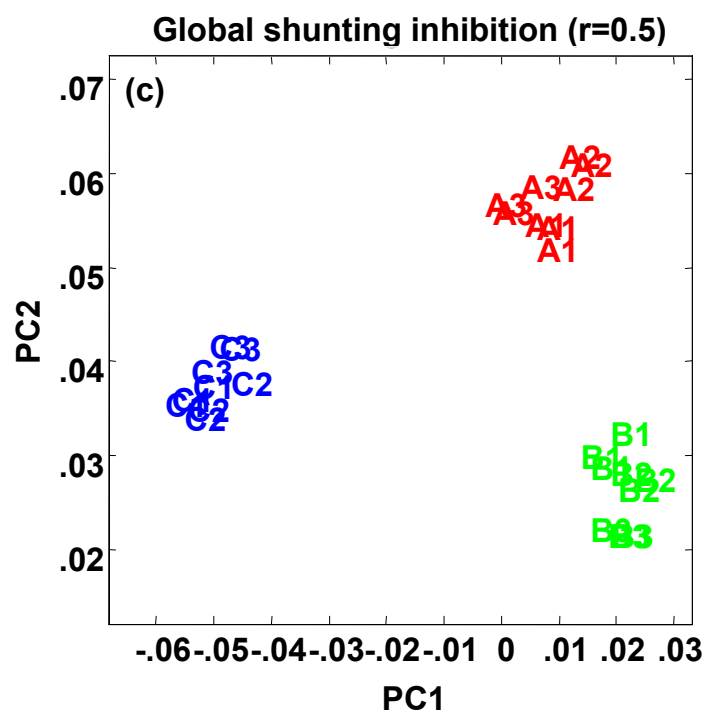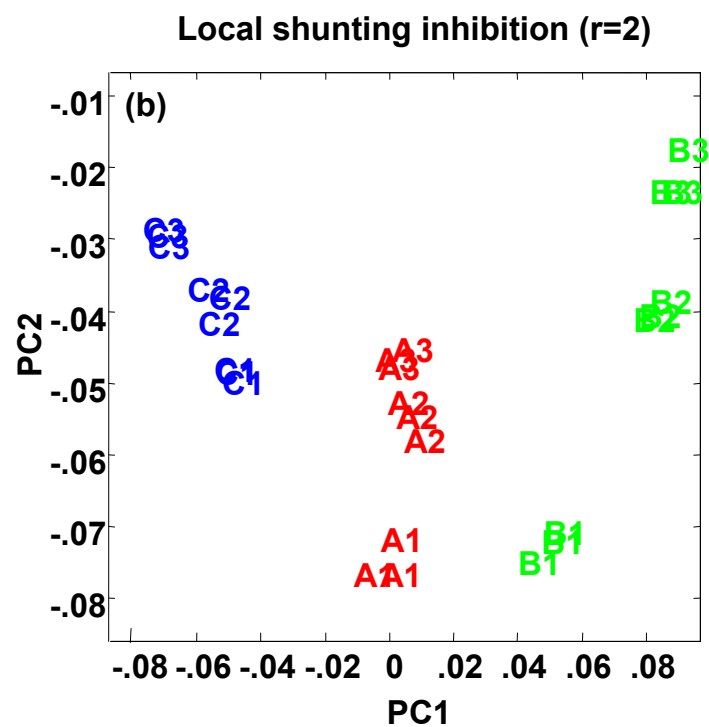
(Fig. 36: continued)

IV.2.1. Characterization of the model

Based on the class separability measure in Chapter III, we define two different measures to quantify the performance of the model: concentration-invariant separability and concentration information. Assuming a three-odor problem (merely to simplify the notation), the *concentration-invariant separability* is measured by:

$$J_{odor} = w_1 J_{AB} + w_2 J_{BC} + w_3 J_{CA} \tag{4.5}$$

where J_{AB}, J_{BC}, and J_{CA} are the separability between odors A and B, B and C, and C and A, respectively, and w_1, w_2, and w_3 are normalization weights to prevent any pair of odors from dominating the metric.

The *concentration information* within each odor class is defined by:

$$J_{conc} = w_4 J_{a1a2a3} + w_5 J_{b1b2b3} + w_6 J_{c1c2c3} \tag{4.6}$$

where J_{a1a2a3}, J_{b1b2b3}, and J_{c1c2c3} are the separability among the three concentrations within an odor, and w_4, w_5, and w_6 are normalization weights to balance the relative contribution of these three terms. The normalization weights are set as the inverse of the maximum possible value of the corresponding term across all values of r, the width of lateral connections (e.g. $w_1 = \dfrac{1}{\max\limits_{\forall r}(J_{AB})}$). This scales each term J_{AB}, J_{BC}, J_{CA}, J_{a1a2a3}, J_{b1b2b3}, J_{c1c2c3} between 0 and 1 making their contribution to J_{odor} and J_{conc} comparable.

IV.2.2. Spread of the lateral connections (r)

In this section we characterize the width of lateral inhibition using the two separability measure proposed in the previous section. Fig. 37(a) shows the *concentration-invariant*

separability measure (J_{odor}) as a function of the width of the shunting inhibitory connections. Maximum separability between odors is achieved for small *r* (global connections). Global connections remove most of the concentration information, a result that follows from the steady-state response in equation (4.3) and is also consistent with the scatterplot in Fig. 36(c). In contrast, reduction in the width of the shunting inhibition allows the within class-scatter to increase, thereby reducing J_{odor}.

Fig. 37(b) shows the *concentration information* measure (J_{conc}) as a function of the width of the shunting inhibitory connections. Maximum separability is achieved for no shunting inhibition (*r=20*; i.e., the size of the lattice). In this case, concentration information serves as the principal source of variance, as was shown in Fig. 36(a). As the connections become global, most of the concentration information is removed. In between the two extremes, different degrees of separability can be achieved among concentration levels of the same odor.

In summary, the width of the lateral inhibition can be used to select an appropriate tradeoff between odor class information (between class-scatter) and odor concentration information (within class-scatter). This prediction is consistent with recent work by Christensen et al. (2001) suggesting that local neurons (analogous to PG cells) in the antennal lobe (analogous to the mammalian olfactory bulb) of sphinx moth can operate as multifunctional units, causing local inhibition at lower odor concentrations and global inhibition at higher concentrations. Their study is particularly relevant to this work as it identifies a possible biological mechanism for modulating

inhibitory width. The model can therefore be used to predict the effect that modulation of inhibitory width may have during the processing of odor signals.
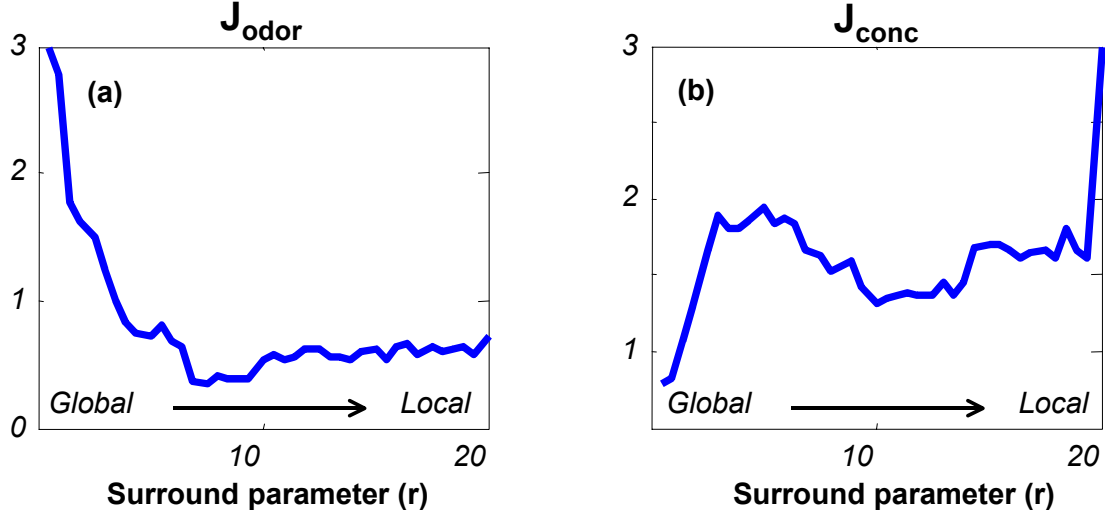
Fig. 37: Characterization of the model; small *r* represents global connections, and large *r* represents local connections. (a) Measure of concentration-invariant separability (J_{odor}) as a function of the width of shunting lateral inhibition. (b) Measure of concentration information (J_{conc}) as a function of the width of shunting lateral inhibition.

IV.2.3. Rate of exponential decay (D)

Fig. 38(a, b) shows the *concentration-invariant separability* and *concentration information* measures as a function of decay rate *D*. For small value of *D* ($D << \sum_{k} G_{k}^{O}$), the model achieves concentration compression similar to the L1 norm, thereby improving separability between odors as shown in Fig. 38(a). For large *D* values ($D >> \sum_{k} G_{k}^{O}$), the steady state response of the model is a scaled version of its

inputs and hence the model retains all the concentration information, as shown in Fig. 38(b). Therefore, for a fixed spread of lateral connections, the exponential decay rate D can also be used to control the amount of concentration compression. These results suggest that the time constant of the PG cells may have a role in the degree of normalization performed by the network. This prediction has yet to be confirmed by experimental studies on animal models.
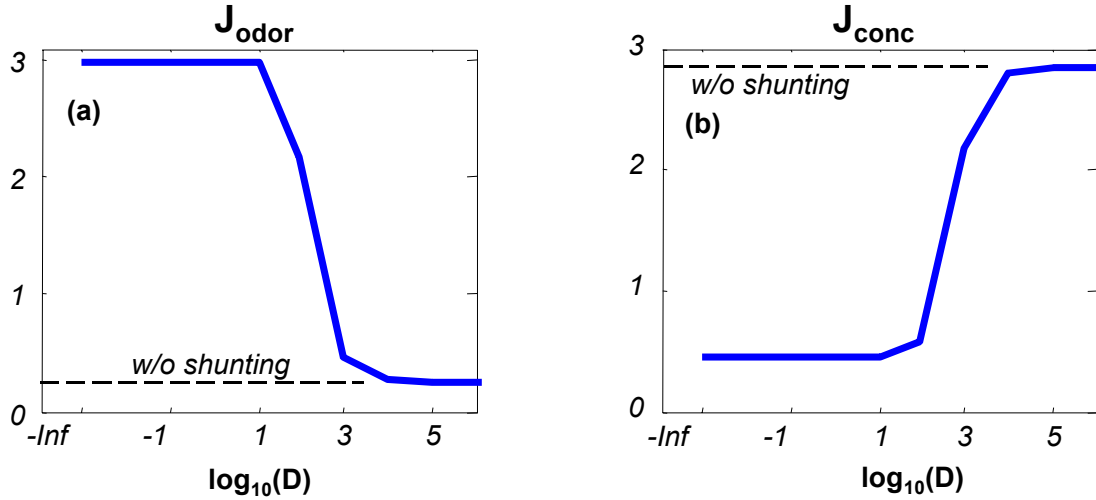
Fig. 38: Characterization of the exponential decay rate (D) (a) Measure of concentration-invariant separability (J_{odor}) as a function of the decay parameter D. (b) Measure of concentration information (J_{conc}) as a function of the decay parameter D. (model parameters $r=0.5$ and $c_{ki}=1 \ \forall \ k,i$). Dashed line indicates separability without shunting-inhibition normalization.

IV.3. Summary

In this chapter, we have presented a neurodynamic model of the first stage of lateral inhibition in the olfactory bulb, that mediated by periglomerular interneurons. Our results show that global connections remove most of the concentration information, increasing the separability between odors. Local connections, on the other hand, retain most of the concentration information at the expense of discriminatory power among odor classes. Thus, different degrees of concentration normalization can be achieved by modulating the width of the lateral connections (or the rate of decay of the neurons). We have analyzed the role of periglomerular inhibition in isolation. Next, we present an additive model of OB lateral interactions for further contrast enhancements and their integration with the gain control circuits.

CHAPTER V

CONTRAST ENHANCEMENT THROUGH CENTER ON-OFF SURROUND LATERAL INHIBITION

Following shunting inhibition, glomerular inputs are further transformed by a layer of additive lateral interaction between mitral and inhibitory granule (G) cells at the output of the OB (Freeman 1983). Two roles have been suggested for this granule-mediated circuit: (i) sharpening of the molecular tuning range of individual mitral cells (Mori et al. 1999), and (ii) global redistribution of activity (Laurent 1999). According to the latter hypothesis, it is the bulb-wide representation of an odorant that becomes specific and concise over time, rather than the tuning range of individual mitral cells. More recently, granule-mediated circuits have been found to be center on-off surround inhibitory (Aungst et al. 2003; Luo and Katz 2001; Lei et al. 2004), an organization reminiscent of the classical receptive fields mediated by ganglion cells in the retina (Kuffler 1953). This form of lateral inhibition performs a winner-take-all competition, where strongly excited units suppress weakly excited ones. In this chapter, we present a computational model of these lateral inhibitory circuits for contrast enhancement of the spatial patterns obtained through chemotopic convergence. We validate the model on the *Selectivity* and *Illumina* datasets.

V.1. Additive lateral inhibition model

We capture this center on-off surround circuit with the classical additive model of Grossberg (Haykin 1999, p. 676), whose general form is:

$$\frac{dv_j(t)}{dt} = -\frac{v_j(t)}{\tau_j} + \sum_{k=1}^{M} L_{kj}\varphi\big(v_k(t)\big) + I_j \tag{5.1}$$

where v_j is the activity of mitral neuron j, τ_j is the time constant that captures the dynamics of the neuron, L_{kj} is the synaptic weight between neurons k and j, M is the number of neurons, and I_j is the external input in equation (5.1) properly scaled to balance the contribution of receptor and lateral inputs ($I_j = 10G_j$). Our model assumes a one-to-one mapping between GL and mitral neurons (refer to Fig. 39); although in some animal species GL are known to project to several mitral neurons, the computational function of this divergence mapping is largely unknown. The non-linear activation $\varphi(\cdot)$ is the logistic function defined by:

$$\varphi(v_j) = \frac{1}{1 + \exp(-a_1 \cdot (v_j - a_2))} \tag{5.2}$$

where the constants a_1 and a_2 are adjusted to match the dynamic range of the input signals. For simplicity, all mitral neurons are assumed to have the same time constant $\tau=10ms$.
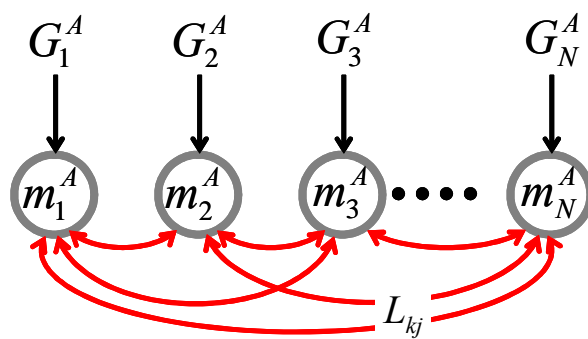
Fig. 39: Additive lateral inhibition at the output of the olfactory bulb.

Integration of equation (5.1) with Euler's method leads to a difference equation:

$$v_j(t + \Delta t) \cong v_j(t) + \Delta t \frac{dv_j(t)}{dt} =$$

$$\left(1 - \frac{\Delta t}{\tau}\right) v_j(t) + \sum_{k=1}^{M} L_{kj} \varphi(v_k(t)) \Delta t + I_j \Delta t$$

(5.3)

where the integration time step Δt is set to *1ms*.

To model center on-off surround, each neuron makes excitatory synapses to nearby units, and inhibitory synapses with distant units as follows:

$$L_{kj} = \begin{cases} U(a,b) & d(k,j) \leq \dfrac{\sqrt{M}}{r} \\ U(-b,a) & \dfrac{\sqrt{M}}{r} < d(k,j) < \dfrac{2\sqrt{M}}{r} \\ 0 & d(k,j) \geq \dfrac{\sqrt{M}}{r} \end{cases}$$

(5.4)

where $U(a,b)$ is a uniform distribution between *a* and *b*, *d* is the distance between units measured as a Euclidean distance within the lattice ($d = \sqrt{(row_k - row_j)^2 + (col_k - col_j)^2}$; *row* and *col* being the row and column coordinates of a neuron in the lattice), and *r* determines the receptive-field width of the lateral connections. Thus, the output of a given mitral neuron is determined by the combined effect of external inputs from ORNs, center on–off surround interactions with collateral neurons, as well as by its own dynamics. An example of the center on-off surround receptive field described by equation (5.4) is shown in Fig. 40.
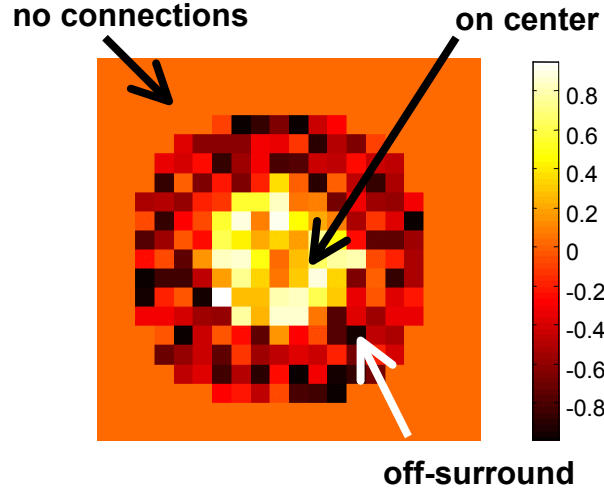
Fig. 40: An example center on-off surround receptive field in a 20x20 lattice for *r=5*.

V.2.   Validation on the Selectivity dataset

Following the convergence model described in Chapter III, temperature-modulated sensor patterns are first chemotopically projected onto a GL layer with 400 nodes, arranged as a 20x20 SOM lattice. The 400 outputs of the convergence model are used as inputs to the center-surround OB network. The parameter a_1 and a_2 of the non-linear activation function are set to *0.0336* and *60.0335* respectively to match the dynamic range of the input signals.   A systematic study of the improvements in pattern separability provided by the OB model as a function of the width of center-surround connections is presented next.

V.2.1. Effect of receptive field width for the center surround connections

The width of the center on-off surround connections is an important parameter for the purpose of pattern formation and generalization. An appropriate value for receptive field

width must provide both stability and good separability. Though the exact optimal value may depend on the database used, the general characteristics described below hold across various databases.

Fig. 41(a-c) shows the measures of concentration-invariant recognition (J_{odor}), concentration separability (J_{conc}), and their combination $J_{balance}$ ($J_{balance} = J_{odor} + J_{conc}$) as a function of the receptive field widths. Small receptive fields (*r>4*) are primarily driven by inputs and hence show high stability (converge to a fixed-point attractor) and less variance. For large receptive fields (*r≤4*), the net value of the lateral connections becomes excitatory, and the system fails to converge into fixed-point attractors. Hence we will not consider them for determining the optimal parameter value for this odor database.

Fig. 41(a,b) shows the separability between various odors (J_{odor}) and across different concentrations within each odor (J_{conc}) as a function of the receptive field width (*r*). From these results, it is clear that that the separability between pairs of odors increases as the width of the receptive field increases, whereas maximum concentration separability is achieved with small receptive fields. The maximum of the objective function $J_{balance}$, which combines concentration-invariant separability and concentration separability, occurs at *r=5*, as shown in Fig. 41(c). This receptive field width will be used to quantify the benefits of the proposed model.
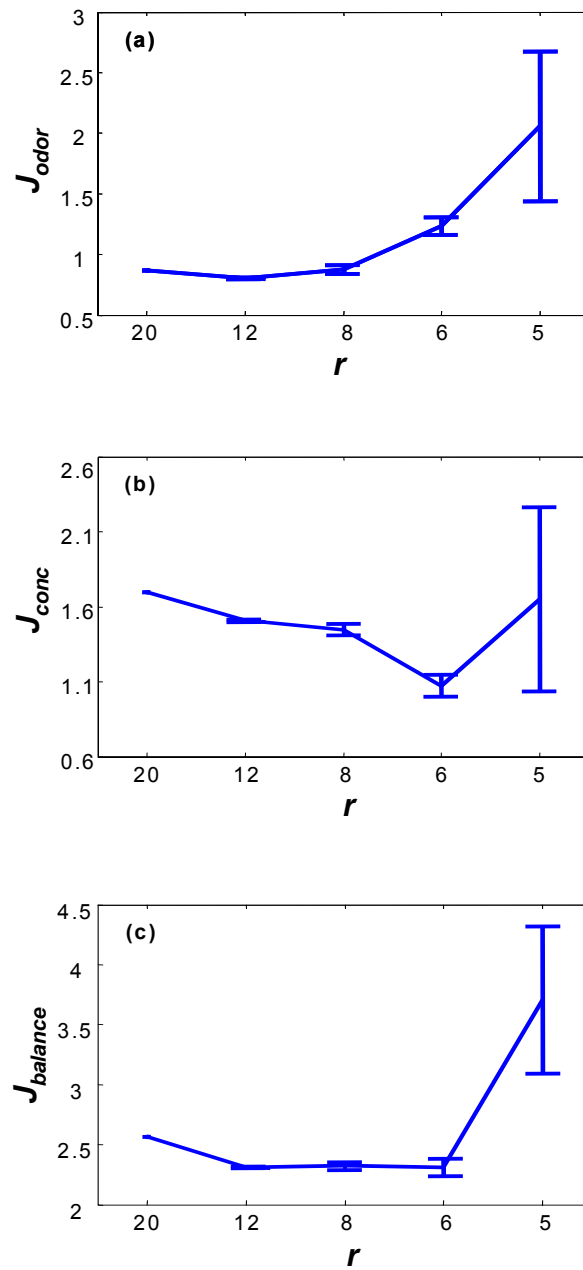
Fig. 41: Discriminatory information of GL patterns as a function of receptive field width: (a) separability between odors J_{odor} (b) separability between concentrations within an odor J_{conc}, and (c) separability across odors and across concentrations (*Selectivity dataset*).

The steady-state spatial patterns for various receptive field widths (*r>4*) are shown in Fig. 42. Global connections lead to sparse representation (fewer active mitral cells) since highly active GL regions are able to suppress activity in other regions in the lattice with weak activity. This causes reduction in the overlap across patterns and improves odor separability.
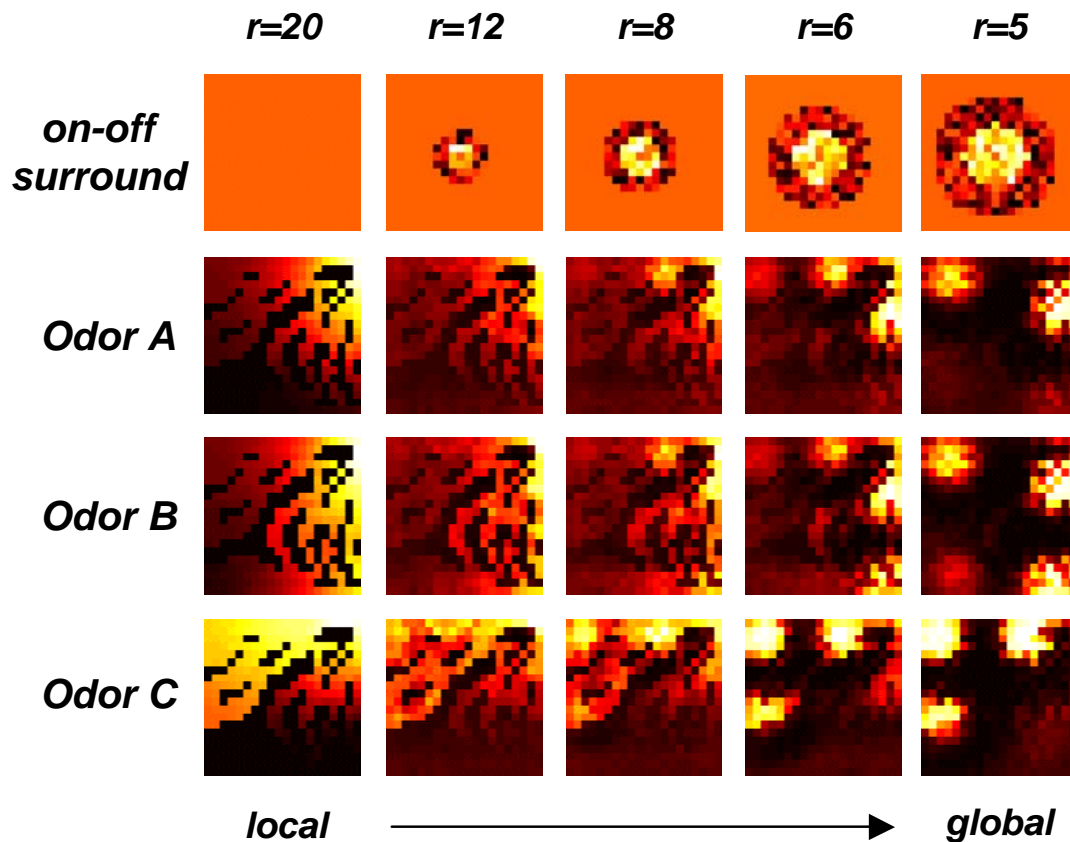
Fig. 42: Characteristics of the spatial odor code for various receptive-field widths of center on-off surround lateral connections. Global connections result in more sparse patterns that provide better odor separability.

V.2.2. Spatial patterning of MOS sensor responses

In this section we qualitatively analyze the improvements in pattern separability that result from the center on-off surround connections ($r=5$). Fig. 43 (top row of each block) shows the spatial pattern that result from sensory convergence at the input of the OB. As a result of the chemotopic mapping, each odor generates a unique spatial pattern across units in the SOM. However, these spatial patterns are highly overlapping due to the collinearity of the sensors. Fig. 43 (bottom row of each block) shows the resulting spatial activities following stabilization of the center-surround lateral interactions in equation (5.1). Odor A leads to heavy activation on two highly-localized regions (spatial code: 13). Odor B produces similar activation in regions 1 and 3, but also high activation in region 4 (spatial code: 134). This unique region 4 corresponds to pseudo-sensors in the smaller peak that occurs for odor B alone (refer Fig. 18). Odor C produces heavy activation of regions 1, 2 and 5 (spatial code: 125). It is important to note that the location of these activation regions is concentration-invariant, but their amplitude and spread increases with concentration, in consistency with recent finding in neurobiology (Friedrich and Korsching 1997).
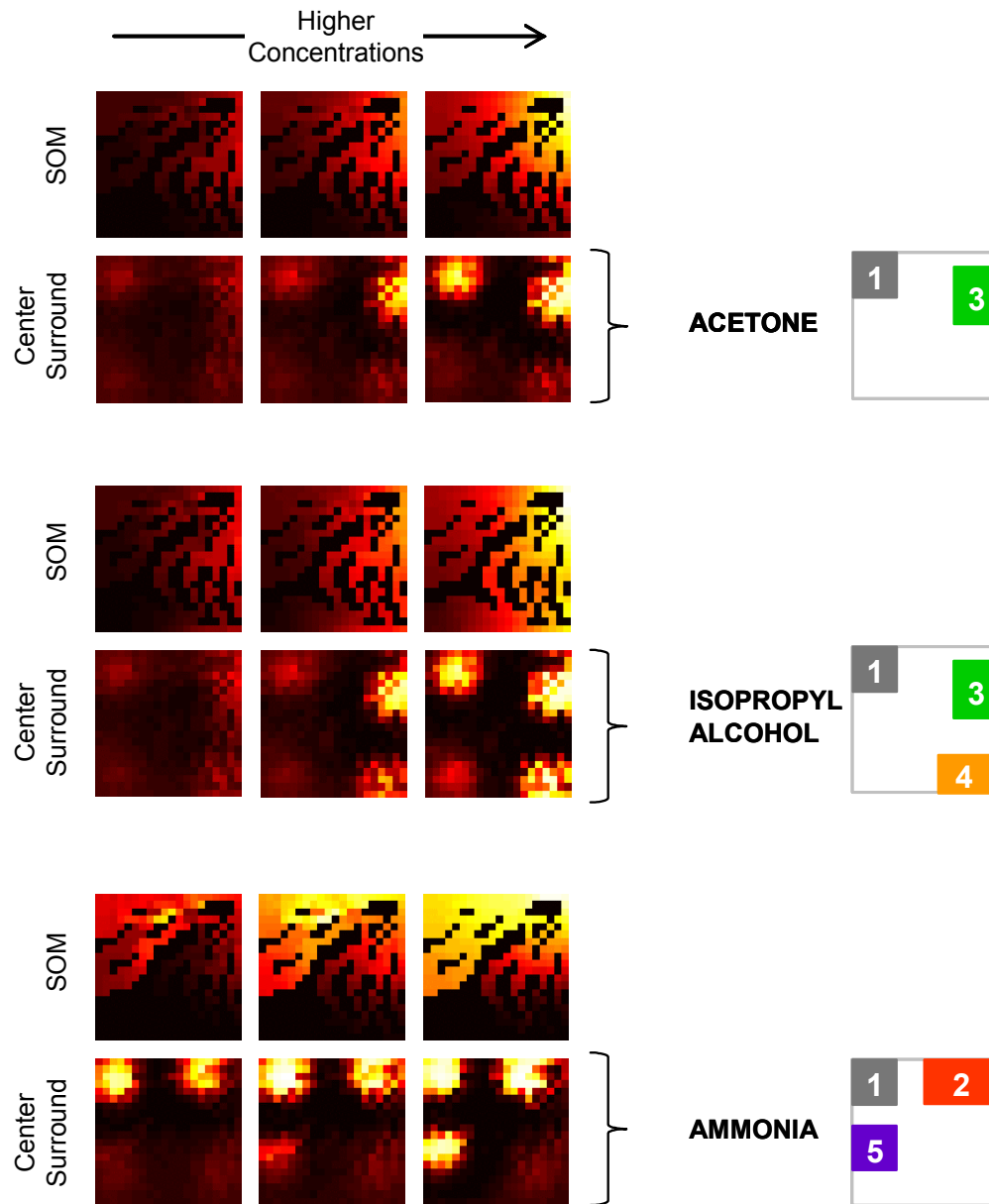
Fig. 43: Spatial maps generated from temperature modulated MOS sensor response at the input (top row of each block) and output (bottom row of each block) of the olfactory-bulb network. Three blocks are shown corresponding to three odors: acetone (first block), isopropyl alcohol (second block) and ammonia (third block). Five sparse coding regions that emerge as a result of the lateral interactions are shown on the right.

V.2.3. Temporal evolution of the odor trajectories

The spatial patterns in Fig. 43 only describe the information content in the steady-state response of the model. To analyze the temporal trajectory of each dynamic attractor, the 400-dimensional (20x20) space was projected onto the first three principal components of the data, which are shown in Fig. 44. Trajectories for each odor and concentration originate at nearby locations in state space, which correspond to the highly overlapping spatial patterns at the input of OB, shown in Fig. 43 (top row). As a result of center on-off-surround lateral connections, the activity for each odor slowly moves away from the initial location and settle into odor-specific fixed-point attractors, which correspond to the localized spatial patterns in Fig. 43 (middle row).

Visual inspection of the steady-state response in Fig. 43 and the transient trajectories in Fig. 44 clearly shows that the lateral inhibitory network is able to significantly increase the contrast between different odors. Parallels between this odor code and recent findings in neurobiology are discussed in section V.2.4. The separability of these patterns is analyzed systematically in section V.2.5.
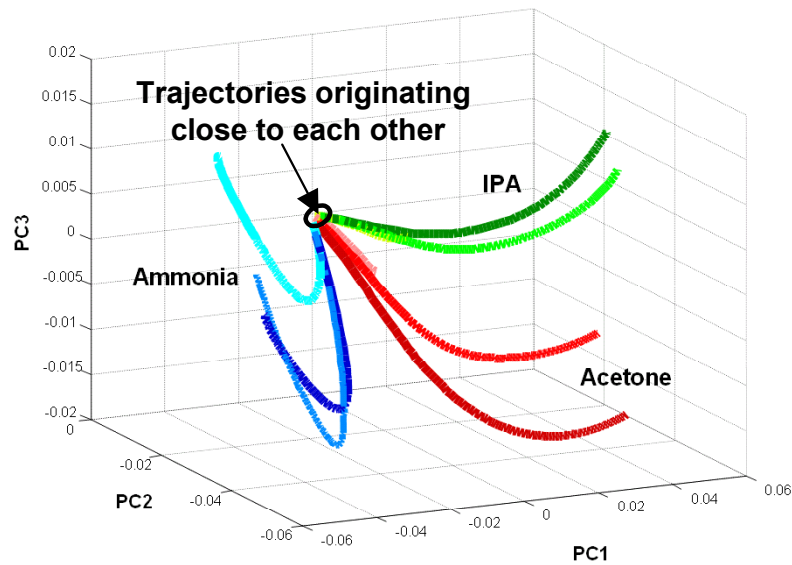
Fig. 44: Evolution of OB activity along the first three principal components of the data. Nine trajectories are shown, one per odor and concentration in the data. The initial points in the trajectories are the spatial maps at the input of the OB network. Odor separability is improved as a result of lateral inhibition.

V.2.4. Discussion: Temporal coding in the biological olfactory system and our model

A recent study of spatio-temporal activity of projection neurons (PN) in the honeybee antennal lobe (analogous to M cells in mammalian OB) by Galan et al. (2003), reveals evolution and convergence of the network activity into odor-specific attractors. Fig. 45(a) shows the projection of the spatio-temporal response of the twenty-one PNs along their first three principal components. These trajectories begin close to each other, and evolve over time to converge into odor specific regions. These experimental results are consistent with the attractor patterns emerging from our model. Furthermore, in-vivo

experiments conducted by Stopfer et al. (2003), to study odor identity and intensity coding in the locusts show hierarchical groupings of spatio-temporal PN activity according to odor identity, followed by odor intensity. Fig. 45(b) illustrates this grouping in the activity of fourteen PNs when exposed to three odors at five concentrations. Again, these results closely resemble the grouping of attractors in our model, shown in Fig. 44.
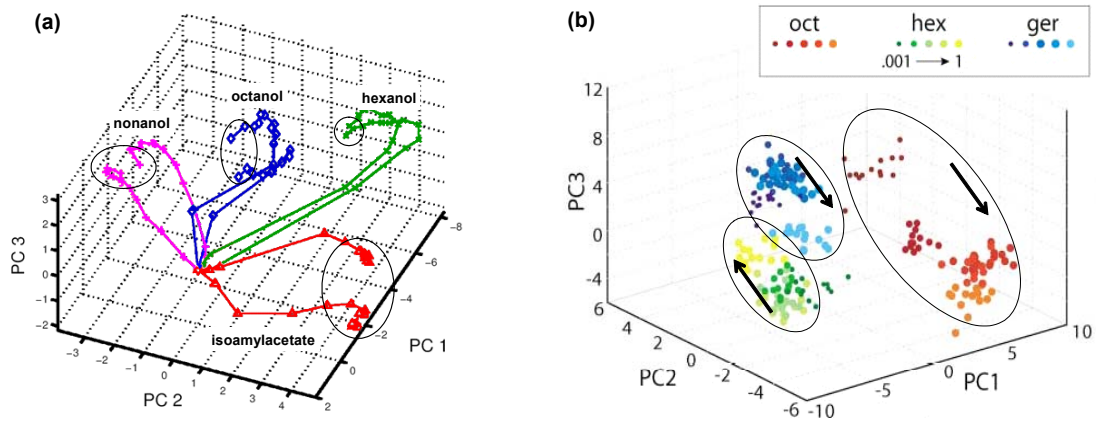
Fig. 45: (a) Odor trajectories formed by spatio-temporal activity in the honeybee AL (adapted from Galan et al. 2003). (b) Identity and intensity clustering of spatio-temporal activity in the locust AL (adapted from Stopfer et al. 2003); arrows indicate the direction of increasing concentration.

V.2.5. Temporal evolution of pattern separability

To illustrate the benefits of the proposed model, we compare the resulting pattern-separability against that which is available (1) from raw sensor data, (2) following chemotopic convergence, (3) at the output of the OB network without lateral connections, and (4) at the output of the OB network with random lateral connections. Fig. 46(a-c) shows the temporal evolution of the separability measures J_{odor}, J_{conc} and $J_{balance}$ for each of these cases. Fig. 46(a) indicates that chemotopic convergence provides better concentration-invariant separability than raw temperature-modulated signals. On the other hand, Fig. 46(b) shows that random connections can in some cases provide better concentration discrimination than center-surround connections, but have significantly lower concentration-invariant separability as shown in Fig. 46(a). Overall, center on-off surround lateral connections (three repetitions are shown using different initial weights) provides maximum contrast between odor patterns amongst the compared schemes, and yields maximum value for the joint objective function $J_{balance}$ as shown in Fig. 46(c).
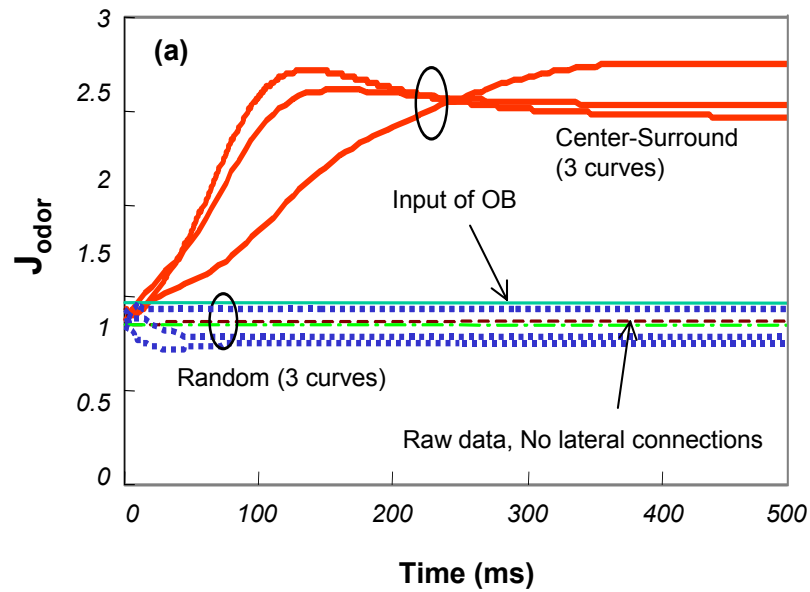
Fig. 46: Comparison of the additive model of OB lateral inhibition with center-surround lateral connections (three repetitions are shown) against (1) raw temperature-modulated data, (2) following chemotopic convergence, (3) at the output of OB with no lateral connections, and (4) at the output of OB with random lateral connections (three repetitions). (a) Concentration-invariant recognition measure J_{odor}, (b) concentration discrimination measure J_{conc}, and (c) balanced measure $J_{balance}$.
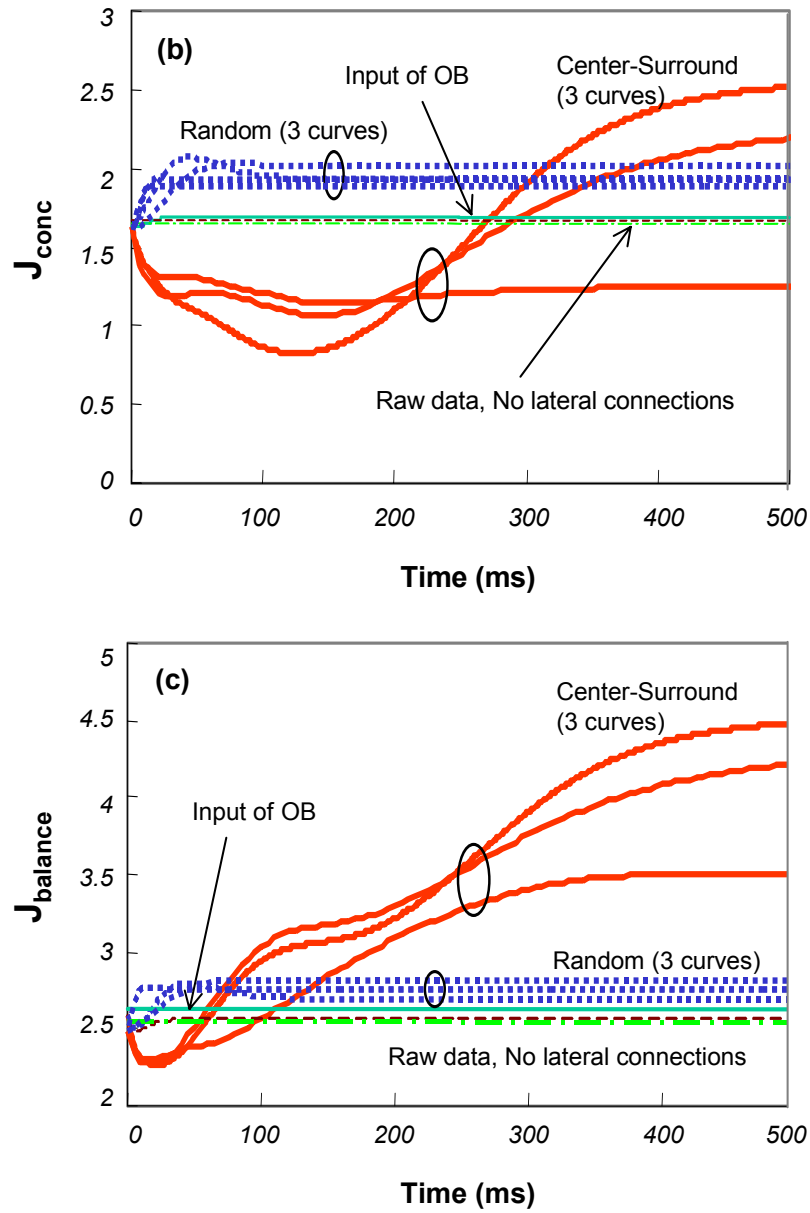
(Fig. 46: continued)

V.3. Validation on the Illumina dataset

In this section, we characterize the center-surround lateral inhibition model on the *Illumina* dataset and present the improvements in odor separability achieved on this

dataset. The microbead array response is chemotopically projected onto a GL layer with 400 nodes, arranged as a 20x20 SOM lattice. The outputs of the convergence model are then used as the input for the neurodynamic OB model. The parameter a_1 and a_2 of the non-linear activation function are set to *0.0589* and *49.9999* respectively to match the dynamic range of the input signal from microbead arrays. The appropriate lateral inhibition spread (parameter *r*) is determined experimentally in a manner similar to the previous study on the *Selectivity* dataset. Results are shown in Fig. 47; separability between pairs of odors increases with the receptive field width till *r=5*. For receptive field width greater than *r=5*, small variations in the inputs are amplified considerably increasing the within-class scatter.
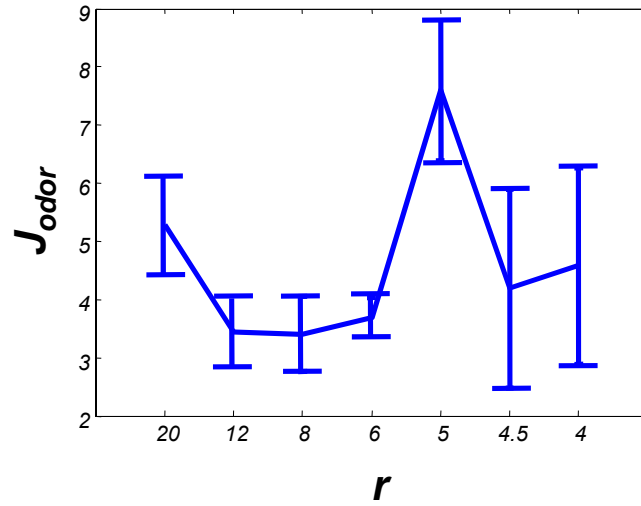
Fig. 47: Discriminatory information of GL patterns as a function of receptive field width (*r*). Since the dataset contains the response of the optical microbeads to a single concentration of five odors, the optimum center-surround width (*r*) can only be selected based on odor separability (J_{odor}).

V.3.1. Spatial patterning of microbead array responses

In this section, we qualitatively analyze the improvements in pattern separability that result from the center on-off surround connections ($r=5$). Fig. 48 (top row) shows the spatial patterns that result from sensory convergence at the input of the OB to five odors: (i) acetone (ACE), (ii) ehtyl alcohol (EA), (iii) ethyl hydroxide (Et-OH), (iv) methyl hydroxide (Me-OH) and (v) toluene (TOL). Each odor generates a unique spatial pattern across SOM units. Fig. 48 (middle row) shows the resulting spatial activities following stabilization of the center-surround lateral interactions. ACE leads to heavy activation on four highly-localized regions (spatial code: 123'4). EA and Et-OH produce similar activation as ACE in regions 2 and 4, but produce slightly different activation in regions 1 and 3 (spatial code: EA - 1'234; Et-OH - 1'234). Me-OH produces heavy activation of region 3 alone (spatial code: 3). TOL produces heavy activation of region 1, 2 and 4 (spatial code: 124). The spatial patterns after center-surround interactions are sparser than the chemotopic odor maps and provide better odor separability.
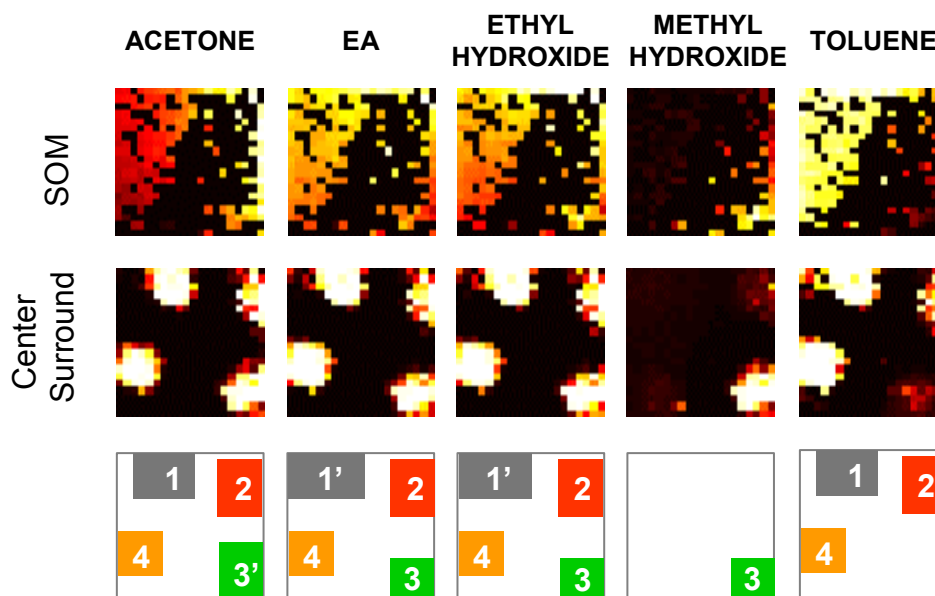
Fig. 48: Spatial maps at the input (top row) and output (middle row) of the OB network for the *Illumina dataset*. The bottom row shows the four sparse coding regions that emerge as a result of the lateral interactions.

V.3.2. Temporal patterning

To study the temporal odor code, the 400-dimensional (20x20) OB model response is projected onto the first three principal components of the data, as shown in Fig. 49. Trajectories for each odor sample originate at nearby locations in state space. As a result of center on-off-surround lateral connections, the activity for each odor slowly moves away from the initial location and settles into odor-specific fixed-point attractors. The repeatability of the odor trajectories is illustrated by visualizing all twenty-five trajectories (five samples per odor) in the dataset. These results are qualitatively similar to those obtained on the *Selectivity* dataset (Fig. 44).
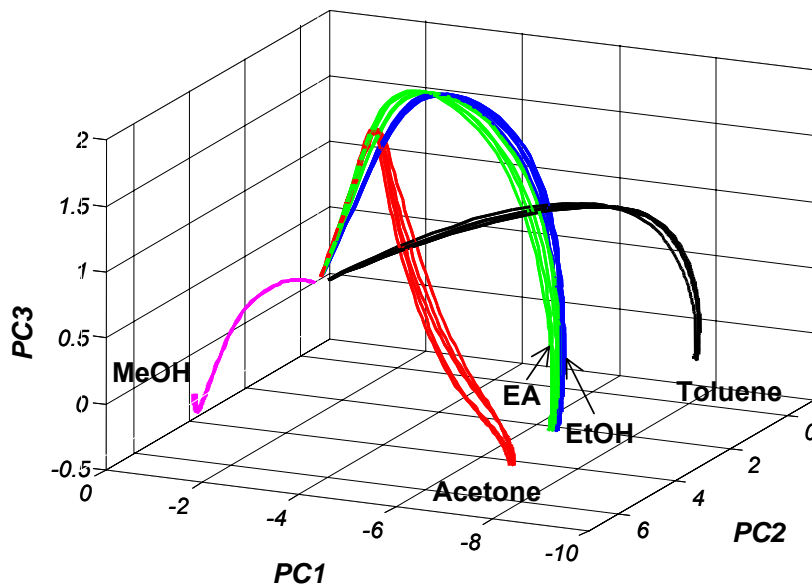
Fig. 49: Evolution of OB activity for the *Illumina dataset* along the first three principal components. Twenty-five trajectories are shown, one per odor sample in the dataset. The initial points in the trajectories are the spatial maps at the input of the OB network, shown in Fig. 48 (top row). Odor separability is improved as a result of lateral inhibition.

V.3.3. Temporal evolution of pattern separability

To illustrate the benefits of the proposed model, we compare the resulting pattern-separability against that which is available (1) from raw sensor data, (2) following chemotopic convergence, (3) at the output of the OB network without lateral connections, and (4) at the output of the OB network with random lateral connections. Fig. 50 shows the temporal evolution of the odor separability for each of these cases. Similar to the results observed in the *Selectivity* dataset, center on-off surround lateral

connection provides maximum contrast between odor patterns amongst the compared schemes.
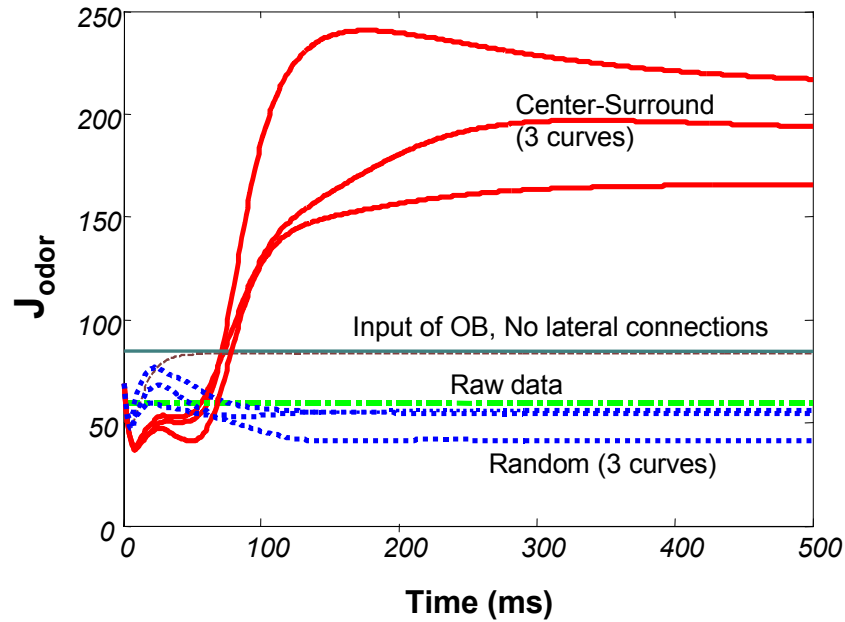
Fig. 50: Comparison of the OB network with center-surround lateral connections (three repetitions are shown) against (1) raw temperature-modulated data, (2) following chemotopic convergence, (3) at the output of OB with no lateral connections, and (4) at the output of OB with random lateral connections (three repetitions).

V.4. Summary

In this chapter, we have presented an additive model of lateral inhibition with center on-off surround receptive fields to model the circuits at the output of the bulb. This network is able to significantly reduce the overlap between the spatial odor patterns, and produces a sparser representation on a few selected mitral cells. The spatial and temporal odor code resulting from the center-surround interactions are consistent with

recent results from neurobiology. The next stage of processing involves synthetic processing of the odor signals in the cortex, and modulatory feedback to the bulb.

CHAPTER VI

MIXTURE SEGMENTATION AND BACKGROUND SUPPRESSION THROUGH BULB-CORTEX INTERACTION

The last two olfactory primitives are concerned with the recognition of odorants against complex backgrounds, and the identification of the constituents in an odor mixture. Several studies have suggested that cortical feedback to the bulb may play an essential role in achieving these computational functions. Ambrose-Ingerson et al. (1990) have modeled the cortical feedback connections to account for hierarchical recognition of odors by humans. In this model, cues common to a subset of odorants are recognized before those that are odorant-specific. Li and Hertz (2000) have shown that centrifugal connections may cause odor-specific adaptation, leading to segmentation of odor mixtures. Grossberg (1976) has proposed that cortical connections to the bulb may selectively filter the bulb input and cause resonance between the two regions. Finally, Yao and Freeman (1990) have implicated these feedback connections with chaotic dynamics in the bulb. In this chapter, we will present a model of olfactory bulb–cortex interaction, and show that two different computational functions can be achieved (mixture segmentation, weaker odor/background suppression) depending upon the learning rule used to establish the cortical feedback connections to the bulb: anti-Hebbian or Hebbian, respectively. We validate these computational models to handle odor mixture signals on simulated odor patterns.

VI.1. Model of bulb-cortex interaction

The olfactory bulb sends non-topographic and many-to-many projections to the olfactory cortex. These convergent and divergent (many-to-many) projections suggest that cortical neurons detect combinations of co-occurring molecular features of the odorant, and therefore function as "coincidence detectors" (Wilson and Stevenson 2003). Fig. 51 illustrates the synthetic processing of odor signals through coincidence detection mechanism in the cortex. Since the number of possible combinations to be detected is extremely large, Laurent (1999) has suggested that these cortical cells perform a random sampling of this space. In our model with only few neurons, we simplify these circuits, and manually label the cortical cells to detect combinations of features for the odors in our datasets.

Apart from these forward connections, the cortex is characterized by excitatory and inhibitory lateral connections that are known to play an important role in the storage of odors with minimum interference and pattern completion of degraded stimuli (Wilson and Bower 1988). Together, these two architectural features of the piriform cortex (many-to-many connection from OB, and lateral association connections between cortical cells) form the basis for the synthetic processing of odors (Wilson and Stevenson 2003).
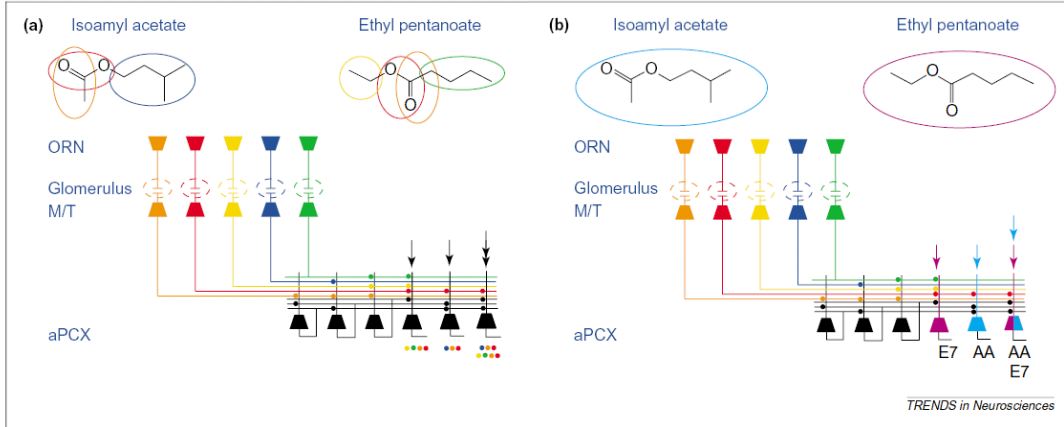
Fig. 51: Synthetic processing by the cortical neurons through coincidence detection mechanism. (a) In response to a new odor the cortical neurons detect a particular combination of co-occurring molecular features identified by the mitral cells. (b) Adaptation of the afferent and association connections through learning enables the cortical neurons respond to odors as a whole when presented subsequently (reprinted from Wilson and Stevenson 2003).

We model these olfactory circuits using an additive model, similar to the olfactory bulb model presented in Chapter V, as follows:

$$\frac{dy_i^O(t)}{dt} = -\frac{y_i^O(t)}{\lambda_i} + \sum_{\substack{k=1 \\ k \neq i}}^{P} AC_{ki}\varphi\left(y_k^O(t)\right) + \sum_{j=1}^{M} FF_{ji}\varphi\left(v_j^O(t)\right) \tag{6.1}$$

where y_j is the activity of cortical pyramidal neuron i, λ_i is the time constant of the neuron, AC_{ki} is the synaptic weight between neurons k and i obtained through Hebbian learning, P is the number of neurons, FF is the feedforward connectivity matrix established through Hebbian learning, and v_j is the activity of bulb neuron j.

Feedforward connections *FF* from bulb to cortex are established through a simple Hebbian learning rule as follows:

$$FF = \delta(VY^T) \qquad (Hebbian) \qquad (6.2)$$

where *Y* is the matrix of cortical neuron outputs to different pure odors (row vectors manually labeled to recognized different odors), *V* is the matrix of bulb neuron outputs to pure odors (row vectors), and δ is a scaling parameter.

Associational connections *AC* within cortex are established through a Hebbian update rule proposed in (Gutierrez-Galvez and Gutierrez-Osuna 2005) as follows:

$$AC = \alpha \cdot \sum_{O_1=1}^{N} Y^{O_1} \cdot (Y^{O_1})^T - \beta \cdot \sum_{O_1=1}^{N} \sum_{\substack{O_2=1 \\ O_2 \neq O_1}}^{N} Y^{O_1} \cdot (Y^{O_2})^T \qquad (6.3)$$

where Y^{O_1} is the cortical response for odor O_1, α and β are scaling parameters, which provide a necessary tradeoff between the first correlation term and the second decorrelation term. This form of update has been shown to enhance the contrast between input patterns (Gutierrez-Galvez and Gutierrez-Osuna 2005). In this case, this update rule results in associational connections such that neurons that code for *at least* one common odor have purely excitatory connections between them, and neurons that encode for different odors (no common odor) have purely inhibitory connections between them. Excitatory lateral connections perform pattern-completion of degraded inputs from the bulb (Wilson and Bower 1988), whereas the inhibitory connections introduce winner-take-all competition among cortical neurons (Xie et al. 2001).

The last component of the model involves feedback connections from the cortex to the bulb. The cortical feedback is integrated to the OB model as follows:

$$\frac{dv_j^O(t)}{dt} = -\frac{v_j^O(t)}{\tau_j} + \sum_{k=1}^{M} L_{kj}\varphi\left(v_k^O(t)\right) + I_j^O + \sum_{i=1}^{P} FB_{ij}\varphi\left(y_i^O(t)\right) \qquad (6.4)$$

where v_j is the activity of bulb neuron j, τ_j is the time constant that captures the dynamics of the neuron, L_{kj} is the synaptic weight between neurons k and j, M is the number of neurons, I_j is the external input from the olfactory epithelium, FB is the feedback connectivity matrix, and y_i is the activity of cortical neuron i.

To model these feedback connections (*FB)* in equation (6.4), we use either anti-Hebbian or Hebbian rule as follows:

$$\begin{aligned} FB &= \gamma(-YV^T) & (anti-Hebbian) \\ FB &= \gamma(YV^T) & (Hebbian) \end{aligned} \qquad (6.5)$$

where Y is the matrix of cortical neuron outputs to different pure odors (organized as row vectors), V is the matrix of bulb neuron outputs to pure odors (row vectors), and γ is a scaling parameter.

In the case of anti-Hebbian learning, all connections are initialized to *0.* The anti-Hebbian update forms feedback connections between the cortical and the bulb neurons that respond to *at least* one common odor. The resulting feedback from cortex inhibits bulbar neurons responsible for the cortical response, in a manner akin to the model proposed by Ambrose-Ingerson et al. (1990), resulting in the temporal segmentation of binary mixtures.

In the case of Hebbian learning, all connections are initialized to *−1*. The Hebbian update retains only those connections between cortical neurons and bulb

neurons that respond to different odors (no common odor). The resulting feedback from cortex inhibits bulbar neurons other than those responsible for the cortical response, causing cortical activity to resonate with OB activity as suggested by Grossberg (1976). This type of resonance allows the model to lock onto a particular odor and suppress the background/weaker odor.

VI.1.1. Illustration of the bulb-cortex interaction

Proof of concept for this model is best illustrated with an example. Let the encoding of two simulated odors at the bulb be $OB_A=[1,0,0,1,1,0]^T$ and $OB_B=[0,1,1,1,0,0]^T$, and the encoding at the cortex be $OC_A=[1,1,0,0,0,0]^T$ and $OC_B=[0,0,1,1,0,0]^T$, respectively. Using these patterns, lateral connections in the OB (not shown in Fig. 52) and associational connections within cortex (shown in Fig. 52 (a)) were established through Hebbian learning as described in the previous section. Time constants were set to 10ms and 5ms for bulb and cortical neurons, respectively. Model parameters were set as follows: $\gamma=1$ and $\delta=0.25$.
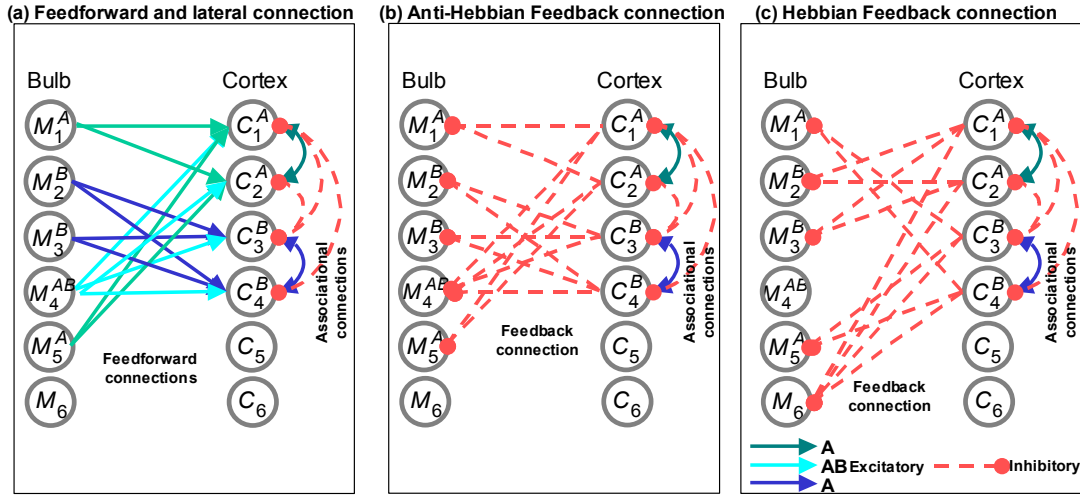
Fig. 52: Bulb-cortex interaction. (a) Lateral connections in OC are learned through Hebbian updates (single analytes used for training). (b) Feedback connections established through anti-Hebbian updates. (c) Feedback connections established through Hebbian updates.

VI.1.2. Case 1: Anti-Hebbian learning leads to temporal segmentation

Anti-Hebbian feedback connections are shown in Fig. 52(b). Note that these connections are the reverse of the forward connections in Fig. 52(a). Following learning with pure odors, the model is exposed to a mixture of odor A and B [0.8, 0.5, 0.5, 0.6, 0.8, 0.0]^T. As a result of lateral inhibition, OB activity for the stronger odor A suppresses the weaker activity of odor B. Hence odor A is first recognized by the cortex. Subsequently, feedback from cortex suppresses activity in the bulb due to odor A, allowing odor B to win the competition. To illustrate this effect, Fig. 53 shows the activity in the OB and the OC over the course of several periods. The activity of B1 and

B5, which code for odor A, become out of phase with B2 and B3, which code for odor B. The common mode B4 is removed. Further, the activity of C1 and C2, which code for odor A, becomes out of phase with C3 and C4, which code for odor B. Hence anti-Hebbian learning of centrifugal projections realizes temporal segmentation of odor mixtures in both bulb and cortex.
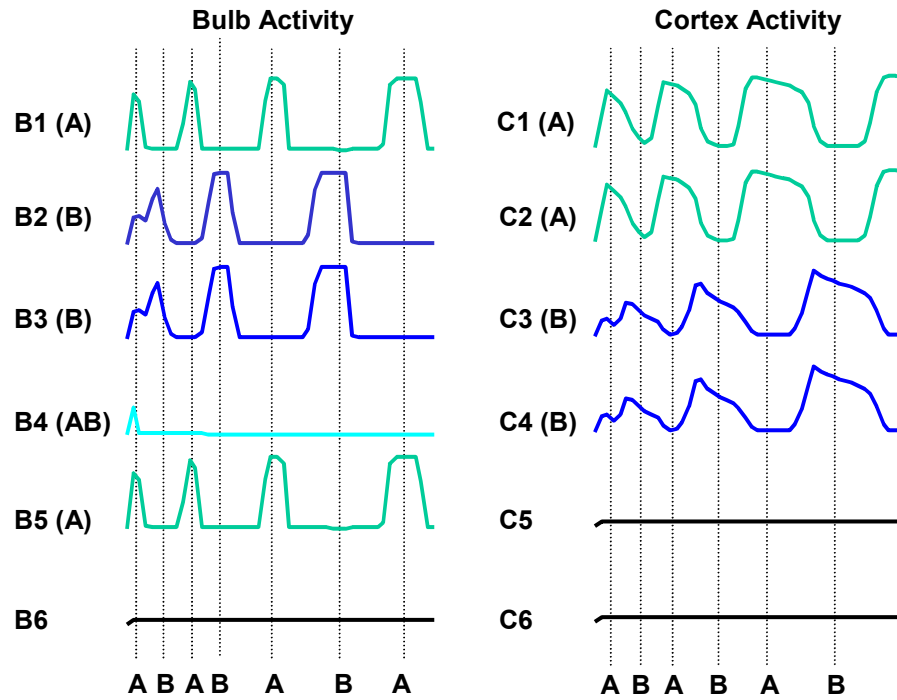
Fig. 53: Temporal segmentation of binary mixtures through anti-Hebbian feedback connections. In response to a mixture of odors A and B $[0.8, 0.5, 0.5, 0.6, 0.8, 0.0]^T$., the cortex first recognizes the stronger odor A. Subsequently, feedback from cortex suppresses activity in the bulb due to odor A, allowing odor B to win the competition. This process is repeated, allowing recognition of mixture components in alternate cycles (see odor labels below).

VI.1.3. Case 2: Hebbian learning leads to background suppression

Hebbian feedback connections are shown in Fig. 52(c). Following learning with pure odors, the model is exposed to a mixture of odors A and B [0.8, 0.5, 0.5, 0.6, 0.8, 0.0]^T. In this case, cortical feedback suppresses the weaker background odor (B) immediately and resonates with odor A, as shown in Fig. 54.
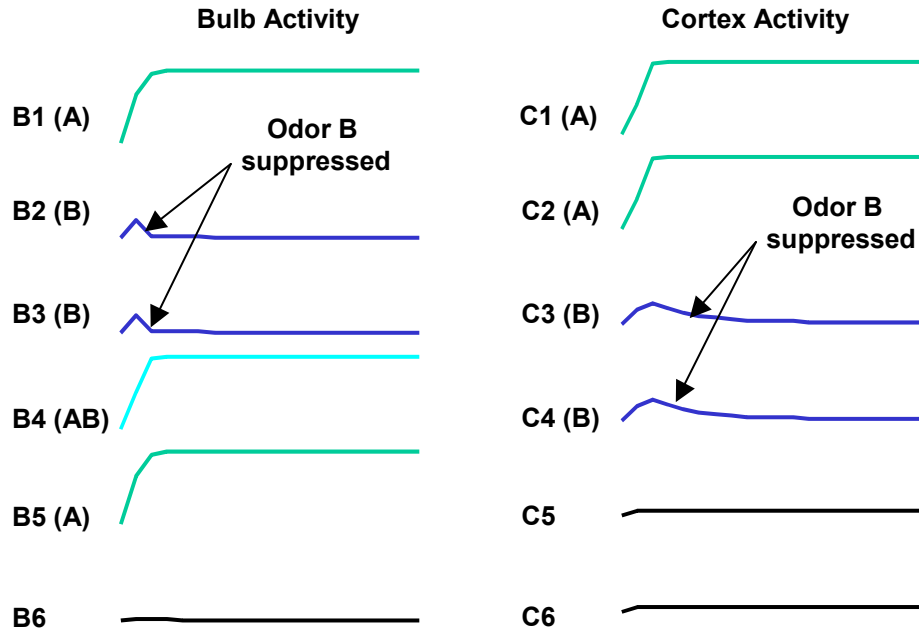
Fig. 54: Suppression of background/weaker odor through Hebbian feedback connections. In response to a mixture of odors A and B [0.8, 0.5, 0.5, 0.6, 0.8, 0.0]^T, the cortical feedback suppresses the weaker background odor (B) and allows the stronger odor A to be easily detected.

VI.2. Summary

In this chapter, we have presented a neurodynamic model of bulbar-cortical interactions. The cortical neurons respond to odors as a whole, synthesizing the features detected by the OB model. Evidence for this kind of processing has emerged recently. Laurent and his colleagues (2005) have shown that Kenyon cells (cortical cells analogue in locusts) respond selectively to one or a few odors. Fig. 55 shows the response of a single KC cell over time (columns) to different repetition (rows) of ten different odors. The KC responds reliable to odor nine alone, clearly indicating that cortical neurons recognize one or at most a few odors (Laurent 2005). This further supports synthetic odor processing in the cortex.

To model the feedback from cortex to bulb both Hebbian and anti-Hebbian learning mechanisms were used. Depending on the type of update rule used to learn these feedback connections, Hebbian or anti-Hebbian, the model realizes background suppression or mixture segmentation functions, respectively. Anti-Hebbian feedback connections result in the identification of binary mixture components as a time series (Liang and Jinks 2001). Hebbian feedback connections allow the olfactory cortex to selectively filter the background or weaker odor input from the bulb, in analogy with the selective attention mechanism proposed by Grossberg (1976).

Fig. 55: Response of a single Kenyon cell (analogue of mammalian pyramidal cell) to ten different odors in locust's mushroom body (analogue of mammalian cortex). Rows show multiple repetitions to the same odor; columns show response of the cortical neuron over time. Gray bar denotes the duration of odor exposure. The recorded cell shows reliable response (shown as dots) only to odor nine, a result that suggests a more holistic processing occurs at the cortical level (reprinted from Laurent 2005).

CHAPTER VII

INTEGRATION

The objective of this chapter is to integrate the computational models of the olfactory signal processing primitives presented in the earlier chapters. This integration is performed in two-stages. First, we integrate the olfactory bulb primitives: chemotopic convergence, shunting lateral inhibition and additive center-surround lateral interactions, and study the benefit of having two levels of lateral inhibition in the bulb. Next, we combine the integrated OB model with the cortical primitives to perform mixture segmentation and background suppression on experimental data. We validate the integrated model using the *Selectivity* dataset, which includes temperature-modulated MOS sensor responses to single analytes at different concentrations, and to their binary and ternary mixtures.

VII.1. Integrated model of the bulb

A unified model of the olfactory bulb is shown in Fig. 56. The high-dimensional odor code from the sensors is first transformed into an organized spatial pattern (i.e., an odor image) using the model of chemotopic convergence presented in Chapter III. The odor images are further transformed in the olfactory bulb by means of two distinct lateral inhibitory circuits (Aungst et al. 2003). First, the outputs of the convergence mapping are input to the shunting lateral inhibition model with global connections (Sache and Galizia 2002), which performs gain control. The outputs of the gain control circuits are

subsequently input to the additive model of lateral inhibition with local center-surround connections (Sache and Galizia 2002). These circuits enhance the sparseness and contrast of the odor patterns.
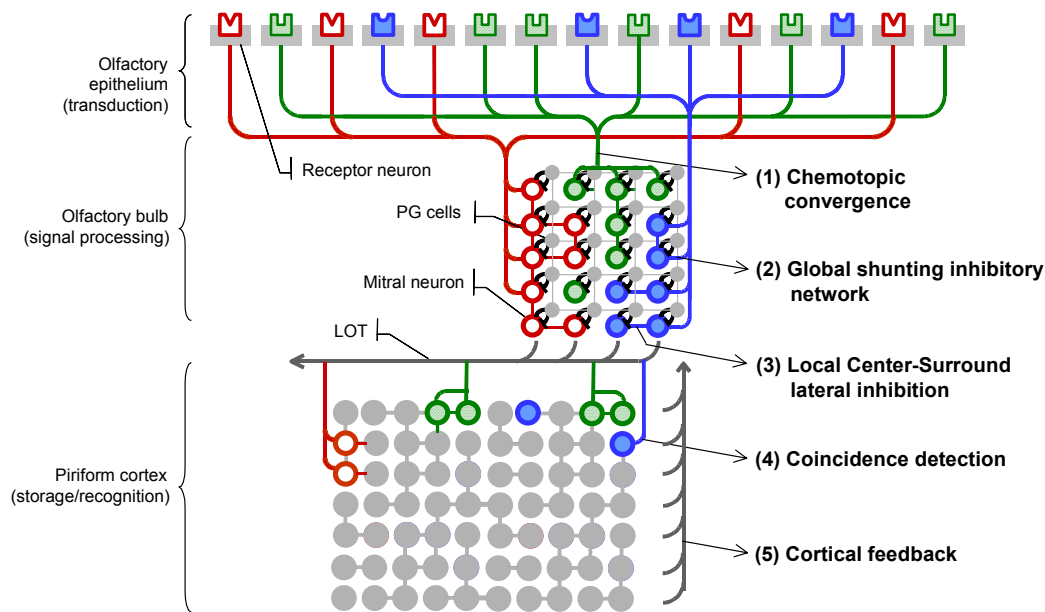
Fig. 56: Structure of the integrated model. Receptor neurons in the olfactory epithelium converge onto the olfactory bulb in a chemotopic manner, forming the first organized representation of a stimulus: an olfactory image. The odor images are further transformed in the olfactory bulb by means of two distinct lateral inhibitory circuits: a global gain control circuit followed by a local center-surround contrast enhancement circuit (Sache and Galiza 2002). The output of the olfactory bulb is projected in a non-topographic, many to many fashion onto the cortex. These convergent and divergent (many-to-many) projections allow the cortical neurons to detect combinations of co-occurring molecular features of the odorant and function as "coincidence detectors". Feedback from cortex modulates the activity in the bulb.

VII.1.1. Validation on the Selectivity dataset

To validate the integrated model of olfactory bulb, the temperature-modulated patterns

for three analytes (acetone (A), isopropyl alcohol (B) and ammonia (C), at three different

concentrations) are first chemotopically projected onto a GL layer with 400 nodes,

arranged as a 20x20 SOM lattice. The outputs of the convergence model (i.e., activity

across the SOM lattice) are first input to the shunting inhibition model in equation 4.1

with global connections ($r=0.5$), which performs pattern normalization. The outputs of

the gain control circuits are subsequently input to the center-surround circuit in equation

5.1 with local connections ($r=5$).

Fig. 57 (top row of each 3×3 image stack) shows the highly overlapping spatial

patterns that result from sensory convergence at the input of the OB in response to the

three analytes. The spatial pattern following stabilization of the center-surround lateral

interactions in equation (5.1) are shown in the middle row of each block. As discussed

earlier, the center-surround interaction improves the contrast between the spatial

patterns. However, due to its local nature, center-surround does not suppress the activity

of mitral cells weakly activated in regions far from the peak activity (e.g., region 1 in the

acetone map). This makes the mechanism sensitive to noise. Further, since these

circuits amplify differences between odor patterns, they require a preprocessing stage to

perform noise reduction and pattern normalization of the inputs (Aungst et al. 2003).

This is precisely what is accomplished in the integrated model, where the global

shunting-inhibitory layer first performs pattern normalization and noise reduction before

the center-surround layer attempts to improve sparseness and contrast. Fig. 57 (bottom

row of each block) shows the resulting spatial activity following stabilization of the global shunting inhibition and local center-surround lateral interactions. It can be observed that only those regions corresponding to peak activity are used to encode each odor. Note that the weakly activated region 1 for acetone and isopropyl alcohol, and region 5 for ammonia, are suppressed.
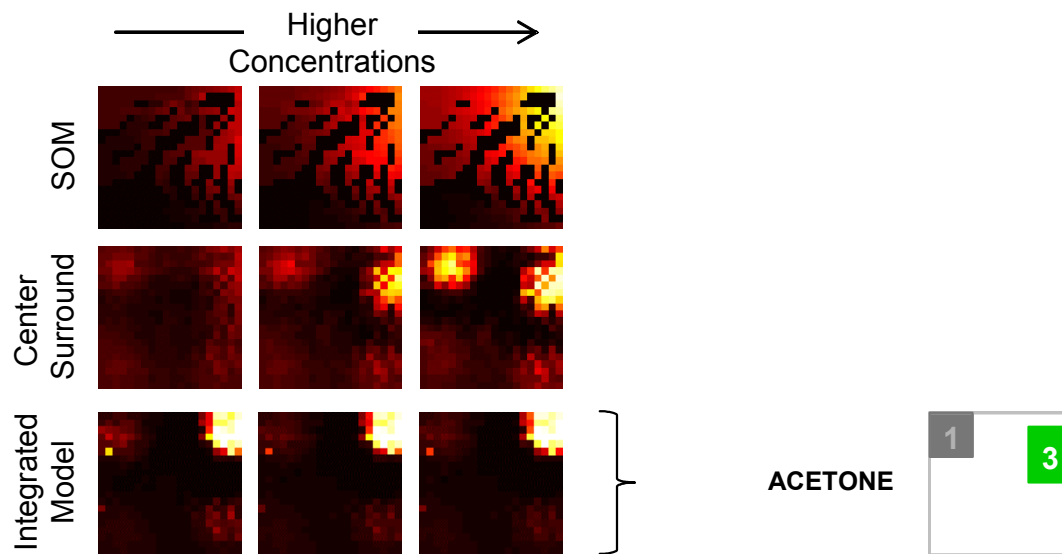
Fig. 57: Spatial maps after (a) chemotopic convergence (top row of each block), (b) only center-surround inhibition (middle row of each block), and (c) integrated OB network with shunting inhibition (model parameters $B=10$, $D=0.1$, $r=0.5$) and center-surround inhibition (model parameters: $a1=0.064$, $a2=45.99$, $r=5$). Three blocks are shown corresponding to three odors: acetone (first block), isopropyl alcohol (second block) and ammonia (third block).

SOM

Center Surround

Integrated Model

ISOPROPYL ALCOHOL

SOM

Center Surround

Integrated Model

AMMONIA
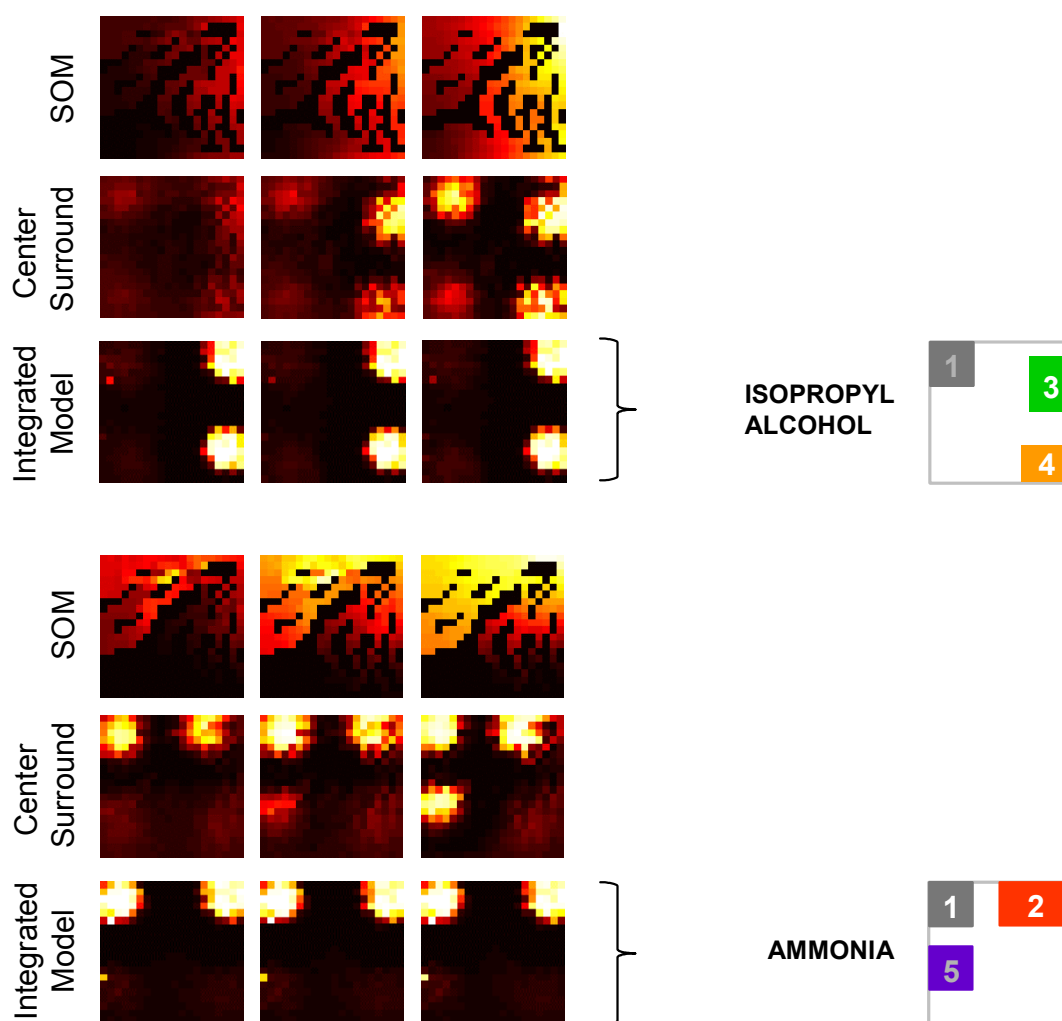
(Fig. 57: continued)

Fig. 58 compares the odor separability between the raw data, chemotopic convergence and the three forms of lateral inhibition (shunting, center-surround and the combination of both). Chemotopic convergence of pseudo-sensors averages out uncorrelated noise and enhances the signal-to-noise-ratio compared to that available in the raw data. The shunting-inhibitory layer performs pattern normalization (L1-norm), which results in a decrease of the within-class scatter and an improvement in odor

separability. The center-surround, on the other hand, produces more sparse and orthogonal patterns than those available at the input. However, in the absence of concentration normalization, the center-surround also tends to emphasize discrimination among the various concentration levels of each odor, which increases the within-class scatter of each odor. The integrated model combines the benefits of both inhibitory mechanisms and convergence, improving the separability between odor patterns significantly than those provided by any of those mechanisms individually.
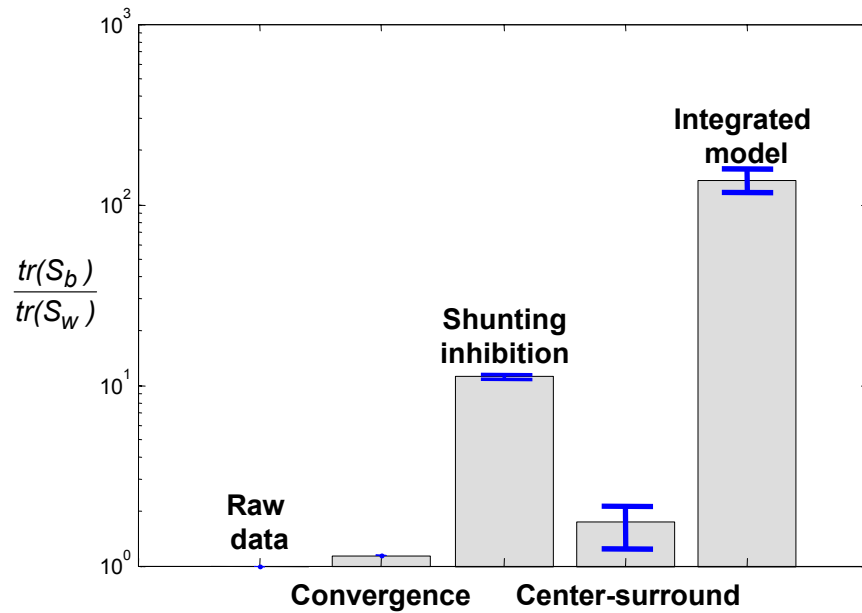
Fig. 58: Comparison of odor separability between (a) raw-data, (b) chemotopic convergence, (c) shunting inhibition, (d) center-surround lateral inhibition and (e) integrated model.

VII.2. Integration with cortical primitives

Next, we integrate the bulbar circuits with the cortical primitives presented in Chapter VI to perform mixture segmentation and background suppression on experimental data. The output of the integrated OB model is input to a cortical network with six manually labeled neurons. Cortical feedback to the bulb is modeled using either anti-Hebbian or Hebbian update rules presented in equation 6.5.

VII.2.1. Mixture segmentation with anti-Hebbian feedback

In order to perform binary mixture segmentation on the experimental datasets, the OB-OC network is initially trained using the three pure odors. Feedforward and feedback connections are learned by considering only the steady-state response of the bulb to the single analytes at their highest concentrations (Fig. 57; 3rd row of each block). The resulting Hebbian feedforward and anti-Hebbian feedback connections are shown in the Fig. 59; each image represents the connection from all bulbar units onto a particular cortical unit. Note that the anti-Hebbian connections are the reverse of the forward connections. The activity of the trained network with anti-Hebbian feedback connections when exposed to a binary mixture of isopropyl alcohol and ammonia and the ternary mixture is shown in Fig. 60. As mentioned in section VI.1, anti-Hebbian feedback results in the removal of bulb activity that is responsible for activity in the cortex. In the case of the binary mixture, isopropyl alcohol is first recognized in the cortex since it is the stronger odor in the mixture. Subsequently, feedback from cortex inhibits bulb neurons responsible for this cortical activity, allowing ammonia to be

detected. These segmentation results are in agreement with results from psychophysical studies on mixtures, which report recognition of components of some binary mixtures in series (Liang and Jinks 2001).
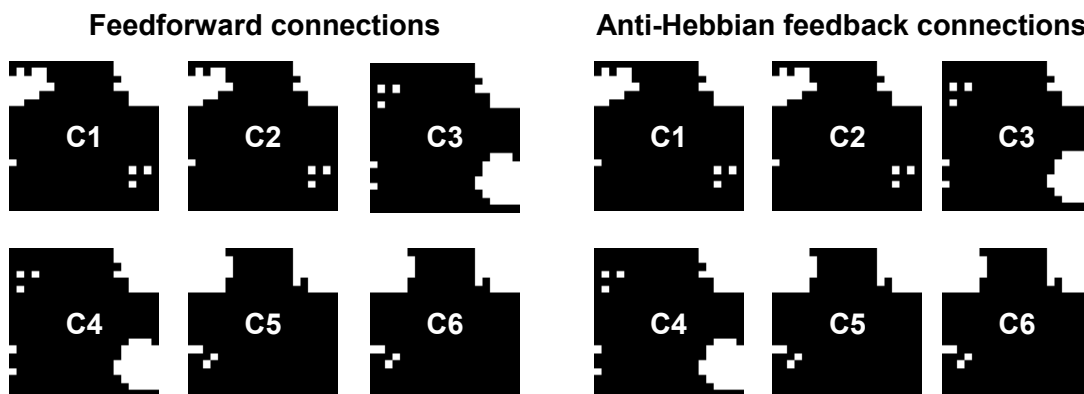
Fig. 59: Feedforward connections from bulb (left) and anti-Hebbian feedback connections from cortex (right). Lighter areas in the Fig. identify bulbar neurons that send or receive connections from cortical neurons, which were manually labeled. These connections were obtained using the steady-state response of the bulb to single analytes at their highest concentration. Cortical neurons C1 and C2 detect Acetone, C3 and C4 detect Isopropyl alcohol, and, C5 and C6 detect Ammonia.
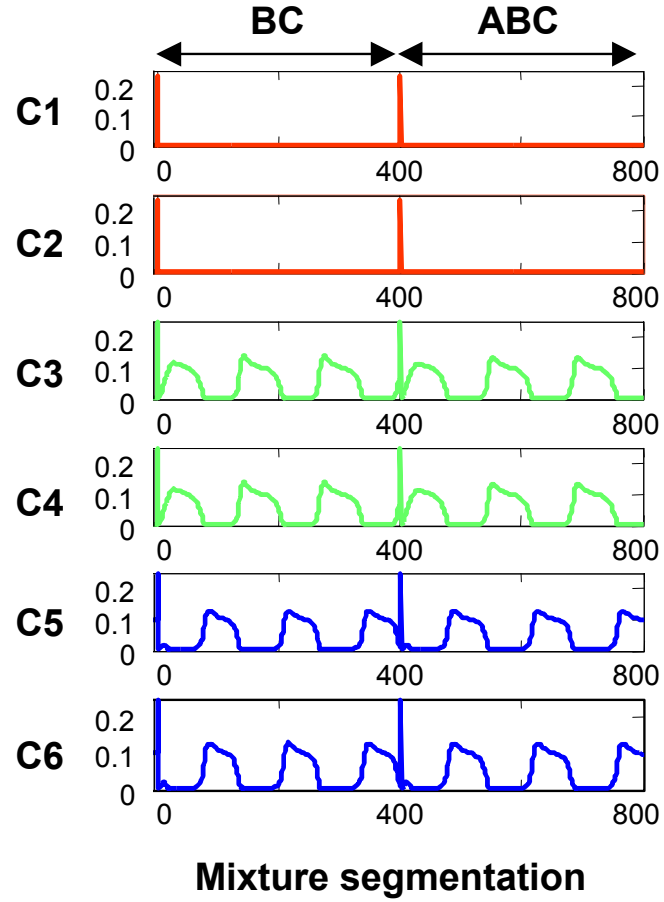
Fig. 60: Segmentation of binary mixture of isopropyl alcohol and ammonia and the ternary mixture by anti-Hebbian cortical feedback. Parameters are set as follows: $\tau=$ *10ms, $\lambda=10ms$, $\gamma=40$* and *$\delta=0.1$*.

Similar behavior can be observed in the case of the ternary mixtures. However, the region corresponding to acetone is inhibited at all times since it is common across all odors in the dataset. This prevents identification of acetone in the ternary mixture and in other binary mixtures containing acetone (not shown). Behavioral experiments in rats have shown that this kind of odor masking is also a common phenomenon while

processing some odor mixtures (Chandra and Smith 1998; Liang et al. 1989). The proposed anti-Hebbian feedback mechanism also appears to be limited to the segmentation of binary odor mixtures whose sensor responses are relatively additive.

VII.2.2. Background suppression with Hebbian feedback

In order to perform background suppression, the OB-OC network is initially trained using the three pure odors at their highest concentration. The resulting Hebbian feedforward and feedback connections are shown in Fig. 61. Note that the Hebbian connections are complementary to the forward connections. The activity of the trained network when exposed to the each of three binary mixtures is shown in Fig. 62. In binary mixtures involving isopropyl alcohol, as well as in the ternary mixture, cortical feedback from the stronger odor (isopropyl alcohol) suppresses the weaker odor (acetone and ammonia, respectively). In the binary mixture containing acetone and ammonia, cortical cells detecting ammonia receive greater input than those that detect acetone. As a result, cortical activity suppresses acetone, in this case the weaker odor. The steady state OB activity for the three binary mixtures and the ternary mixture with and without cortical feedback is shown in Fig. 63. Without cortical feedback, the regions corresponding to different constituents show some activity. The Hebbian cortical feedback helps filter these inputs and lock on to the stronger odor in the mixture, in this case isopropyl alcohol.

Feedforward connections   **Hebbian feedback connections**
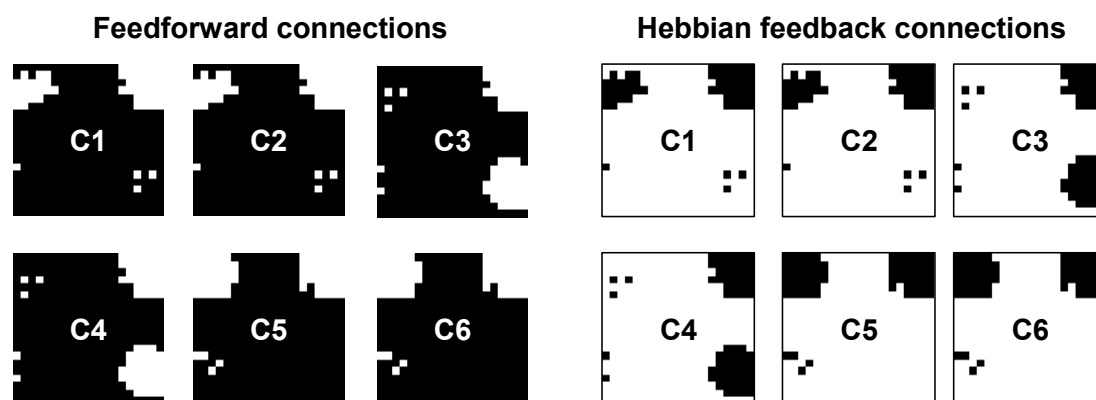
Fig. 61: Feedforward connections from bulb onto cortex (left), and anti-Hebbian feedback connections from cortex (right). Lighter areas in the Fig. identify bulb neurons that send or receive connections from cortical neurons. These connections were obtained using the steady-state response of the bulb to single analytes at their highest concentration. Cortical neurons C1 and C2 detect acetone, C3 and C4 detect isopropyl alcohol, and, C5 and C6 detect ammonia.
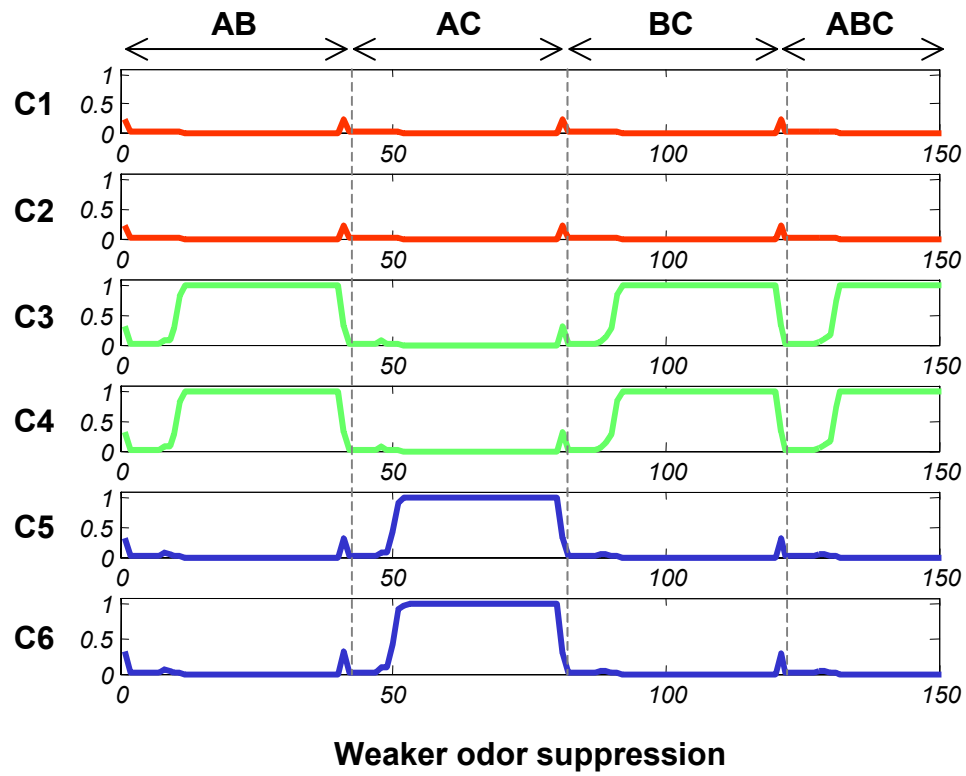
Fig. 62: Background/weaker odor suppression by Hebbian cortical feedback. Parameters were set as follows: τ= 10ms, λ=10ms, γ=1 and δ=0.1.
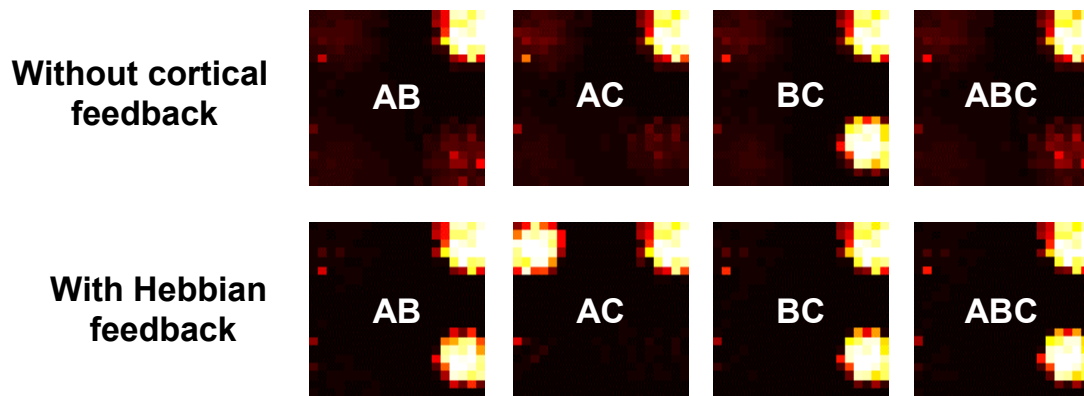
Fig. 63: Comparison of activity in the bulb with and without Hebbian cortical feedback to the binary and ternary mixtures. Without cortical feedback, regions corresponding to different constituents show some activity. With cortical feedback bulbar activity resembles the response to the stronger odor alone.

VII.3. Summary

In this chapter we have integrated the models of the six olfactory signal-processing primitives presented in the earlier chapters. The model of bulb with chemotopic convergence, shunting lateral inhibition and center-surround lateral inhibition enhances the separability between odor patterns significantly that those provided by any of those mechanisms individually. This is a direct result of the global shunting network complementing the local center-surround circuits, which allows the combined model to synergistically enhance the contrast of the odor patterns. Integration of the bulbar circuits with the cortical primitives allows the model to perform mixture segmentation and background suppression on experimental datasets.

CHAPTER VIII

CONCLUSIONS

In this dissertation, I have proposed a biologically-inspired approach for pattern recognition for chemical sensor arrays. I have presented computational models of six signal processing primitives in the olfactory pathway: (i) population coding by olfactory receptor neurons (ORNs), (ii) dimensionality and noise reduction through chemotopic convergence of ORNs, (iii) gain control through lateral inhibition from periglomerular (PG) cells, (iv) contrast enhancement through lateral inhibition from granule (GR) cells, (5) storage of odors in the olfactory cortex, and, (6) mixture segmentation and background suppression through cortical feedback. These computational models were integrated into a neuromorphic architecture as shown in Fig. 64.
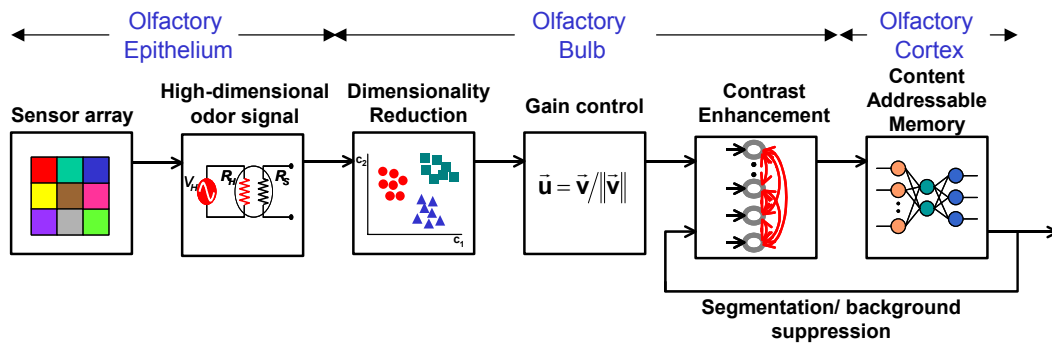
Fig. 64: Building blocks of a biologically inspired pattern recognition architecture for chemical sensor arrays. Each of the six stages corresponds to a signal processing primitive in the olfactory pathway.

Our approach can be summarized as follows. First a high dimensional odor signal was generated from chemical sensor arrays. Three approaches have been proposed to generate a combinatorial and high dimensional odor signal: temperature modulation of metal-oxide sensors, a large population of optical microbead sensors, and infrared spectroscopy. These approaches overcome the dimensionality mismatch between the artificial olfactory system and its biological counterpart. In addition to these approaches, a receptor model has also been presented in Appendix B to generate a high-dimensional response from a low-dimensional feature space, such as the one available in conventional datasets with small sensor arrays (2-32 sensors).

Following combinatorial coding, the resulting high-dimensional odor signal was subject to dimensionality reduction using a self-organizing model of chemotopic convergence. This convergence transforms the initial combinatorial, high-dimensional code into an organized spatial pattern (i.e., an odor image), which decouples odor identity from intensity. Odor images formed through convergence are however highly overlapping due to collinearity of sensor input, and require further processing.

Two lateral inhibitory circuits, subsequently process the overlapping odor images obtained after chemotopic convergence. The first shunting lateral inhibition circuits perform gain control enabling identification of the odorant across a wide range of concentration. We have shown that the spread of lateral inhibition can be used to control the degree of concentration removal performed by this circuit. The second circuit is modeled using additive model of lateral inhibition with center-surround connections. These lateral interactions improve contrast between odor images producing more sparse

and orthogonal patterns compared to that available at the input. Furthermore, we have shown that the odor-evoked responses evolve continuously and settle into odor-specific fixed-point attractors. These attractors have been shown to cluster by identity followed by intensity and are consistent with recent findings in neurobiology. Integration of these two lateral inhibitory mechanisms resulted in significant improvement in odor separability, better than those provided by any of these lateral inhibition mechanisms individually. This was a direct result of the global shunting network complementing the local center-surround circuits, which allows the combined model to synergistically enhance the contrast of the odor patterns.

The sharpened odor image was stored in a simple cortical circuit, also modeled using an additive neurodynamics model. We showed that depending upon the learning rule used to establish the cortical feedback to bulb: anti-Hebbian or Hebbian, mixture segmentation and weaker odor/background suppression were achieved, respectively.

The proposed models are not tied to a particular input representation. We have presented a receptor model in Appendix B, which allows these models to work with traditional feature space with fewer dimensions. Also it should be noted that the identified signal processing primitives are not tied to any particular neural network model. To illustrate this point, we have presented a spiking model of the olfactory bulb circuits in Appendix C.

The neuromorphic approach to signal processing presented in this dissertation represents a unique departure from current practices in the e-nose community. We expect this approach to move the electronic nose technology beyond multivariate

chemical sensing and in the direction of true machine olfaction: relating sensor/instrumental signals to the perceptual characteristics of the odorant being sensed (structure-odor relationships). A preliminary study in this direction was included in this dissertation involving our chemotopic convergence model and IR absorption spectroscopy. Our results show that the chemical clusters obtained from the IR data match those from rat OB images. More interestingly, each of these clusters uniquely identified a specific smell descriptor: *Fruity*, *Cheese* or *Sweat*, *Fat* or *Citrus* and *Nuts*. These results provide evidence supporting the proposed biologically inspired approach for machine olfaction.

VIII.1. Future work

The computational models presented can also be used to gain insight into and predict the functions of various olfactory processing mechanisms:

- The receptor model presented in Appendix B predicts that maximum separability is achieved using convergence mapping with receptor neurons whose receptive field width is neither too broad nor too narrow. This is *in agreement* with theoretical work on biological and artificial chemical sensors, which indicates that maximum mutual information between the sensor response and the set of odors to be identified is obtained with an array of receptors/sensors that are tuned to 25-35% of the entire stimuli set (Alkasab et al. 2002).

  Our model has employed a homogeneous receptor population. However, theoretical predictions by Alkasab et al., (2002) indicate that maximum mutual

information is achieved with a heterogeneous population of receptors/sensors. It is therefore possible to further improve pattern separability by employing a non-uniform distribution of receptor field widths.

An additional but related study involves the trade-off between selectivity and generality. In (Raman et al., 2005), we argue that receptors with narrow receptive fields allow effective discrimination of odors in the training set, whereas broadly-tuned receptors allow detection of new, unknown odors. Therefore, *we predict* that a non-uniform distribution of receptor-field width is necessary to strike an appropriate balance between selectivity and generalization capabilities. A related *prediction* is that receptors may be sharply tuned if they detect odors in well-sampled regions of feature space to improve selectivity, whereas, receptors that identify odors in under-sampled regions may be broadly tuned to allow identification of new odors. These predictions are yet to be confirmed by experimental studies.

- Based on the results presented in Chapter III, *we predict* that convergence mapping combined with IR absorption spectra may be an appropriate method to capture perceptual characteristics of the odorants. Though encouraging, our results with IR data are preliminary at best. Further investigations are required to unveil the relationships that exist across the three representations of an odorant: stereo-chemical molecular features (Pelosi and Persaud 2000), olfactory bulb images (Johnson and Leon 2000), and organoleptic descriptors (Dravnieks 1985).

- Results from our shunting-inhibition model suggest that the width of the lateral inhibition can be used to control the amount of concentration normalization achieved at the input of the OB. This *prediction is consistent* with recent work by Christensen et al., (2001), which suggests that local neurons in the antennal lobe (analogous to PG cells in the mammalian olfactory bulb) of sphinx moth can operate as multifunctional units, causing local inhibition at lower odor concentrations and global inhibition at higher concentrations. Their study is particularly relevant to our work as it identifies a possible biological mechanism for modulating inhibitory width. Our shunting inhibition model can therefore be used to *predict* the effect that modulation of inhibitory width may have during the processing of odor signals.

- Results from the contrast-enhancement circuits indicate that removal of lateral inhibition between mitral cells through granule inter-neurons can reduce odor discriminability (refer to Figure 46, Figure 50). These *predictions are similar* to those made by Bazhenov et al., (2001), and are *consistent* with recent experimental results on locusts (Stopfer et al. 1997; Laurent 1999).

   Further, *the model predicts* that excitatory lateral connections are responsible for spreading mitral cell activity and moving odor-specific attractors (Galan et al. 2003) away from their initial coordinates. Hence removal of the glutamatergic (excitatory) lateral interactions between mitral cells should affect the temporal and spatial characteristics of the odor code, specifically causing

odor attractors to remain close to one another. This prediction has yet to be confirmed by experimental studies.

- The model of bulb-cortex interaction predicts two roles for the cortical feedback depending on the update rule used to establish these connections. Anti-Hebbian connections result in the identification of binary mixture components as a time series. On the contrary, Hebbian feedback allows the olfactory cortex to selectively filter the background or weaker odor input from the bulb, in analogy with the selective attention mechanism proposed by Grossberg (1976).

    Both mixture segmentation (Liang and Jinks 2001) and background suppression (Chandra and Smith, 1998; Liang et al. 1989) have been reported by psychophysical studies on the processing of odor mixtures. A possible explanation may be that both types of connections co-exist and the type of feedback may be determined by the importance of the odor to the animal. For example, cortical neurons that recognize odors of a prey or a predator may have Hebbian feedback to the bulb, whereas other less important odors may have anti-Hebbian feedback. This prediction has yet to be confirmed by experimental studies on animal models.

Our modeling efforts in this dissertation research have focused on capturing the principal signal processing circuits in the early olfactory pathway. Incorporation of adaptation mechanisms such as neurogenesis (Cecchi et al. 2002) and synaptogensis (Jefferis et al. 2004)] will allow the models to deal with additional problems, such as sensor drift. Here, we anticipate that a specific case of synaptogenesis, the wiring of

newly born ORNs onto PNs (Jefferis et al. 2004), could be combined with disposable sensor arrays to prevent drift.

This work has concentrated primarily on chemosensory signals. However the developed models have a broader application to problems with high-dimensional data, such as face recognition, image processing and DNA microarray analysis. Future research will investigate the issue of abstracting the models of chemotopic convergence and lateral inhibition circuits and formulating them as novel pattern recognition schemes.

REFERENCES

Alkasab TK, White J, Kauer JS (2002) A computational system for simulating and analyzing arrays of biological and artificial chemical sensors. Chemical Senses 27:261-275

Ambros-Ingerson J, Granger R, Lynch G (1990) Simulation of paleocortex performs hierarchical clustering. Science 247:1344-1348

Amoore JE (1970) Molecular Basis of Odor. C.C. Thomas, Pub., Springfield, Illinois

Aungst JL, Heyward PM, Puche AC, Karnup SC, Hayar A, Szabo G and Shipley MT (2003) Center-surround inhibition among olfactory bulb glomeruli. Nature 26:623- 629

Axel R (1995) The molecular logic of smell. Scientific American 273(4):154-159

Bazhenov M, Stopfer M, Rabinovich M, Heurta R, Abarbanel H, Sejnowski TJ, Laurent G (2001) Model of transient oscillatory synchronization in the locust antennal lobe. Neuron 30:553-567

Buck L (1996) Information coding in the vertebrate olfactory system. Annual Review of Neuroscience 19:517-544

Buck L, Axel R (1991) A novel multigene family may encode odor receptors: a molecular basis for odor recognition. Cell 65(1):178-187

Bulfone et al. (1998) An olfactory sensory map develops in the absence of normal projection neurons or GABAergic Interneurons. Neuron 21(6):1273-1282

Capone S, Siciliano P, Barsan N, Weimer U, Vasanelli L (2001) Analysis of CO and CH$_4$ mixtures by using a micromachine sensor array. Sensors and Actuators (B) 78:40-48

Cecchi GA, Petreanu L, Alvarez-buylla A, Magnasco M (2002) Unsupervised learning and adaptation in a model of adult neurogenesis. Journal of Computational Neuroscience 11(2):175-182

Chandra S, Smith B (1998) An analysis of synthetic processing of odor mixtures in the honeybee (Apis Mellifera). The Journal of Experimental Biology 210:3113-3121

Christensen TA, D'Alessandro G, Lega J, Hildebrand JG (2001) Morphometric modeling of olfactory circuits in the insect antennal lobe: I. Simulations of spiking local interneurons. Biosystems 61:143-153

Claussnitzer U, Quarder S, Otto M (2001) Interpretation of analytical patterns from the output of chaotic dynamical memories. Fresenius Journal of Analytical Chemistry 369:698-703

Davis JL, Eichenbaum H (1991) Olfaction: A Model System for Computational Neuroscience. MIT Press, Cambridge

DeCoste D, Burl MC, Hopkins A, Lewis NS (2001) Support vector machines and kernel Fisher discriminants: A case study using electronic nose data. In: Fourth Workshop on Mining Scientific Datasets held in conjunction with Knowledge Discovery and Data mining (KDD'01), San Francisco, California

Dickinson TA, Michael KL, Kauer JS, Walt DR (1999) Convergent, self-encoded bead sensor array in the design of an artificial nose. Journal of Analytical Chemistry, 71: 2192-2198

Dickinson TA, White J, Kauer JS, Walt DR (1996) A chemical detecting system based on cross-reactive optical sensor array. Nature 382(22):697-700

Dravnieks A (1985) Atlas of Odor Character Profiles, Data Series DS 61, ASTM, Philadelphia, PA

Dyson GM (1938) The scientific basis of odor. Chem. Ind. 57:647-651

Figaro Engineering, Inc. (MOS Sensors), Osaka, Japan, 1996.

Firestein S (2001) How the olfactory system makes sense of scents. Nature 413:211-218

Freeman W (1973) A model of the olfactory system. In: Brazier MAB, Walter DO, Schneider E (eds), Neural Modeling, Brain Information Service Report No.1, University of California Press, Los Angeles, pp 41-62

Freeman W (1999) Olfactory system: odorant detection and classification. In: Amit D, Parisi G (eds), Building blocks for intelligent systems: Brain components as elements of intelligent function, Academic Press, New York, pp 1-27

Friedrich RW, Korsching SI (1997) Combinatorial and chemotopic odorant coding in the zebrafish olfactory bulb visualized by optical imaging. Neuron 18:737-752

Fukunaga K (1990) Introduction to Statistical Pattern Recognition, Second Edition. Academic Press, New York

Galán RF, Sachse S, Galizia CG, Herz AV (2004) Odor-driven attractor dynamics in the antennal lobe allow for simple and rapid olfactory pattern classification. Neural Computation 16(5):999-1012

Georgopoulos A, Schwartz AB, Kettner RE (1986) Neuronal population coding of movement direction. Science 233(4771):1416-1419

Gerstner W, Kistler W (2002) Spiking Neuron Models: Single Neurons, Populations, Plasticity. University Press, Cambridge

Gill DS, Pearce TC (2003) Wiring the olfactory bulb – activity dependent models of axonal targeting in the developing olfactory pathway. Reviews in Neuroscience 14:63-72

Grossberg S (1976) Adaptive pattern classification and universal recording: I parallel development and coding of neural feature detectors. Biological Cybernetics 23:121-134

Grossberg S (1976) Adaptive pattern classification and universal recording: II. feedback, expectation, olfaction and illusion. Biological Cybernetics 23:187-02

Gutierrez-Galvez A, Gutierrez-Osuna R (2005) Contrast enhancement and background suppression of chemosensor array patterns with the KIII model. International Journal of Intelligent Systems (in press)

Gutierrez-Osuna R (1998) Signal processing and pattern recognition for an electronic nose. Ph.D. Dissertation, Department of Computer Engineering, North Carolina State University, Raleigh

Gutierrez-Osuna R (2000) Drift reduction for metal-oxide sensors using canonical correlation regression and partial least squares. In: Proc 7th International symposium on Olfaction & Electronic Nose, Brighton, England

Gutierrez-Osuna R (2002) Pattern analysis for machine olfaction: A review. IEEE Sensors Journal 2(3):189-202

Gutierrez-Osuna R (2002) A self-organizing model of chemotopic convergence for olfactory coding. In: Proc 2nd Joint EMBS-BMES Conference, Houston, TX, pp 23-26.

Gutierrez-Osuna R, Gutierrez-Galvez A (2003) Habituation in the KIII olfactory model with chemical sensor arrays. IEEE Transactions on Neural Networks 16:649-656

Gutierrez-Osuna R, Powar NU (2003) Odor mixtures and chemosensory adaptation in gas sensor arrays. International Journal on Artificial Intelligence Tools 12(1):1-16

Gutierrez-Osuna R, Raman B (2004) Cancellation of chemical backgrounds with generalized Fischer's linear discriminants. In: Proc 3rd IEEE Sensors conference, Vienna, Austria

Haykin S (1999) Neural Networks, A Comprehensive Foundation, 2nd edition. Prentice Hall, Upper Saddle River, NJ

Hildebrand JG, Shepherd GM (1997) Mechanisms of olfactory discrimination: converging principles across phyla. Annual Reviews of Neuroscience 20:595-631

Holmberg M, Arthursson T (2002) Drift compensation, standards, calibration methods. In: Pearce TC, Schiffman SS, Nagle HT, Gardner JW (eds), Handbook of

Machine Olfaction: Electronic Nose Technology, Wiley-VCH, Weinhiem, Germany, pp 325-346

Jefferis GS, Vyas RM, Berdnik D, Ramaekers A, Stocker RF,Tanaka N, Ito K, Luo L (2004) Developmental origin of wiring specificity in the olfactory system of drosophila. Development 131:117-130

Joerges J, Küttner A, Galizia CG, Menzel R (1997) Representations of odours and odour mixtures visualized in the honeybee brain. Nature 387:285-288

Johnson BA, Leon L (2000) Modular representation of odorants in the glomerular layer of the rat olfactory bulb and the effects of stimulus concentration. Journal of Comparative Neurology 422:496-509

Kohonen T (1982) Self-organized formation of topologically correct feature maps. Biological Cybernetics 43:59-69

Kuffler SW (1953) Discharge patterns and functional organization of mammalian retina. Journal of Neurophysiology 16:37-68

Laaksonen J, Koskela M, Oja E (2003) Probability interpretation of distributions on SOM surfaces. In: Proc Workshop on Self-Organizing Maps (WSOM'03), Hibikino, Kitakyushu, Japan, pp 77-82

Laing DG, Panhuber H, Slotnick BM (1989) Odor masking in the rat. Phyisological Behavior 45(4):689-694

Laing DG, Jinks AL (2001) Psychophysical analysis of complex odor mixtures. Chimia 55:413-420

Lancet D, Sadovsky E, Seidemann E (1993) Probability models for molecular recognitionin biological receptor repertoires: Significance to the olfactory system. PNAS 90:3715-3719

Laurent G (1999) A systems perspective on early olfactory coding. Science 286(22):723-728

Laurent G (2005) The sense of smell: A window into the brain and memory. Ernest C. Watson Lecture series, Cal Tech, Pasadena

Lee AP, Reedy BJ (1999) Temperature modulation in semiconductor gas sensing. Sensors and Actuators (B) 60:35-42

Leffingwell JC (2002) Olfaction: A review. Leffingwell Reports 2(1):1-34 (available at http://www.leffingwell.com; accessed October 17, 2005)

Lei H, Christensen T, Hildebrand JG (2004) Spatial and temporal organization of ensemble representations for different odor classes in the moth antennal lobe. The Journal of Neuroscience 24(49):11108-11119

Li Z, Hertz J (2000) Odor recognition and segmentation by a model olfactory bulb and cortex. Network: Computation in Neural Systems 11:83-102

Linstrom PJ, Mallard WJ (2003) NIST Chemistry WebBook. NIST Standard Reference Database Number 69, National Institute of Standards and Technology, Gaithersburg (http://webbook.nist.gov; accessed October 17, 2005)

Luo M, Katz LC (2001) Response correlation maps of neurons in the mammalian olfactory bulb. Neuron 32:1165-1179

Malaka R, Ragg T, Hammer M (1995) A model for chemosensory reception. In: Tesauro G, Touretzky DS, Leen TK (eds), Advances in Neural Information Processing Systems 7, MIT Press, Cambridge, pp 61-68

Meister M, Bonhoeffer T (2001) Tuning and topography in an odor map on the rat olfactory bulb. Journal of Neuroscience 21(4):1351-1360

Mombaerts P (2004) Genes and ligands for odorants, vomeronasal and taste receptors. Nature reviews Neuroscience 5:263-278.

Moncrieff RW (1949) What is odor. A new theory. Am. Perfumer 54:453

Mori K, Nagao H, Yoshihara Y (1999) The olfactory bulb: coding and processing of odor molecule information. Science 286:711-715

Nagle HT, Schiffman SS, Gutierrez-Osuna R (1998) The how and why of electronic noses. IEEE Spectrum 35(9):22-34

Ortega A, Marco S, Sundic T, Samitier J (2000) New pattern recognition systems designed for electronic noses. Sensors and Actuators (B) 69:302-307

Otto M, Quarder S, Claußnitzer U, Lerchner J (2000) A nonlinear dynamic system for recognizing chemicals based on chemical sensors and optical spectra. In: Proc World Multiconference on Systemics, Cybernetics and Informatics (SCI-2000), pp 413-418

Pearce TC (1997) Computational parallels between the biological olfactory pathway and its analogue 'The Electronic Nose': Part I. Biological olfaction. BioSystems 41:43-67

Pearce TC (1997) Computational parallels between the biological olfactory pathway and its analogue 'The Electronic Nose': Part II. Sensor-based machine olfaction. BioSystems 41:69-90

Pearce TC, Verschure PFMJ, White J, Kauer JS (2001) Robust stimulus encoding in olfactory processing: hyperacuity and efficient signal transmission. In: Wermter S, Austin J, Willshaw D (eds), Emergent Neural Computation Architectures Based on Neuroscience, Springer-Verlag, London, pp 461-479

Pelosi P, Persaud KC (2000) Physiological and artificial systems for odour recognition. In: Proc. 2nd Italian Workshop on Chemical Sensors and Biosensors, Rome, Italy, pp 37-55

Perera A, Papamichail N, Barsan N, Weimer U, Marco S (2003) On-line event detection by recursive dynamic principal component analysis and gas sensor arrays under drift conditions. In: Proc IEEE Sensors conference, pp 860-865

Persaud KC, Dodd GH (1982) Analysis of discrimination mechanisms of the mammalian olfactory system using a model nose. Nature 299:352-355

Powar N (2002) Temperature modulation and transient analysis for tin-oxide sensor arrays. M.S. Thesis, Department of Computer Science and Engineering, Wright State University, Dayton, Ohio

Quarder S, Claussnitzer U, Otto M (2001) Using singular-value decompositions to classify spatial patterns generated by a nonlinear dynamic model of the olfactory system. Chemometrics and Intelligent Laboratory Systems 1248:45-51

Raman B, Sun P, Gutierrez-Galvez A, Gutierrez-Osuna R (2005), Processing of chemical sensor arrays with a biologically-inspired model of olfactory coding. IEEE Transactions of Neural Networks (to appear).

Ratton L, Kunt T, McAvoy T, Fuja T, Cavicchi R, Semancik S (1997) A comparative study of signal processing techniques for clustering microsensor data (a first step towards an artificial nose). Sensors & Actuators (B) 41(1-3):105-120

Sache S, Galizia CG (2002) Role of inhibition for temporal and spatial odor representation in olfactory output neurons: a calcium imaging study. Journal of Neurophysiology 87:1106-1117

Schiffman SS, Pearce TC (2003) Introduction to olfaction: perception, anatomy, physiology, and molecular biology. In: Pearce TC, Schiffman SS, Nagle HT, Gardner JW (eds), Handbook of Machine Olfaction: Electronic Nose Technology, Wiley-VCH, Weinheim, Germany, pp 1-32

Segev I (1999) Taming the time in the olfactory bulb. Nature Neuroscience 12(12):1041-1042

Shepherd GM (1987) A molecular vocabulary for olfaction. In: Roper SD, Atema J (eds), Olfaction and Taste X, Annals of New York Academy of Sciences, NY, USA, pp 98-103

Shepherd GM, Chen WR, Greer CA (2003) The olfactory bulb. In: Shepherd GM (ed), The Synaptic Organization of the Brain (fifth edition), Oxford University Press, New York, pp 165-216

Sicard G, Holley A (1984) Receptor cell responses to odorants: Similarities and differences among odorants. Brain Research 292:283–296

Stopfer M, Baghavan M, Smith BH, Laurent G (1997) Impaired odor discrimination on desynchronization of odor-encoding neural assemblies. Nature 390:70-74

Stopfer M, Jayaraman V, Laurent G (2003) Intensity versus identity coding in an olfactory system. Neuron 39:991-1004

Sundic T, Marco S, Perera A, Pardo A, Hahn S, Barsan N, Weimer U (2003) Fuzzy inference systems for sensor array calibration: prediction of CO and CH4 levels in variable humidity conditions. Chemometrics and Intelligent Laboratory Systems 64:103-122

Turin L (1996) A spectroscopic mechanism for primary olfactory reception. Chemical Senses 21(6):773-791

Vassar R, Chao SK, Sitcheran R, Nunez JM, Voshall LB, Axel R (1994) Topographic organization of sensory projections to the olfactory bulb. Cell 79:981-991

White J, Dickinson TA, Walt DR, Kauer JS (1998) An olfactory neural network for vapor recognition in an artificial nose. Biological Cybernetics 78:245-251, 1998.

White J, Kauer JS (1999) Odor recognition in an artificial nose by spatio-temporal processing using an olfactory neuronal network. Neurocomputing 26-27:919-924

Wilson HR (1999) Spikes Decision and Actions, Dynamical Foundations of Neuroscience. Oxford University Press, New York

Wilson MA, Bower JM (1988) A computer simulation of olfactory cortex with functional implications for storage and retrieval of olfactory information. In:

Anderson DZ (ed), Neural Information Processing Systems, MIT Press, Cambridge, pp 114-126

Wilson DA, Stevenson RJ (2003) The fundamental role of memory in olfactory perception. Trends in Neurosciences 26(5):243-247

Wright RH (1982) The Sense of Smell. CRC Press, Boca Raton

Xie XH, Hahnloser R, Seung HS (2001) Learning winner-take-all competition between groups of neurons in lateral inhibitory networks. In: Leen TK, Dietterich TG, Tresp V (eds), Advances in Neural Information Processing Systems 13, MIT Press, Cambridge, pp 350-356

Yamanaka T (2004) Study of smell reproduction using chemical sensing system. Ph.D. Dissertation, Tokyo Institute of Technology, Tokyo, Japan

Yao Y, Freeman WJ (1990) Model of biological pattern recognition with spatially chaotic dynamics. Neural Networks 3:153-170

Yinon J (2003) Detection of explosives by electronic noses. Analytical Chemistry 75:99A-105A

Yokoi M, Mori K, Nakanishi S (1995) Refinement of odor molecule tuning by dendrodendritic synaptic inhibition in the olfactory bulb. PNAS 9:3371–3375

Zhang K, Sejnowski TJ (1999) Neuronal tuning: to sharpen or broaden. Neural Computation 11: 75-84

Zheng C, Firestein P, Mombarets T, Rodriguez I, Mombarets P (2000) Peripheral olfactory projections are differentially affected in mice deficient in a cyclic nucleotide channel subunit. Neuron 26:81-91

APPENDIX A

IR ABSORPTIONS FOR DIFFERENT FUNCTIONAL GROUPS[6]

Functional Class	Range (wave numbers)	Assignment
Alkanes	2850-3000	CH_3, CH_2 & CH 2 or 3 bands
	1350-1470	CH_2 & CH_3 deformation
	1370-1390	CH_3 deformation
	720-725	CH_2 rocking
Alkenes	3020-3100	=C-H & =CH_2 (usually sharp)
	1630-1680	C=C (symmetry reduces intensity)
	1900-2000	C=C asymmetric stretch
	880-995	=C-H & =CH_2
	780-850	(out-of-plane bending)
	675-730	cis-RCH=CHR
Alkynes	3300	C-H (usually sharp)
	2100-2250	C≡C (symmetry reduces intensity)
	600-700	C-H deformation
Arenes	3030	C-H (may be several bands)
	1600 & 1500	C=C (in ring) (2 bands)
		(3 if conjugated)
	690-900	C-H bending &
		ring puckering
Alcohols & Phenols	3580-3650	O-H (free), usually sharp
	3200-3550	O-H (H-bonded), usually broad
	970-1250	C-O
	1330-1430	O-H bending (in-plane)
	650-770	O-H bend (out-of-plane)

[6] http://www.cem.msu.edu/~reusch/VirtualText/Spectrpy/InfraRed/infrared.htm

Amines	3400-3500 (dil. soln.)	N-H (1°-amines), 2 bands
	3300-3400 (dil. soln.)	N-H (2°-amines)
	1000-1250	C-N
	1550-1650	NH$_2$ scissoring (1°-amines)
	660-900	NH$_2$ & N-H wagging
		(shifts on H-bonding)
Aldehydes & Ketones	2690-2840(2 bands)	C-H (aldehyde C-H)
	1720-1740	C=O (saturated aldehyde)
	1710-1720	C=O (saturated ketone)
	1690	aryl ketone
	1675	α, β-unsaturation
	1745	cyclopentanone
	1780	cyclobutanone
	1350-1360	α-CH$_3$ bending
	1400-1450	α-CH$_2$ bending
	1100	C-C-C bending
Carboxylic Acids & Derivatives	2500-3300 (acids) overlap	O-H (very broad)
	C-H	C=O (H-bonded)
	1705-1720 (acids)	O-C (sometimes 2-peaks)
	1210-1320 (acids)	
	1785-1815 (acyl halides)	C=O
	1750 & 1820 (anhydrides)	C=O (2-bands)
	1040-1100	O-C
	1735-1750 (esters)	C=O
	1000-1300	O-C (2-bands)
	1630-1695(amides)	C=O (amide I band)
	1395-1440	
	1590-1650	C-O-H bending
	1500-1560	N-H (1¡-amide) II band
		N-H (2¡-amide) II band

Nitriles	2240-2260	C≡N (sharp)
Isocyanates,Isot hiocyanates, Diimides, Azides & Ketenes	2100-2270	-N=C=O, -N=C=S -N=C=N-, -N_3, C=C=O

APPENDIX B

RECEPTOR MODEL

Our computational model has been validated on high-dimensional data from three chemical sensor arrays. In this appendix we propose a computational model for olfactory receptors that can be used to generate high-dimensional signals from the low-dimensional feature spaces typically obtained with e-nose instruments.

To simulate an ORN population from a low-dimensional feature space, we present the following receptor model. The receptor model transforms a *n*-dimensional sensor response $\overrightarrow{S^A} = \left[S_1^A, S_2^A, ..., S_n^A\right]$, where S_j^A is the response of sensor *j* to odor A, onto an *m*-dimensional response $\overrightarrow{R^A} = \left[R_1^A, R_2^A, ..., R_m^A\right]$ across a population of *m (m>>n)* ORNs. The selectivity of each simulated ORN is given by a n-dimensional unit-vector $\overrightarrow{V_i} = \left[V_1, V_2, ..., V_n\right]$ defined in feature space, as illustrated in Fig. 65(a). The response of receptor *i* to odor *A* is then given by

$$R_i^A = \sigma\left(\left|\mathbf{S^A}\right| \cdot \cos\left(\theta_{V_i, S^A}\right)^p\right) \tag{B.1}$$

where $|S^A|$ is the length of the odor vector, which captures concentration information, θ_{V_i, S^A} is the angle between the vectors $\overrightarrow{V_i}$ and $\overrightarrow{S^A}$, which is related to the identity of the odor, *p* defines the receptive field width of this receptor (refer Fig. 65(b)), and $\sigma(\cdot)$ is a logistic function that models saturation. The cosine weighting of the form shown in

equation (B.1) is common in the primary motor neurons used to code movement directions (Georgopoulos et al. 1986), and has been suggested to be a primary requirement for performing vector computations on sensory inputs (Wilson 1999).

Let us illustrate this mapping with an example. Consider a synthetic problem with two gas sensors (1 and 2) and three receptors (*A, B,* and *C*). The surface plot in Fig. 66 shows the response of each simulated ORN to all possible combinations of sensor 1 and sensor 2 responses. Receptor A is selective to odors that produce high response in sensor 2 and low response in sensor 1. Receptor B and C, which have similar selectivity, respond maximally to odors that generate high response in sensor 1 but low response in sensor 2. Furthermore, the response of the receptors increases with an increase in concentration (represented by an increase in the amplitude of the sensor response) until saturation sets in. By sampling the sensor space with a population of such simulated receptors, a high dimensional odor signal can be obtained that preserves the topology and proximity relationships of the sensor space.
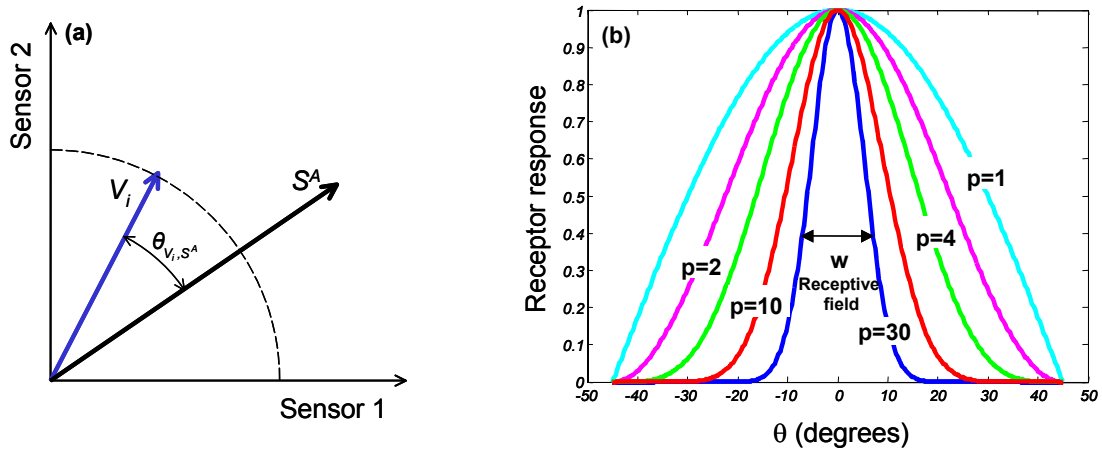
Fig. 65: (a) Illustration of the receptor model: The selectivity of receptor neuron *i* is defined by the unit-vector V_i in a two-dimensional sensor space. The response of this receptor to odor A depends on the angle θ_{V_i,S^A} between V_i and the sensor response to the odor $S_A=[S_1,\ S_2]^T$. (b) Effect of parameter *p* on the cosine weights: increasing values of *p* correspond to narrower receptive field widths.
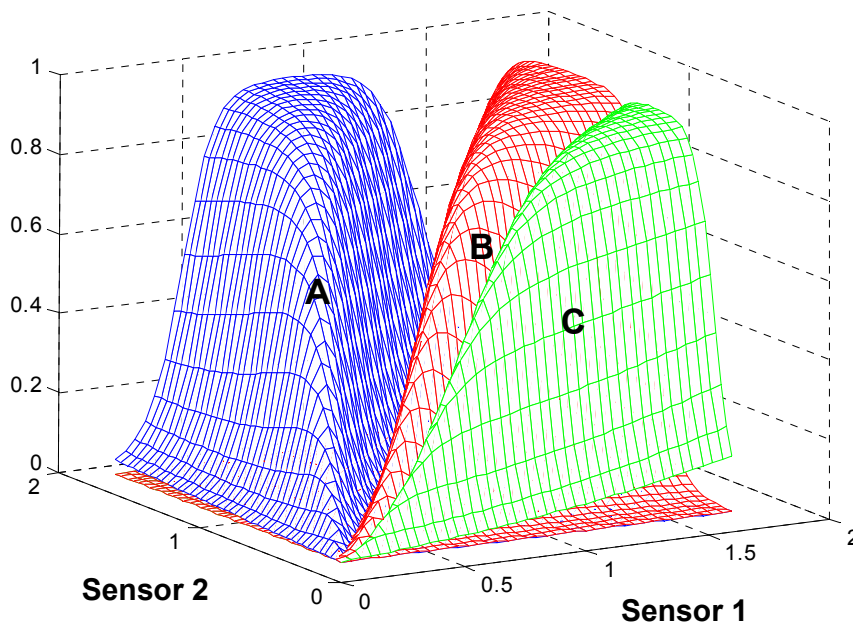
Fig. 66: Illustration of the receptor mapping: Three receptors and their receptive field defined in a synthetic two dimensional sensor space.

Experimental results

In order to evaluate the proposed receptor model on experimental datasets, we use the temperature-modulated MOS sensor response from the *Selectivity* dataset. To generate a low dimensional sensor response each transient is now decimated into 10 equally spaced measurements per sensor, generating a 20-dimensional input signal. The sensor response (only one out of three replicates) to each of the three analytes (acetone (A), isopropyl alcohol (B) and ammonia (C)) at their highest concentration is used to train the system. A population of 5,000 ORNs is simulated by aligning the ORNs in the direction of the three training odor vectors with the addition of uniformly distributed noise to each

dimension (±25% of the maximum value). This is done to overcome the difficulty in uniformly sampling the 20-dimensional space with 5,000 ORNs and also to prevent overfitting. Subsequently, the high dimensional ORN response is chemotopically projected onto a GL layer with 400 nodes, arranged as a 20x20 SOM lattice. Fig. 67 shows the simulated glomerular images (SOM activity) for the three analytes at three concentration levels. The SOM learns three odor-specific loci corresponding to the three odors. The concentration information is captured by the amplitude and spread of this pattern. These results are qualitatively similar to those obtained in Chapter III.
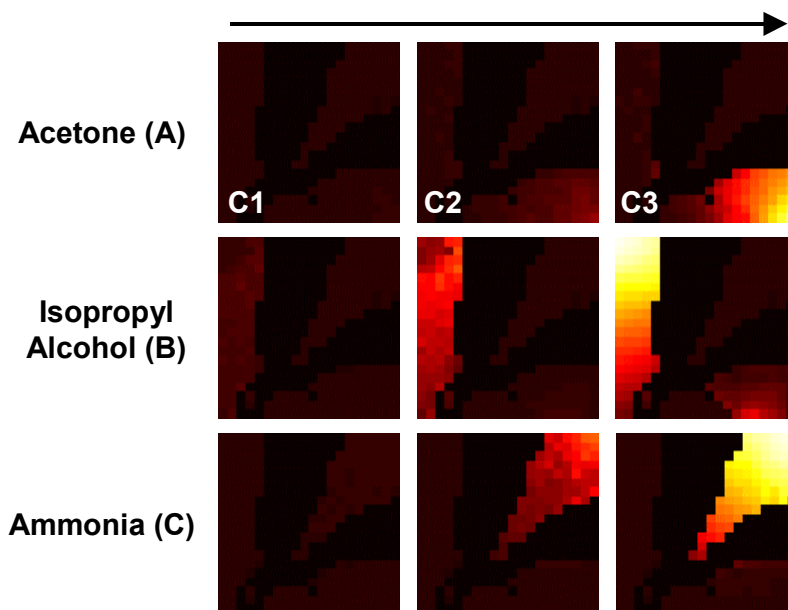

Fig. 67: Glomerular images of the three analytes generated using an experimental database of temperature-modulated MOS sensors exposed to acetone, isopropyl alcohol, and ammonia at three different concentrations levels (*Selectivity database*). A population of 5,000 sharply tuned receptor neurons (*p=30*) and a 20×20 SOM lattice was used to generate these spatial maps.

Broad vs. sharp tuning of receptors

Next we use the model to study the relationship between receptor neuron tuning width and odor separability. The tuning width of the simulated ORNs can be controlled by adjusting the value of the parameter p in equation B.1. Large p values correspond to sharply tuned ORNs, whereas small p values correspond to broad receptive field widths. Fig. 68 shows the separability between the three analytes (all concentrations included) when computed from raw sensor data (20 dimensions), principal components (first two eigenvectors), and following convergence mapping. Maximum separability is achieved using convergence mapping with receptor neurons whose receptive field width is neither too broad nor too narrow ($p=8$ to $p=12$). This is in agreement with theoretical work on biological and artificial chemical sensors, which indicates that maximum mutual information between the sensor response and the set of odors to be identified is obtained by using an array of receptors/sensors that are tuned to 25-35% of the entire stimulus set (Alkasab et al. 2002). Furthermore, our results show that convergence (for $6 \leq p \leq 15$) leads to an increase in odor separability when compared with the raw signals or the PCA projection. This improvement in signal-to-noise-ratio is again a direct result of the supervised nature of the convergence mapping, which leads to more orthogonal patterns than those available at the input.
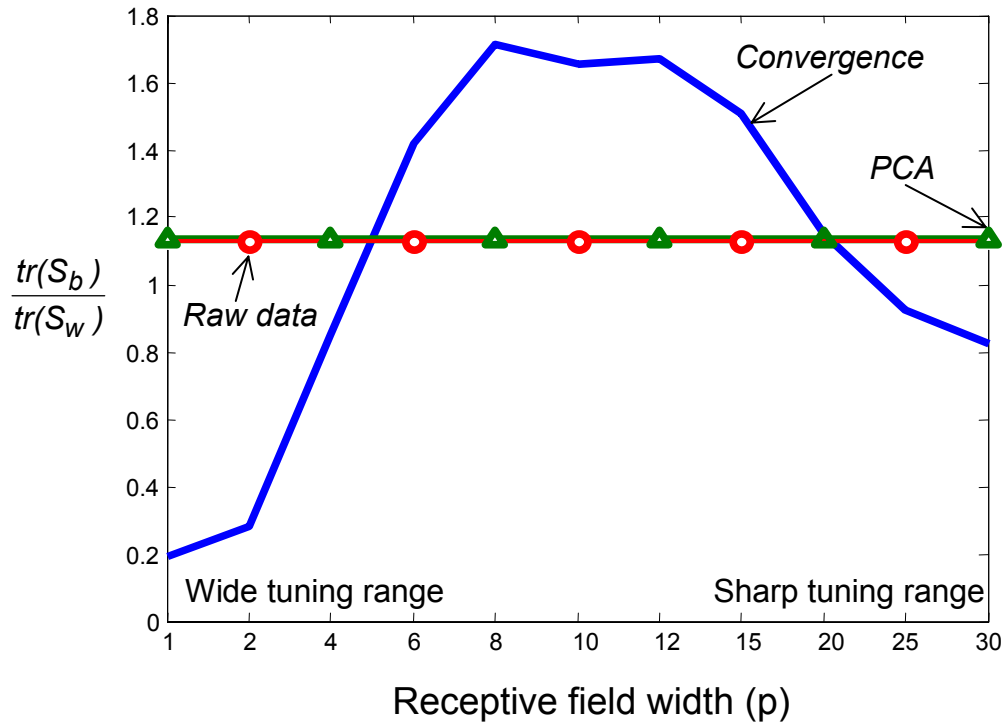
Fig. 68: Comparison of pattern separability using (a) raw sensor data, (b) PCA, and (c) convergence (maximum separability is achieved in the region p=8 to p=12).

APPENDIX C

SPIKING MODEL OF THE OLFACTORY BULB NETWORK

The proposed signal-processing primitives have been demonstrated on a rate model of the olfactory pathway. These primitives, however, are not tied to a particular neural network model. To illustrate this point, this section presents a spiking model of the olfactory bulb circuits described in Chapter V.

Each M cell is now modeled using a leaky integrate-and-fire spiking neuron (Gerstner and Kitler 2002). The input current $I(t)$ and change in membrane potential $u(t)$ of a neuron is now given by:

$$I(t) = \frac{u(t)}{R} + C\frac{du}{dt}$$

$$\tau\frac{du}{dt} = -u(t) + R \cdot I(t) \quad [\tau = RC]$$

(4.1)

Each M cell receives current I_{input} from ORNs and current $I_{lateral}$ from lateral connections with other M cells:

$$I_{input}(j) = \sum_i W_{ij} \cdot ORN_i$$

$$I_{lateral}(j,t) = \sum_k L_{kj} \cdot \alpha(k, t-1)$$

(4.2)

where W_{ij} indicates the presence/absence of a synapse between ORN_i and M_j, as determined by the chemotopic mapping, L_{kj} is the efficacy of the lateral connection between M_k and M_j, and $\alpha(k,t\text{-}1)$ is the post-synaptic current generated by a spike at M_k:

$$\alpha(k, t-1) = -g(k, t-1) \cdot [u(j, t-1)_+ - E_{syn}] \qquad (4.3)$$

$g(k,t-1)$ is the conductance of the synapse between M_k and M_j at time t-1, $u(j,t-1)$ is the membrane potential of M_j at time t-1 and the $+$ subscript indicates this value becomes zero if negative, and E_{syn} is the reverse synaptic potential. The change in conductance of post-synaptic membrane is:

$$\dot{g}(k, t) = \frac{dg(k, t)}{dt} = \frac{-g(k, t)}{\tau_{syn}} + z(k, t)$$

$$\dot{z}(k, t) = \frac{dz(k, t)}{dt} = \frac{-z(k, t)}{\tau_{syn}} + g_{norm} \cdot spk(k, t) \qquad (4.4)$$

where $z(.)$ and $g(.)$ are low pass filters of the form $exp(-t/\tau_{syn})$ and $t \cdot exp(-t/\tau_{syn})$, respectively, τ_{syn} is the synaptic time constant, g_{norm} is a normalization constant, and $spk(j,t)$ marks the occurrence of a spike in neuron i at time t:

$$spk(j, t) = \begin{cases} 1 & u(j, t) = V_{spike} \\ 0 & u(j, t) \neq V_{spike} \end{cases} \qquad (4.5)$$

Combining equations (4.3) and (4.4), the membrane potential can be expressed as:

$$\dot{u}(j, t) = \frac{du(j, t)}{dt} = \frac{-u(j, t)}{RC} + \frac{I_{lateral}(j, t)}{C} + \frac{I_{input}(j)}{C}$$

$$u(j, t) = \begin{cases} u(j, t-1) + \dot{u}(j, t-1) \cdot dt & u(j, t) < V_{threshold} \\ V_{spike} & u(j, t) \geq V_{threshold} \end{cases} \qquad (4.6)$$

When the membrane potential reaches $V_{threshold}$, a spike is generated, and the membrane potential is reset to V_{rest}. Any further inputs to the neuron are ignored during the subsequent refractory period. Model parameters are summarized in Table 1.

Table 1. Parameters of the OB spiking neuron lattice

Parameter	Value	Parameter	Value
Peak synaptic conductance (G_{peak})	0.01	Synaptic time constants (τ_{syn})	10 ms
Capacitance (C)	1 nF	Total simulation time (t_{tot})	500 ms
Resistance (R)	10 MOhm	Integration time step (dt)	1 ms
Spike voltage (V_{spike})	70 mV	Refractory period (t_{ref})	3 ms
Threshold voltage ($V_{threshold}$)	5 mV	Number of mitral cells (N)	400
Synapse Reverse potential (E_{syn})	70 mV	Normalization constant (g_{norm})	0.0027

Experimental Results

The temperature-modulated sensor patterns for three analytes acetone (A), isopropyl alcohol (B) and ammonia (C), at three different concentrations are chemotopically projected onto a GL layer with 400 nodes, arranged as a 20x20 SOM lattice, based on the convergence model described in Chapter III. The 400 outputs of the convergence model are used as the inputs to the spiking OB model.

Fig. 69 shows the projection of membrane potential of the 400 M cells along their first three principal components. Three trajectories are shown per analyte, which correspond to the sensor response to the highest analyte concentration on three separate days of data collection. Similar to the results from the firing rate model, the trajectories originate close to each other, but slowly migrate and converge into unique odor-specific attractors, as illustrated by the insets in Fig. 69.
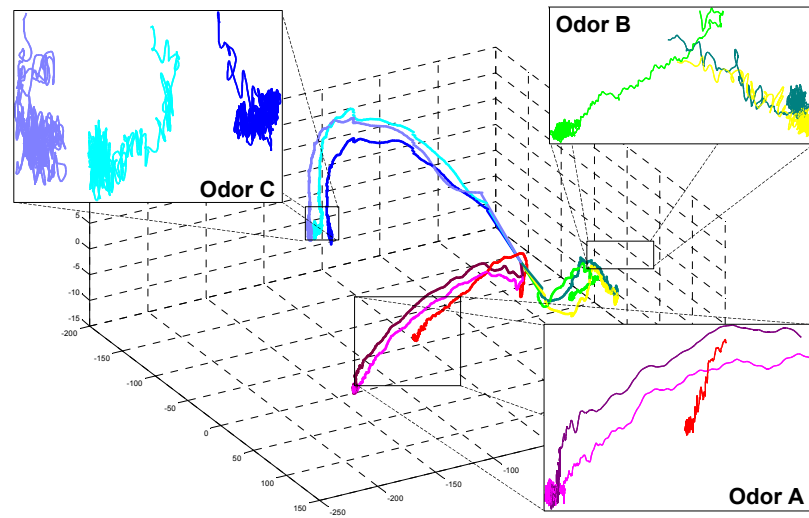
Fig. 69: Odor-specific attractors from experimental sensor data. Three trajectories are shown per analyte, corresponding to the sensor response on three separate days.

To illustrate the coding of identity and intensity performed by the model, Fig. 70 shows the trajectories of the three analytes at three concentrations. The OB network activity evolves to settle into an attractor, where the identity of the stimulus is encoded by the direction of the trajectory relative to the initial position, and the intensity is encoded by the length along the trajectory. This emerging code is consistent with the results generated using the firing rate model presented in Chapter V.

These results show that that the proposed signal-processing primitives are not tied to any particular neural network model.
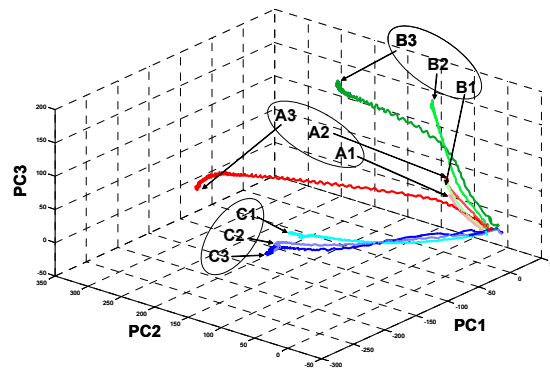
Fig. 70: Identity and intensity coding using dynamic attractors.

VITA

Baranidharan Raman was born in Madras, India on June 20, 1979, the son of R. Raman and R. Sundaralakshmy. He received his Bachelor of Engineering in computer science with distinction from the University of Madras in 2000. He received the M.S. degree from the Department of Computer Science at Texas A&M University in May 2003 and his Ph.D. in computer science in December 2005. He is currently a member of the Pattern Recognition and Intelligent Sensor Machines (PRISM) Laboratory in the Department of Computer Science, Texas A&M University. His research interests include Sensor based Machine Olfaction, Intelligent Systems, Machine learning, Neural Computation, and Robotics.

Permanent Address:

73 Dhanalakshmy colony,

9/4 Natarajan Street, Vadapalani

Chennai, Tamilnadu, India-600026

E-mail: barani@cs.tamu.edu

Web: http:/students.cs.tamu.edu/barani